Thermal Analysis of Polymers Adsorbed on Silica and the Functionalized Mesoporous Silica and Its Application to the Adsorption of Volatile Organic Compounds

By

SHADI ALIZADEH-BAZAZI

Bachelor of Science in Chemistry
Azad University
Tehran, Iran
2002

Master of Science in Inorganic Chemistry
University of Tehran
Tehran, Iran
2006

Submitted to the Faculty of the
Graduate College of the
Oklahoma State University
in partial fulfillment of
the requirements for
the Degree of
DOCTOR OF PHILOSOPHY
July 2015

Thermal Analysis of Polymers Adsorbed on Silica and the Functionalized Mesoporous Silica and Its Application to the Adsorption of Volatile Organic Compounds

Dissertation Approved:

Dr. Nicholas F. Materer

Dissertation Adviser

Dr. Allen Apblett

Dr. Richard Bunce

Dr. Ziad El-Rassi

Dr. Tyler Ley

ACKNOWLEDGEMENTS

I would like to express my deep appreciation and gratitude to my advisor, Dr. Nicholas F. Materer, for the patient guidance and mentorship he provided to me and I am truly fortunate to have had the opportunity to work with him. Also I wish to thank the members of my committee for their help and time.

I would like to thank department of chemistry for providing teaching opportunities for me specially Dr. Frank D. Blum, for supervising the first part of dissertation. I also thank Dr. Iob and Mrs. Halihan for supervising and helping me in my teaching duties.

I appreciate the help in the experimental part of the work provided by Dr. P. Rajasekar, research scientist at Xplosafe LLC.

Special thanks to wonderful human being and great soul Fateme Fashandi. Her persistence, passion and generosity have always impacted my life in such a wonderful way.

I would also like to thank Cheryl and James Malone for become my family in Stillwater. Their constant love and support during my challenging days here is priceless and they will be my forever angles.

Thanks a lot to my best friend and sister Shabnam, and my brother Kamrouz, my wonder of wonders.

Last but certainly not least, I would like to appreciate my lovely and dedicated parents, Iran Basirat and Behrouz Alizadeh for their love and support. They cheered me up and stood by me through the good times and the bad.

Acknowledgements reflect the views of the author and are not endorsed by committee members or Oklahoma State University.

Name: SHADI ALIZADEH BAZAZI

Date of Degree: July 2015

Title of Study: Thermal Analysis of Polymers Adsorbed on Silica and the Functionalized Mesoporous Silica and Its Application to the Adsorption of Volatile Organic Compounds

Major Field: CHEMISTRY

Abstract:
The thermal behavior of adsorbed poly(vinyl acetate) (PVAc) on silica was determined using temperature-modulated differential scanning calorimetry (TMDSC). PVAc samples with different molecular masses (260, 170 and 100 kDa) were studied. PVAc with high and medium molecular masses, had 0.91±0.31 mg/m^2 and 0.66±0.16 mg/m^2 amounts of tightly-bound polymer, respectively. The low molecular mass PVAc had a smaller amount of tightly-bound polymer (about 0.53±0.02 mg/m^2). The ratios of the heat capacity changes in the glass transition region were consistent with the tightly-bound PVAc in a more restricted environment than the bulk polymer.

Functionalized hexagonal mesoporous silica, in powder and pellet forms, was prepared by chemical modification of mesoporous silica with both chlorine-based and alkoxide silylating agents of different chain lengths. The ^{13}C and ^{29}Si NMR and TGA results show that both methods can functionalize the surface of mesoporous silica. Better loading of organic moieties was found when using hexyltrimethoxysilane. A hydrolysis study shows that chlorotrimethylsilane functionalized mesoporous silica can be readily hydrolyzed, but the surfaces generated from the alkoxide silylating agents are stable. Toluene, nitrobenzene, and naphthalene have been used as adsorbents to probe the difference between pure and functionalized mesoporous silica. Heats of vaporization or sublimation for toluene, nitrobenzene and naphthalene have been measured using an optical absorption method for the pure material and pure and functionalized mesoporous silica. Since, mesoporous silica is a hydrophilic material; nitrobenzene binding energy to the hydroxylated mesoporous silica is higher compared with the functionalized mesoporous silica because of the polarity of nitrobenzene resulting in higher affinity to the hydroxyl groups of mesoporous silica. In contrast, the functionalized mesoporous silica samples exhibit hydrophobic properties. Toluene and naphthalene binding energies to the functionalized mesoporous silica are higher than for the hydroxylated mesoporous silica.

TABLE OF CONTENTS

LIST OF TABLES

LIST OF FIGURES

Figures page

CHAPTER I

INTRODUCTION

This introduction, as with the following dissertation, is broken into two parts. The first part of the dissertation (Chapter II) details my research with thermal behavior of adsorbed poly(vinyl acetate) (PVAc) on silica. A two-component model, based on loosely-bound polymer (with a glass transition temperature, T_g, similar to that of bulk) and tightly-bound polymer (with T_g higher than of loosely-bound polymer) was used to interpret the thermograms.

The second part of the dissertation, starting with Chapters III, describes research accomplished with pellets and powders of mesoporous silica functionalized with trimethylchlorosilanes (TMCS) and alkoxysilane groups functionalized hexagonal mesoporous silica, in powder and pellet forms, were prepared by chemical modification of surfactant free mesoporous silica with either chlorine-based or siloxane-based silylating agents of different chain length. The resulting inorganic–organic hybrids were characterized by solid-state ^{29}Si and ^{13}C CP/MAS nuclear magnetic resonance (NMR) spectroscopy, total internal reflection infrared Fourier transform (TRIFT) spectroscopy and thermogravimetric analysis (TGA).

Chapter IV describes an application of functionalized materials to trap volatile organic components. This chapter outlines the spectroscopic determination of enthalpies of evaporation or sublimation of selected volatile organic compounds adsorbed on the functionalized mesoporous silica. In this chapter we report the direct determination of optical and thermodynamic parameters of low-volatile organic compounds in their vapor phase using a UV/Vis spectrophotometer.

1.1 Polymers

In Chapter II, the glass transition temperature (T_g), which is related to the heat capacity of adsorbed polymers, was investigated using temperature-modulated differential scanning calorimetry (TMDSC) and the data was interpreted using a two-component model. In this introduction we discuss how polymers are defined, the important properties related to the experiments, and the standard methods of characterization.

Polymers are formed by chemical reactions in which a large number of molecules called monomers are joined sequentially, forming a chain. In many polymers, only one monomer is used. In others, two or three different monomers may be combined.[1] Polymers range from synthetic polymers such as poly(vinyl acetate) to natural biopolymers such as DNA and proteins that as fundamental to biological structure and function. Current applications of polymers include adhesives, foams, coatings, and packaging materials, textile and industrial fibers, composites, biomedical devices, electronic devices, and optical devices. For several applications, polymers have replaced other important materials such as metal, glass, and ceramics due to their light weight, flexibility, durability, chemical inertness, and inexpensive cost.

Polymers are used in different forms such as in bulk and also in composites. A bulk polymer is defined as a system containing only a single polymeric component, such as a homopolymer. On the other hand, a polymer composite is generally a phase separated multi-component material such as a polymer blend, structured latex, or adsorbed polymer. Polymer composites have become very important due to their designable proporties for specific uses and superior performance, as compared to that available through the use of bulk polymers. The structural and functional properties of polymer composites depend upon the properties and interactions of their components,

especially at interfaces where the different components of multi-phases come into contact. An understanding of the behavior of polymers at interfaces is essential and beneficial for improving their properties or for developing novel materials for specific uses. [2]

Among polymer composites, adsorbed polymers are often part of the materials used. Interactions between polymers adsorbed onto surfaces are important in many systems. The importance of these interactions ranges in applications all the way from adhesion, lubrication, surface protection, stabilization, and controlled flocculation of a colloidal dispersion to biological processes of membrane-polymer interactions and medicinal applications.[3-10] The physical properties of adsorbed polymers are, as expected, more complex than those of bulk polymers since they involve multi-component, polymers and interfaces.

Thin polymeric films that range in thickness from a few to several hundred nanometers are of technological interest for the development of electronic and optical devices.[8,5] Because such thin layers of polymeric films may not survive on their own as free-standing films, a supporting surface is often needed. Accordingly, the physical properties of thin polymeric films become rather complicated since they involve both polymers and surfaces. An understanding of the behavior of adsorbed polymers on a surface is essential for improving properties for specific uses. Studies of polymer adsorption have been approached in several ways.[11-15] In general, adsorption can be described as the attachment of species (in this case for polymers) to the substrate. Studies of polymer adsorption are often based on polymers adsorbed from solution. Polymer adsorption is often a relatively irreversible process, as suggested by the small amounts of desorption observed upon dilution with a solvent.[16] In the dilute solution, where the adsorption is typically of single molecules, monolayer adsorption occurs. Polymers

segments randomly adsorbing on the surface, typically do so as alternating three-dimensional loops and two-dimensional surface contained trains.[15,17]

It is well known that the structures and properties of polymers are time and temperature dependent,[18] most polymer solids are unlikely to achieve true equilibrium because of their relatively large sizes and high molecular masses. Solid polymers often exhibit a range of relaxation times and properties in response to their environment. Their dynamic behavior allows the polymers to restructure or reorient in response to environmental changes to minimize free energy. In different systems, such as bulk and adsorbed polymers, the behavior of these polymers may or may not be the same. Although they have common characteristics, a number of studies have reported that, in some ways, adsorbed polymers behave differently from their bulk counterparts.

In this study, we investigated systems such as that shown in Figure 1.1. The restricted motion of an adsorbed polymer on an attractive surface results in higher and broader glass transition temperatures (T_g) than those found in bulk polymers. The (T_g) is a good indication of the mobility of these adsorbed polymers. [19-21]

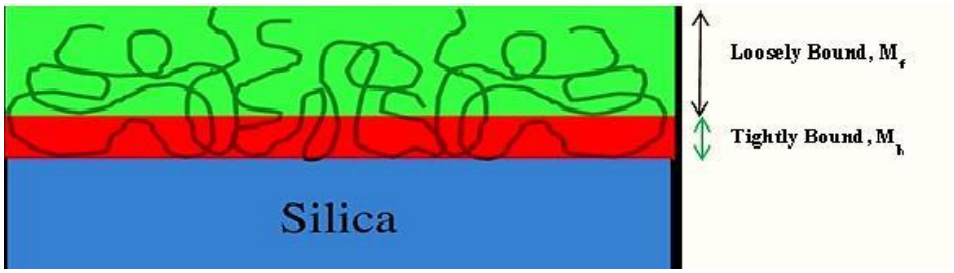

Figure 1.1 A motional gradient of the surfaced-bound polymer. Adapted from reference 22.

A glass transition is a reversible change in an amorphous material (or in amorphous regions within semi-crystalline materials) from a hard and relatively brittle

state into a molten or rubber-like state.[23] For polymers, this change is typically from a hard brittle solid to a viscous or rubbery plastic, or vice versa.[24] The approximate midpoint of the temperature range over which the glass transition occurs is called the "glass transition temperature" (T_g). Amorphous materials are solid (glassy) below the T_g, and are more liquid-like when above the T_g. A glassy state has no long-range order and any long-range transitional molecular motions are essentially frozen, although some motions, such as vibration or other types of local motions can exist. An amorphous polymer exhibits a glass transition, as evidenced by the continuous change in the slope of thermodynamic properties, such as volume (V), enthalpy (H), entropy (S), or by a broad discontinuity in heat capacity (Cp), thermal expansion (α), or compressibility (κ) with temperature.[24,25]

Glass transitions of adsorbed polymers have been probed to investigate their thermal properties, structure, and dynamics. T_g is the region of dramatic and rapid property changes, and thus, it is critical to processing, storage and application of polymers.

1.2 Characterization Techniques for Polymeric Materials

The characterization of polymeric materials, especially for those with multi-components, has been pursued in recent years. However, exploring better techniques of characterization has been challenging and remains so even now. Morphology affects mechanical properties in these materials; therefore, information about morphological parameters, such as the thickness, weight (volume) fraction of interfaces, composition distribution in the phase, phase size/shape, and T_gs is clearly important. Since interfacial properties have a significant impact on the properties of composite materials, an understanding of the interfacial characteristics of these materials and the ability to

optimize its properties are necessary for the improvement and development of polymeric materials.

Many techniques have been used to characterize the morphology of multicomponent polymeric materials.[26] Scattering and microscope techniques have been used to study the shape and size of the domain, and the interface content. For instance, small-angle X-ray (SAXS) and small angle neutron scattering (SANS) have yielded information about interfacial thickness and domain size.[27,28] Transmission electron microscopy (TEM) is a technique that has provided both interfacial thicknesses and information on composition gradients across an interface.[27] It has been used to determine the miscibility, size and shape of domains and their distribution in polymer blends, or phase segregation of interpenetrating polymer networks (IPNs). However, sample preparation can sometimes be difficult due to the need for ultra-thin sections. In addition, electron beams can sometimes cause artifacts and damage to a sample.[29,30] A listing of some of the characterization techniques for multi-component polymeric materials is shown in Table 1.1. However, there is no technique that can provide all the information desired. Therefore, it is very desirable to explore and develop widely applicable techniques for characterizing multi-component polymeric materials that can overcome the disadvantages of existing techniques.

Table 1.1 Comparison of various characterization techniques for multi-component polymeric materials.[31] Adapted from reference 2.

	DSC	SAXS	SANS	SEM	TEM	NMR
Resolution (nm)	20	1	2	20	1	1
Sample Preparation	Easy	Easy	Difficult	Easy	Difficult	Easy

T_g	Quant	No	No	No	No	Qual
Multi-phase information	Yes	Yes	Yes	Yes	Yes	Yes
Interfacial information	Yes	Yes	Yes	No	Yes	Yes
Interfacial thickness	No	Quant	Quant	No	Qual	No
Weight fraction	Qual	No	No	No	No	Yes*
Domain size	No	Yes	Yes	Yes	Yes	No

Qual = qualitative; Quant = quantitative

*Not always possible

Among these, thermal analysis is perhaps the most common and widely used technique for obtaining information on thermodynamic properties, such as the T_g and heat capacity. The heat capacity is primarily based on molecular motions and has been used to evaluate conformational energies of organic molecules.[32]

In this work, we used the temperature modulated differential scanning calorimetry (TMDSC) technique, an advanced version of standard differential scanning calorimetry (DSC). DSC is the most common technique to investigate the thermal transitions in bulk polymers especially at the glass transition temperature.[33,34] Characterization of the behavior of adsorbed polymers at T_g has been studied using temperature modulated DSC (TMDSC). TMDSC is a version of DSC which offers the same information as conventional DSC as well as additional information to understand many aspects of thermal behavior of materials by separating the heat flow data into reversing and non-reversing events.[35] TMDSC has been used to resolve weak transitions and those occurring at close temperatures.[36-38] TMDSC has an ability to separate overlapping

transitions that are difficult to distinguish in conventional DSC. Since the TMDSC separates the total heat flow into reversing and non-reversing components, more information about the thermal properties of materials can be obtained.[39]

1.3 Pure and Functionalized Mesoporous Silica

According to the International Union of Pure and Applied Chemistry (IUPAC), mesoporous are defined as pores with sizes in the range of 2-50 nm. In 1990, Yanagisawa *et al.*[40] described the synthesis of microporous materials. Their preparation method is based on the intercalation of long-chain (typically C-16) alkyltrimethylammonium cations, into the layered silicate kanemite, followed by calcination up to 700 °C to remove the organic species, which is later called surfactants, yielding a mesoporous material. The X-ray powder diffraction gave only an uninformative peak centered at extreme low angles. Unfortunately, there were no further characterization data available leading to an ignoring of the Yanagisawa results.[41] In 1992, scientists at the Mobil research and development corporation published a paper describing synthesis and characterization of mesoporous silica, designated M41S, by a proposed liquid-crystal template mechanism (Figure 1.3).[42] The paper that appeared in the journal Nature is one of the most cited chemistry papers of all time, and the American Chemical Society (ACS) referred to their discovery as one of the most important discoveries in chemistry.[43]

In this work, a unique form of silica with a massively parallel pore structure, arranged in a hexagonal lattice was unveiled and named MCM-41. (Figure 1.2) MCM-41 has been synthesized with uniform channels varying from approximately 15 Å to greater than 100 Å in size. The larger pore materials typically have surface areas above 700 m^2/g. Other members of this family, including a cubic phase and other less well defined phases, have been identified.

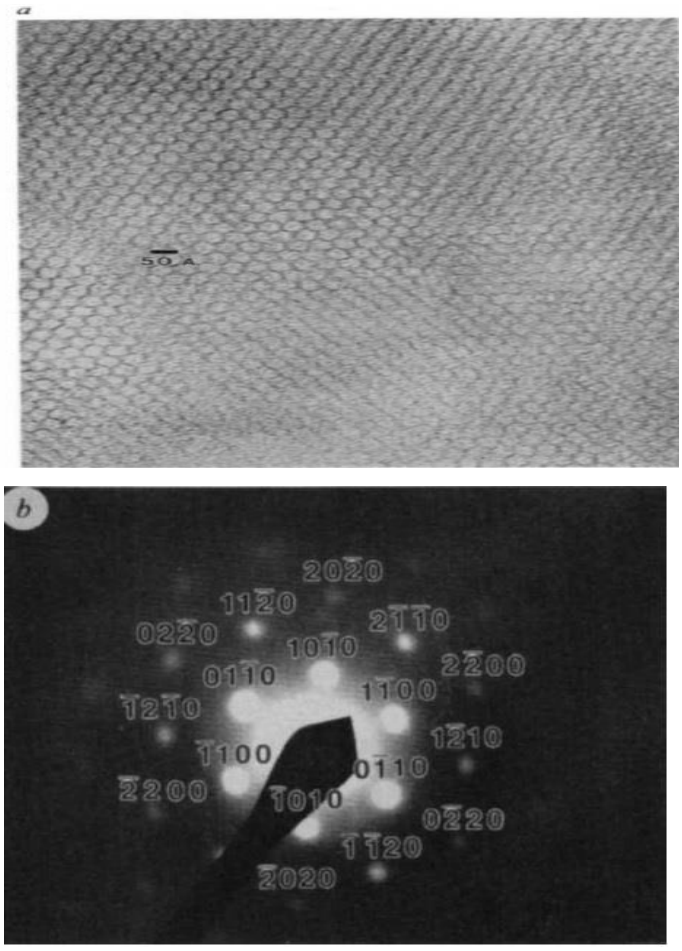

Figure 1.2 a) Representative transmission electron micrograph of MCM-41 and b) Representative electron micrograph of MCM-41. Adapted from reference 42

A liquid crystal templating (LCT) mechanism in which surfactant liquid crystal structures serve as organic templates has been proposed for the formation of these materials (Figure 1.3).[1, 3] The LCT mechanism exploits the continuous solvent (water) region to create inorganic walls between the surfactant liquid crystal structures. It may be that encapsulation occurs because anionic inorganic species enter the solvent region to balance the cationic hydrophilic surfaces of the micelles. Alternatively, perhaps it is the introduction of the inorganic species themselves that mediates the liquid crystal ordering.

In the LCT mechanism, Beck *et al*. proposed that silicate condensation is not the dominant factor in the formation of the structure.[44] They suggested that the structure is defined by the organization of the surfactant molecules into micellar liquid crystals which serve as templates for the formation of the MCM-41 structure.

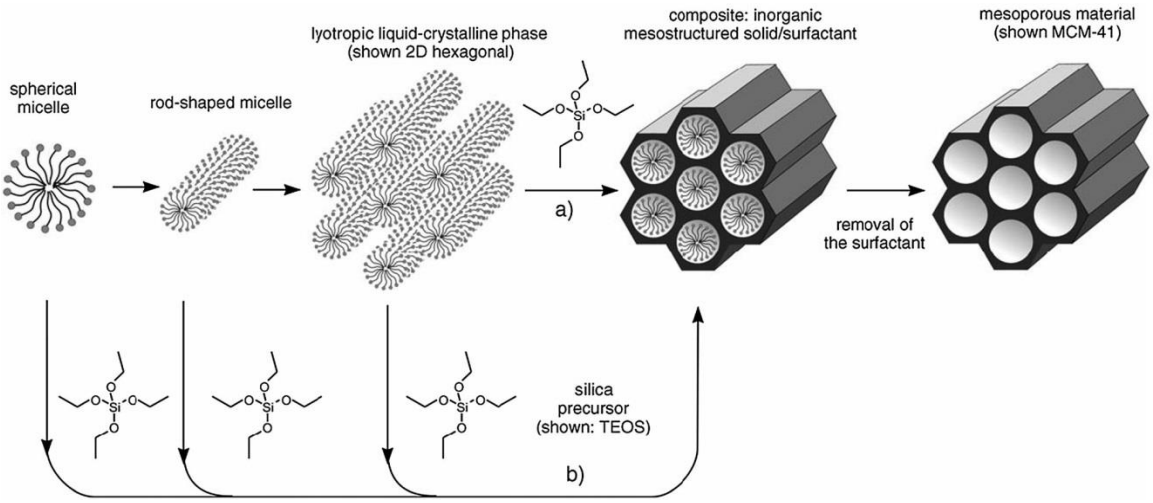

Figure 1.3 Possible mechanistic pathways for the formation of MCM-41: (1) Liquid crystal phase initiated and (2) silicate anion initiated. Adapted from reference 45.

The LCT mechanism has two possible pathways: The first mechanistic model described the addition of silicate to micelles formed using the organic template; the silica polymerizing around the previously formed micelles. The second model proposed that addition of silicate to an aqueous template solution induced ordering of silicate-encased surfactant micelles simultaneously, that is micelle formation required silicate to be present. A schematic illustration of the formation mechanisms is given in Figure 1.3. After polymerization, the mesosilica becomes porous by removing the surfactant template by solvent extraction or calcination.

The diameter of the pores can be varied by changing the alkyl chain length of the cationic surfactant used in the synthesis procedure or adding auxiliary hydrocarbons such as alkylated benzene to the synthesis mixture.[46] When the auxiliary organic species are added to the reaction gel, they will be solubilized inside the hydrophobic regions of micelles, causing an increase in micelle diameter which will lead to an increase in the pore size of the final product.[47] This highly porous morphology results in extremely high surface area, typically 1000 m^2/g or more. In addition because of the parallel orientation of the pores and high degree of order, all of the pores are open-ended, leaving the entire internal pore surfaced accessible to gas-phase or solution-borne chemical species.[48] These properties makes MCM-41 a very promising candidate as a catalyst, catalyst support, sensors, adsorption/separation, environmental pollution control, and stationary phases for different kind of chromatography.[49-58]

Mesoporous materials are interesting supports for organic functional groups due to their high surface area, large and uniform pore size, and narrow pore size distribution. While the silica framework provides thermal and mechanical stability, the surface organic moieties provide control of interfacial and bulk materials properties such as flexibility and optical properties (Figure 1.4).[59]

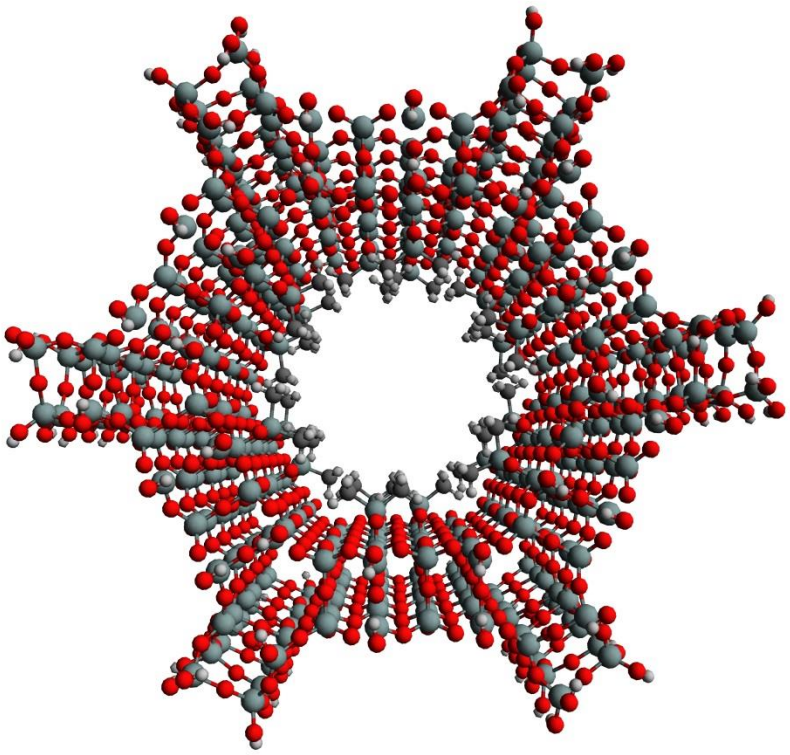

Figure 1.4 Functionalized MCM-41.

In this research, we have synthesized mesoporous silica (OSU-6) with enhanced thermal and hydrothermal stabilities following the method described by Al-Othman and Apblett[60] and studied the structural and surface properties before and after surface modification with chlorine-based silylating agent and alkylsilanes of different alkyl chain lengths and functionalities ($CH_3(CH_2)_nSiR_3$, with n = 1,3,5,7; R =OCH_3,OEt). Modification of the mesoporous surface with alkyl chains provides additional physical or chemical properties to the silica parent material e.g. increases the surface hydrophobicity, passivates the silanol groups to protect the framework against hydrolysis. The pore

diameter can be progressively decreased by using alkyl chains of different lengths and functionalities.[61]

1.4 Spectroscopic Determination of Enthalpies of Evaporation and Sublimation of Volatile Organic Compounds Adsorbed on Functionalized Mesoporous Silica.

Volatile organic compounds (VOCs) are one of the most common air pollutants that need to be controlled according to increasingly strict environmental regulations. The presence of VOCs in the air presents a number of harmful effects related to their toxicity and their contribution to photochemical smog, acting as precursors in the generation of ozone and secondary organic aerosol (SOA). One of the main sources of VOCs is the use of fossil fuels and they are extensively used as solvents, aerosol propellants, and raw materials, resulting in a steadily growing demand and production.[62,63] The quantity of VOCs emitted by processes of distribution and storage of gasoline accounts for about 5% of the total amount of VOCs released to the atmosphere. [64] A number of technologies have been developed and applied commercially for VOC abatement. Numerous technologies, such as adsorption, thermal oxidation, incineration and catalytic reduction, have been developed and applied for the removal of VOCs.[65]

These alternatives are basically classified into two different groups: destructives and nondestructives. In the destructive methods, such as incineration, thermal, and catalytic oxidation, VOCs are transformed into inert or less harmful materials. In the second group, VOCs are retained and removed from the air without suffering any chemical modification. This group includes treatments as adsorption, condensation, and absorption. Adsorption processes are widely used because of the flexibility of the system, low energy consumption cheap operation costs, and the possible recovery of valuable VOCs.[64,66,67]

Activated carbons and hydrophobic zeolites with high Si/Al ratio are the most commonly applied adsorbents for VOCs removal because of easy operation, and low operating cost, although their use involves a number of problems, mainly related to the fact that activated carbons are flammable materials with difficult regeneration procedure and pore clog.[68,69] To circumvent these drawbacks, the replacement of microporous solids by mesoporous adsorbents could be of relevant interest. Mesoporous silica materials involve a high BET surface area coupled to an important pore volume which confers them with high sorption capacities. They are also considered as organophilic solids due to their ability to adsorb significant quantities of organic molecules in the gas phase, such as n-hexane, benzene, toluene as well as various alcohols.[70-72] The surface functionalization of mesoporous silica materials with appropriate organic moieties is expected to minimize the water adsorption within the pores, while increasing the pollutant sorption capacities because of stronger interactions between the adsorbent and the organic pollutant.[73]

Previous studies[74,75] indicated that adsorption characteristics of MCM-41 for polar molecules greatly depends on the concentration of surface silanol groups (SiOH). Mobil Oil Corporation has patented a sorption separation process using modified MCM- 41 for the purification of water.[44] Feng *et al*.[76] reported a functionalized mesoporous adsorbent for the removal of heavy metals from wastewater.

In this research, we report the use of absorbance spectroscopy in the UV region of the electromagnetic spectrum to determine the latent heats of sublimation and evaporation of toluene, nitrobenzene, and naphthalene.

CHAPTER II

THERMAL ANALYSIS OF ADSORBED POLY(VINYL ACETATE) ON SILICA

2.1 Introduction

In bulk polymers, when there are no specific attractions such as hydrogen bonding, ionic bonding (ionomers) or others, the change in heat capacity at the T_g is primarily determined by the change in conformational structures.[77,78] Below the T_g, large-scale conformational motions of the polymers are virtually nonexistent, while at higher temperatures, they are common. In adsorbed polymers, the changes in molecular motion at the glass transition are different from bulk polymers. In the present case, this motion is significantly affected by a specific interaction, namely hydrogen bonding between the carbonyls of PVAc and the surface silanols on the silica. This work was performed in Dr. Blum's research group.

A study of adsorbed PVAc on silica using temperature modulated differential scanning calorimetry (TMDSC) has been reported[79] and a relatively narrow, single glass transition for bulk PVAc, plus broader two-component transitions were found for the adsorbed polymer. A two-state model, based on loosely-bound polymer (T_g similar to bulk) and more tightly-bound polymer (T_g higher than bulk) was used to interpret the thermograms. Based on that work, the ratio of the change in heat capacities for the tightly-bound and the loosely bound polymer at the T_g, and the amount of tightly bound polymer were estimated. In the present work, we have used the same technique based on

this two-state model to study the effect of molecular mass on the adsorption of PVAc on silica.

2.2 DSC Method

In this work, we used the temperature modulated scanning calorimetry (TMDSC) technique, an advanced version of standard DSC. Differential Scanning Calorimetry, DSC, is a technique which combines the quantitative features of calorimetry with measurement during heating and cooling cycles. In DSC, the temperature is measured continuously and the difference in heat flow between a sample and a reference is measured as a function of time and temperature under controlled conditions (time, temperature, and pressure). The most common design of DSC instruments is the heat flux calorimeter, as shown in Figure 2.1 In this design, a metallic disc (constantan) is used to transfer heat between a sample and a reference. A sample is packed in a metal pan such as aluminum, and an empty pan is used as a reference. Those two pans are placed on the raised platform of the metallic disc. When heat is transferred to the disc, the differential heat flow to the sample and to the reference is measured by a thermocouple, which is connected to chromel pieces beneath the metallic disc. An inert gas such as nitrogen, helium, or argon is used for purging to ensure a uniform, stable thermal environment which results in a better baseline and better sensitivity (signal-to-noise). The purge gas enters the sample chamber through an orifice in the heating block.

The differential heat flow is measured by thermocouples with $dQ/dt = \Delta T/R_D$, where dQ/dt is heat flow, ΔT is the temperature difference between the reference and sample, and R_D is the thermal resistance of the metallic disc.

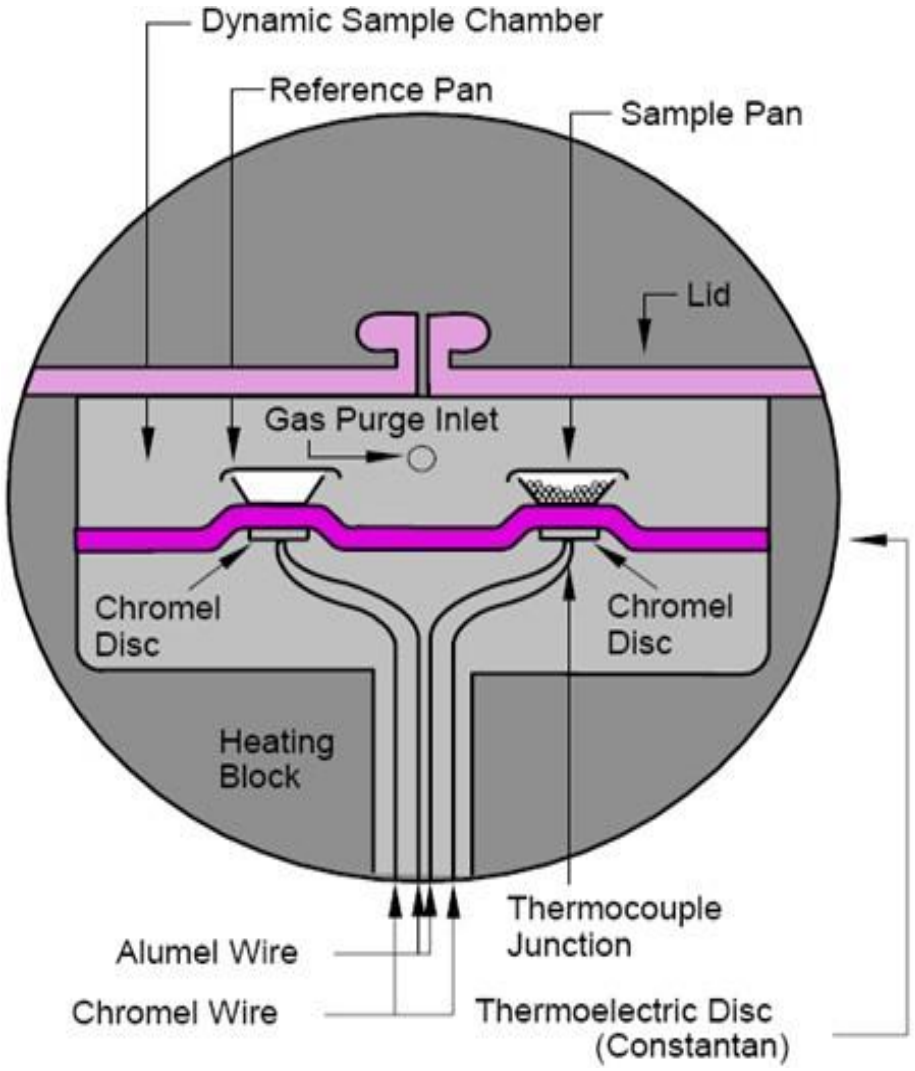

Figure 2.1 Heat flux differential scanning calorimeter. Adapted from reference [80]

DSC is a thermoanalytical technique in which the difference in the amount of heat required to increase the temperature of a sample and reference is measured as a function of time and temperature. It provides quantitative and qualitative analysis information about the physical and chemical changes associated with endothermic and exothermic processes, or changes in heat capacity. DSC is applicable to several kinds of materials,

such as polymers, organic and inorganic compounds. Among thermal analysis techniques, DSC is most widely used because of the reasonable time required for analysis, simple preparation of samples in both liquids and solids, and the wide range of temperatures involved. However, there are some limitations to the use of DSC. Temperature modulated differential scanning calorimetry (TMDSC) is an improved version of the standard DSC, which has overcome most of its previous limitations. TMDSC offers the same information as conventional DSC, with the addition of other unique information that one might not be able to obtain due to limitations in conventional DSC.[81]

TMDSC also measures the difference in heat flow between a sample and an inert reference as a function of time and temperature. The major difference between standard DSC and TMDSC is the application of a sinusoidal modulation (oscillation) imposed on the conventional linear heating or cooling ramp to yield a different temperature profile, since the average temperature of a sample changes with time, in a non-linear fashion. One can simply picture the two experiments being run simultaneously on a sample as a conventional linear (average) heating rate and a sinusoidal (instantaneous) heating rate. The actual rates for these depend on the heating rate, period of modulation, and the temperature amplitude of modulation. The general equation which describes the resulting heat flow for a DSC or a MDSC experiment is

$$dQ/dT = Cp\beta + f(T,t) \quad (2)$$

where dQ/dT is total heat flow, Cp is heat capacity, β is heating rate and f(T,t) is kinetic heat flow (absolute temperature and time dependent) processes.

Conventional DSC only measures the total heat flow, dQ/dT, whereas TMDSC provides those two individual heat flows, Cpβ, (reversing heat flow) and kinetic

component, f(T,t), (nonreversing heat flow), as well as the total heat flow (the sum). In TMDSC, the average heating rate provides total heat flow information, while the sinusoidal heating rate yields heat capacity information from the heat flow that responds to a change in heating rate. The nonreversing heat flow is the difference between the total heat flow and the reversing heat flow. As shown in Figure 2.2, weak or overlapping transitions, such as the glass transition of polymers (which involves enthalpy relaxation), can be accurately obtained from the reversing heat flow component.

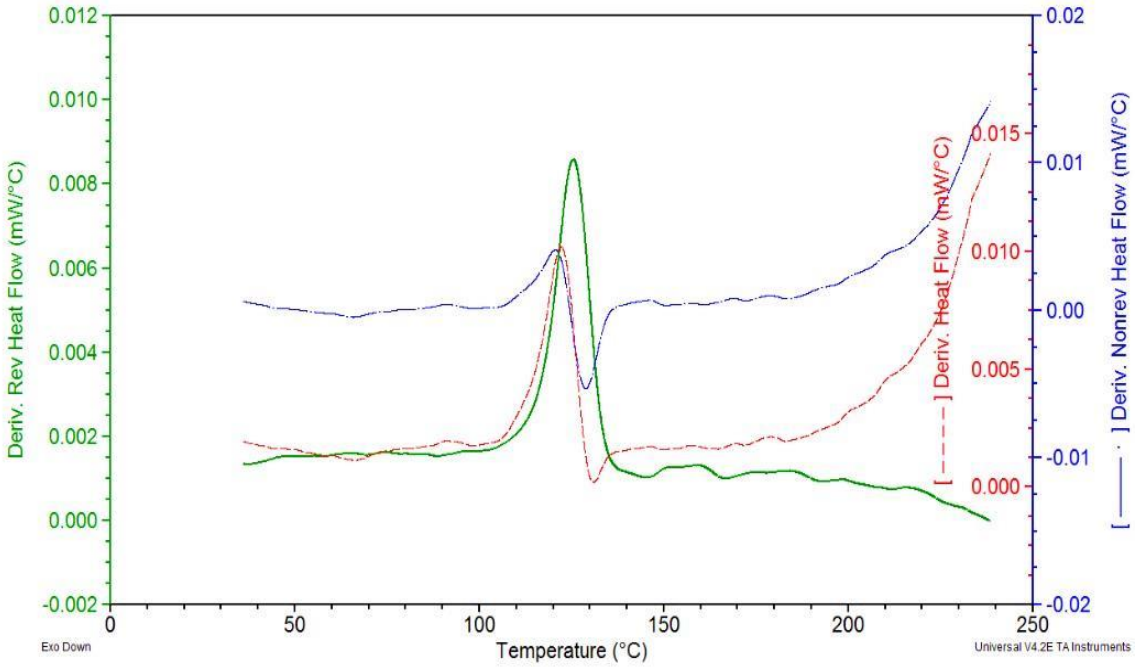

Figure 2.2 The derivatives of total heat flow (a red dashed line), nonreversing heat flow (a blue dash dotted line), and reversing heat flow (a green solid line) of bulk PMMA. Adapted from reference [2]

2.3 Experimental

Three different molecular masses (M_w) of PVAc (260, 170 and 100 kDa) were used as received (*Scientific Polymer Products, Inc.*, Ontario, NY). The molecular masses were determined by using gel permeation chromatography with a Dawn EOS laser light scattering instrument (LLS) and an Optilab refractive index detector (Wyatt Technology, Santa Barbara, CA). The tacticities of these samples have been determined by ^{1}H-NMR and have been reported as percentage of triads as: isotactic triads (mm), atactic triads (rm), and syndiotactic triads (rr). The tacticities were 28.74 (mm), 45.26 (rm), 25.99 (rr) for the 260 kDa sample, 27.84 (mm), 45.27 (rm), 26.89 (rr) for the 170 kDa sample, and 26.02 (mm), 47.70 (rm), 26.28 (rr) for the 100 kDa sample. Cab-O-Sil M-5P silica, with a specific surface area of 200 m^2/g (Cabot Corporation, Tuscola, IL), was used as the substrate.

The silica was dried in an oven at 400 ºC for 24 hour before use. Various concentrations of PVAc solutions of 30, 60, 90, 120, 150 mg/mL in toluene (10 mL) were prepared. 300 mg of silica were added to the PVAc solution. The test tubes containing mixtures of silica and the PVAc solutions were put in a mechanical shaker for 48 hours. The toluene was removed by blowing air at a low flow rate, using a glass pipette, through the adsorbed polymer-silica-solvent dispersion, as it was being agitated. The air-dried samples were put in an oven under vacuum at 50°C, 48 hours to remove any residual solvent.

Thermogravimetric analysis (TGA) measurements were made using a Hi-Res TGA-2950 (TA Instruments, New Castle, DE) to determine the amount of absorbed polymer at the surface of the silica. Samples of approximately 8-12 mg were placed in a platinum pan and heated from 25 to 700 ºC, with a heating rate of 20 ºC/min in air. The mass loss was followed as a function of time (temperature) up to roughly about 250-270 ºC.

The thermal behavior in the glass transition region was measured with a TA Instruments model Q2000 DSC MDSC (TA Instruments, New Castle, DE). The samples were referenced against the empty pans and the cell purged with nitrogen gas at a flow rate of 50 mL/ min. The samples were held at -40 ºC for 3 min, heated to 150 ºC at a rate of 3 ºC/min with a modulation amplitude of +/- 1.0 ºC, and a period of 60 s, held for 3 min, cooled to -40 ºC at the same rate and then held at -40 ºC for 3 min in order to minimize the effects of previous thermal history. After the first heating and cooling scan, the second heating scan was done with the same conditions as the first heating scan. The T_g was determined based on the second heating scan. The results are shown as differential reversing heat flow rate ($dQ_{reversing}/dT$) vs temperature. A 15 ºC smoothing was applied to the thermograms to reduce the high-frequency noise and highlight the broad transitions.

A perpendicular drop method (TA Universal Analysis V4.2E software) was used to estimate the area under the transitions in the ($dQ_{reversing}/dT$) plots. In this method, a straight baseline was chosen over a range of two transition temperatures. The two overlapping transitions were separated by a vertical line that was perpendicular to the baseline at the temperature where the first transition (loosely bound) ended and the second transition (tightly bound) began. The areas under those two transitions were integrated. The T_g of each transition was taken at the peak of the derivative curve. [82]

2.4 Model

A two-state model was previously applied to the thermal analysis of adsorbed polymers.[21] The model will be briefly outlined here. The model was based on loosely bound polymer (with a T_g similar to, but not necessarily equal to that of bulk) and tightly bound polymer (with a T_g higher than that of the loosely bound polymer). A normalized polymer mass, m'_p, was defined as the total mass of adsorbed polymer (from TGA)

divided by the mass of silica used, which is the sum of the masses for the two components, or

$$m'_p = m'_{pA} + m'_{pB} \quad (1)$$

where m'_{pA} is the normalized mass of loosely-bound polymer and m'_{pB} is the normalized mass of tightly-bound polymer.

The ratio of the heat flow changes of components, A (loosely bound) and B (tightly bound), given by r, is related to the ratios of the heat capacities of the components, or:

$$r = \Delta Q_A / \Delta Q_B = m'_{pA} \Delta C_{pA} / (m'_{pB} \Delta C_{pB}) \quad (2)$$

where the ΔQs represent the heat flows and the ΔC_ps represent the changes in heat capacity in the glass transition region.

In effect, the ratio, r, is the ratio of the area under the two transitions in the thermograms. From equations (1) and (2), a linear equation can be made, or

$$\begin{aligned} r &= (m'_p - m'_{pB}) \Delta C_{pA} / (m'_{pB} \Delta C_{pB}) \\ &= [\Delta C_{pA} / (m'_{pB} \Delta C_{pB})] m'_p - \Delta C_{pA} / \Delta C_{pB} \end{aligned} \quad (3)$$

This equation suggests that r should be linear function of m'_p (which is known and related to the adsorbed amount). As noted above, m'p, was defined as the total mass of adsorbed polymer (from TGA), divided by the mass of silica used. Therefore, one can calculate the adsorbed amount of the polymer on the silica from m'_p, based on the specific surface area of the silica.

The bound fraction, f_B, was the ratio of the mass of tightly-bound polymer at the interface to the total amount of polymer. This can be expressed as a function of the experimental observable, r, as

$$f_B = m'_{pB}/m'_p = m_{pB}/m_p = 1/(1+ r\Delta C_{pB}/\Delta C_{pA}) \quad (4)$$

The fraction of bound polymer, f_B, and the ratios of the ΔC_p's can be estimated from the model, using the value of m'_{pB} obtained from the intercept, divided by the slope from the linear regression.

2.5 Results

The bulk T_gs of the three different molecular mass PVAc (260, 170 and 100 kDa) are shown in Figure 2.3 High (260 kDa) and medium (170 kDa) molecular masses have the same T_g for the bulk (43 ºC) region that is slightly higher than T_g of low molecular mass (42 ºC).

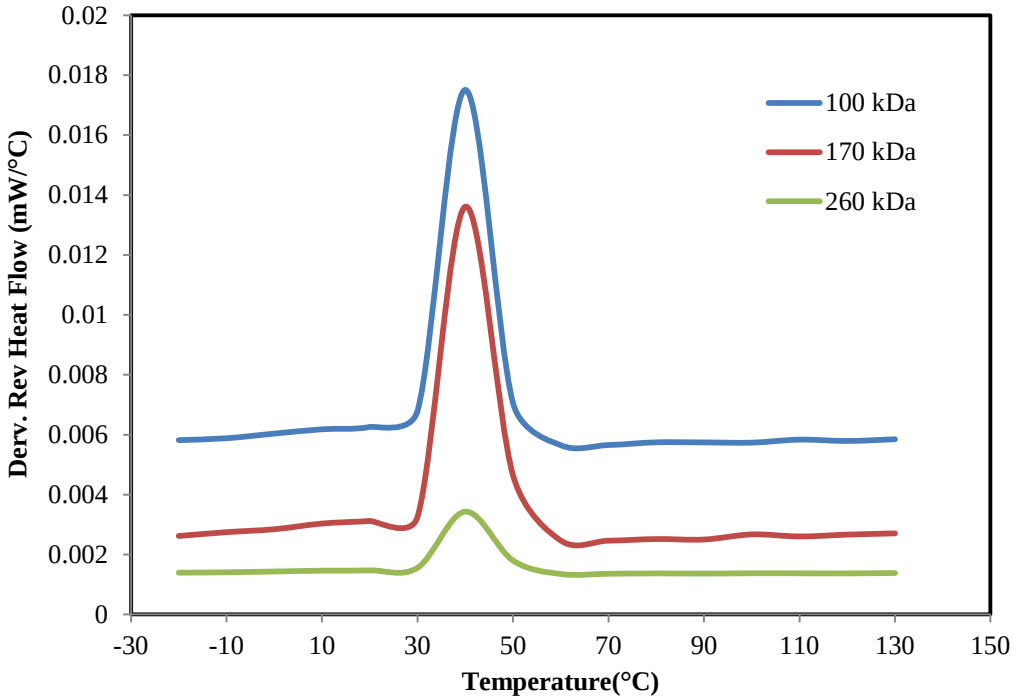

Figure 2.3 TMDSC thermograms of bulk PVAc for three different molecular masses (260 kDa, 170 kDa, and 100 kDa).

The thermograms of the high molecular mass PVAc (260 kDa) adsorbed on silica for different absorbed amounts are shown in Figure 2.4. The vertical scale in the thermograms was shifted to allow comparisons between thermograms. The T_g of the high molecular mass PVAc was about 43.14 ºC for the bulk polymer. The thermograms for the adsorbed polymers showed two distinct peaks, which we refer to as the component A (loosely bound, T_g similar to bulk) and the component B (tightly bound, T_g higher than bulk). As the amounts of adsorbed polymer increased, the area under transition A increased, whereas that of transition B remained roughly constant. For the high molecular mass PVAc, the peak of the transition for the component A was shifted slightly to a

higher temperature than that in the bulk. For 260 kDa, the average glass transition temperature of the peak A (calculated from all adsorbed amounts studied) was 42.81 ± 3.82 ºC (1 S.D.), and that of the component B was about 67.44 ± 11.76 ºC (1 S.D.). The standard deviation (S.D.) was calculated from the T_g of different adsorbed amounts studied. The T_g of the component B was about 24.30 °C higher than that of the bulk polymer.

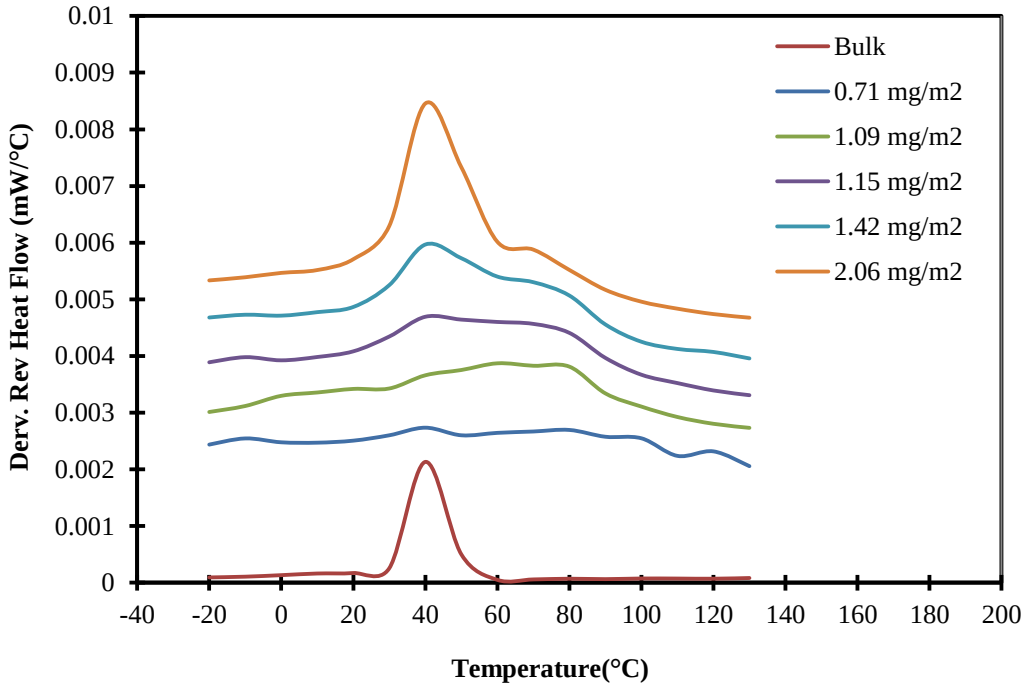

Figure 2.4 TMDSC thermograms of various adsorbed amounts of high molecular mass PVAc (260 kDa) on silica.

The thermograms of different amounts of the medium molecular mass PVAc (170 kDa) adsorbed on silica are shown in Figure 2.5. The bulk T_g for this polymer was about 43.16 ºC. The peak of the transition for the component A increased from that in bulk to 44.30 ± 5.70 ºC (1 S.D.), and the position of the component B was about 62.13 ± 7.56 ºC

(1 S.D.). The T_g for the component B was about 18.97 °C above that for the bulk polymer.

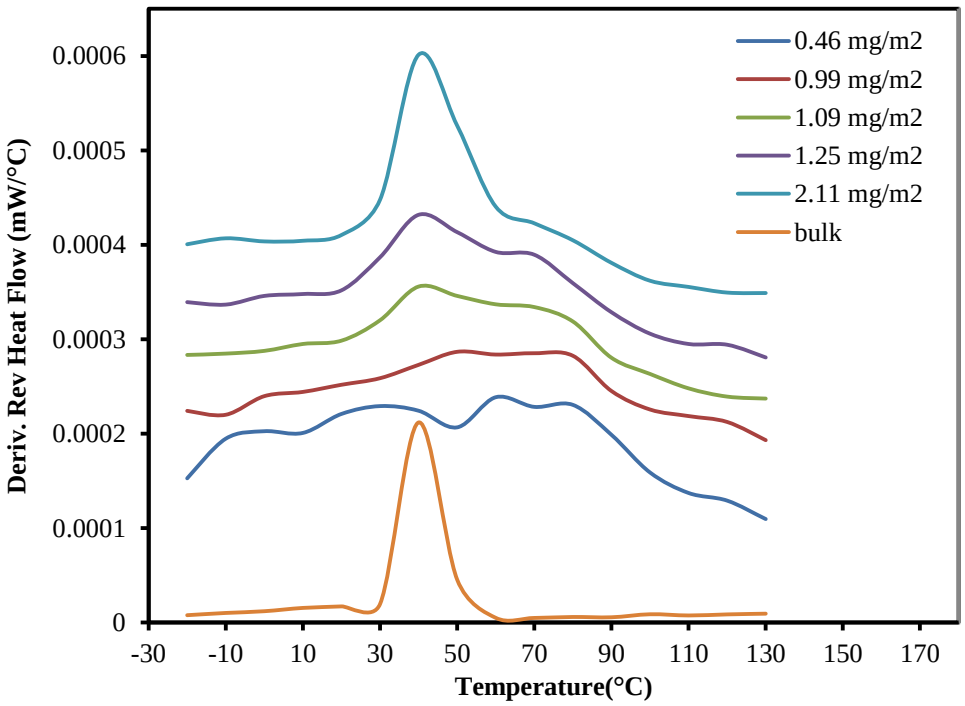

Figure 2.5 TMDSC thermograms of various adsorbed amounts of medium molecular mass PVAc (170 kDa) on silica.

Thermograms of different amounts of low molecular mass PVAc (100 kDa) adsorbed on silica are shown in Figure 2.6. The bulk T_g was about 42.45 ºC. The peak of the transition for the component A increased from that in bulk to 45.66 ± 4.42 ºC (1 S.D.) and the position of the component B was about 66.01 ± 8.48 ºC (1 S.D.). The T_g for the component B was 23.56 °C above that of the bulk polymer. A summary of T_gs for bulk PVAc and absorbed PVAc (including both loosely- and tightly-bound polymers) is shown in Table 2.1.

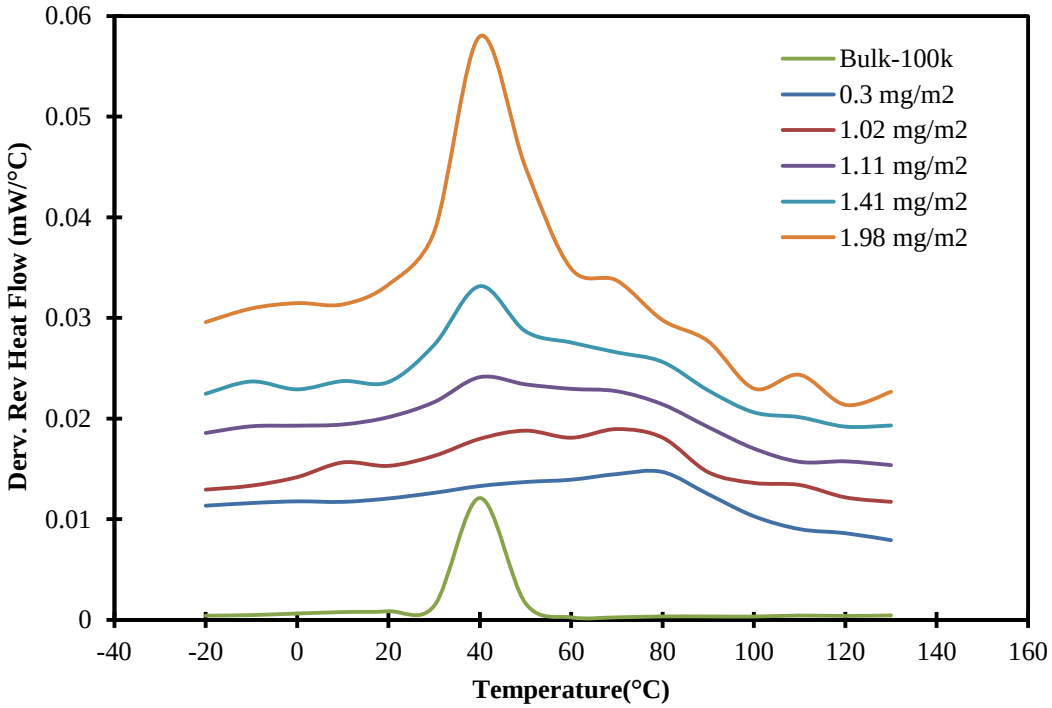

Figure 2.6 TMDSC thermograms of various adsorbed amounts of low molecular mass PVAc (100 kDa) on silica.

Table 2.1 Glass transition temperature (T_g) of different molecular mass PVAc for bulk and surface adsorbed PVAc on silica

Molecular Mass (kDa)	Polydispersity	Bulk T_g (ºC)	Adsorbed T_g (ºC) +/- (1 S.D.[a])	
			Loosely Bound	Tightly Bound
260	3.28	43.14	42.81 ± 3.82	67.44 ± 11.76
170	3.67	43.16	44.30 ± 5.70	62.13 ± 7.56
100	3.69	42.45	45.66 ± 4.42	66.01 ± 8.48

[a] S.D. is the standard deviation from all the different adsorbed amounts for each molecular mass.

As shown in Figure 2.7, a plot of the ratio, r, for the areas of the components of A and B in the derivative thermograms, was a linear function of the total relative mass of polymer (m'_p), or adsorbed amounts (mg polymer/m^2 silica). According to eq. 3, the intercept of the line yields the negative value of the changes in heat capacity ratio, $\Delta C_{pA}/\Delta C_{pB}$, and the slope yields $\Delta C_{pA}/(m'_{pB}\Delta C_{pB})$. The data were linear with positive slopes.

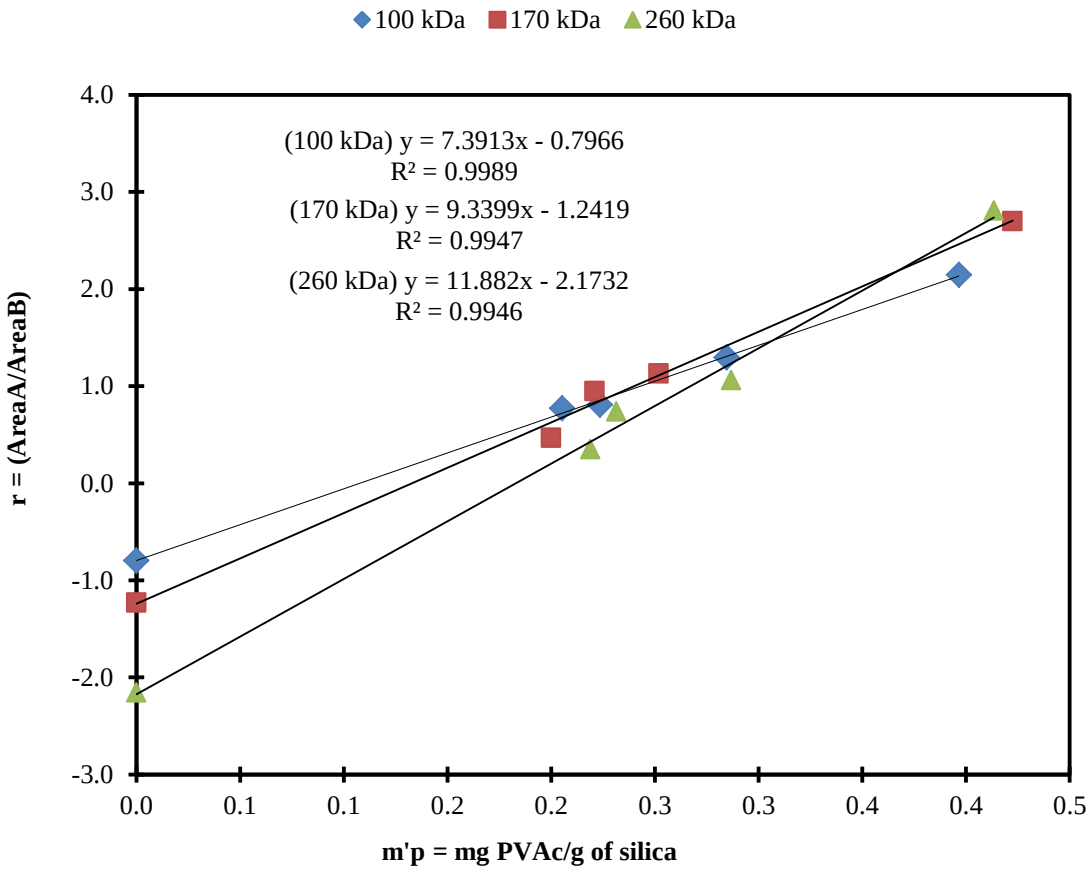

Figure 2.7 The ratio (r) of the areas under the transitions A and B as a function of the adsorbed amounts (mg polymer/m^2 silica) for three different molecular masses of PVAc.

2.6 Discussion

PVAc samples with different molecular masses but same tacticity (260, 170 and 100 kDa) were studied. High (260 kDa) and medium (170 kDa) molecular masses have the almost the same T_g for the bulk (43.14 and 43.16 ºC, respectively) region that is slightly higher than T_g of low molecular mass (42.45 ºC). Low (100 kDa) molecular mass has a higher T_g at bulk-like region (loosely bound polymer) (45 ºC) of the adsorbed

polymers, as compared with that of the medium (170 kDa) and high (260 kDa) molecular mass polymers.

It was also observed that the tightly-bound polymers have a higher T_g than that found in bulk and the loosely-bound region of the same polymer. As mentioned earlier, the adsorbed polymers have more restricted motions than the bulk polymers, which result in shifts to higher T_gs. This effect was pronounced for our systems because of hydrogen bonding between the polymer carbonyls and substrate silanols.[20,21] In addition, a broader range of T_g was also found for adsorbed samples which can be estimated from the width at half height of the transition A and B. The width of the peak at glass transition region for the bulk polymer was approximately about 20 ºC wide, while for the adsorbed polymers, it was 33 ºC wide for the loosely bound polymer, and 43 ºC for the tightly bound polymer. The broadening of the T_gs for adsorbed samples was due to a loss in the cooperative large-amplitude motions. The broadening of the T_g is an important characteristic of a multi-component material, such as an adsorbed polymer.

The amounts of the tightly-bound polymer (M_B) and the corresponding effective thicknesses of three different molecular mass PVAc adsorbed on silica are shown in Table 2. PVAc with a high (260 kDa), and medium (170 kDa) molecular mass , showed a larger amounts of tightly-bound polymer (0.91 and 0.66 mg/ m^2) respectively than that in the 100 kDa (0.53 mg/m^2) polymers. The effective thicknesses corresponding to 0.91, 0.66, and 0.53 mg/m^2 of tightly bound polymer resulted to 9.1 Å, 6.6 and 5.3 Å. The thickness of the tightly bound polymer was calculated using the bulk density of 1.18 g/cm^3 for PVAc. Nevertheless, our current results do correlate well with the thermograms, as shown in Figure 2.3-5. When the amount of tightly bound polymer was greater than the M_B, 0.91 mg/m^2 (260 kDa), 0.66 mg/m^2 (170 kDa) and 0.53 mg/m^2 (100 kDa), a transition for loosely bound region was observed.

Table 2.2 Ratios of heat capacity changes at T_g ($\Delta C_{pA}/\Delta C_{pB}$), tightly bound amount (M_B) and corresponding thickness for PVAcs adsorbed on silica

Molecular mass (kDa)	($\Delta C_{pA}/\Delta C_{pB}$) +/- (1 S.D.)	Tightly bound amount (M_B) mg PVAc/ m^2 silica +/- (1 S.D.[a])	Tightly bound thickness (Å)
260	2.17 +/- 0.61	0.91 +/- 0.31	9.14 +/- 3.11
170	1.24 +/- 0.27	0.66 +/- 0.15	6.64 +/- 1.60
100	0.80 +/- 0.03	0.53 +/- 0.02	5.38 +/- 0.23

[a] 1 S.D. is the standard deviation from the uncertainties in the slope and intercept.

The bound fractions, based on the ratios of the integrals of the different peaks were calculated from Eq. 4 as a function of the amount of adsorbed polymer. Plots of the bound fraction for various adsorbed amounts of polymer in three different molecular mass PVAcs are shown in Figure 2.8. As expected, the bound fraction in all three decreased relatively smoothly when the adsorbed amounts increased. For low molecular mass PVAc (100 kDa), the bound fractions were smaller than those of the high and medium molecular masses.

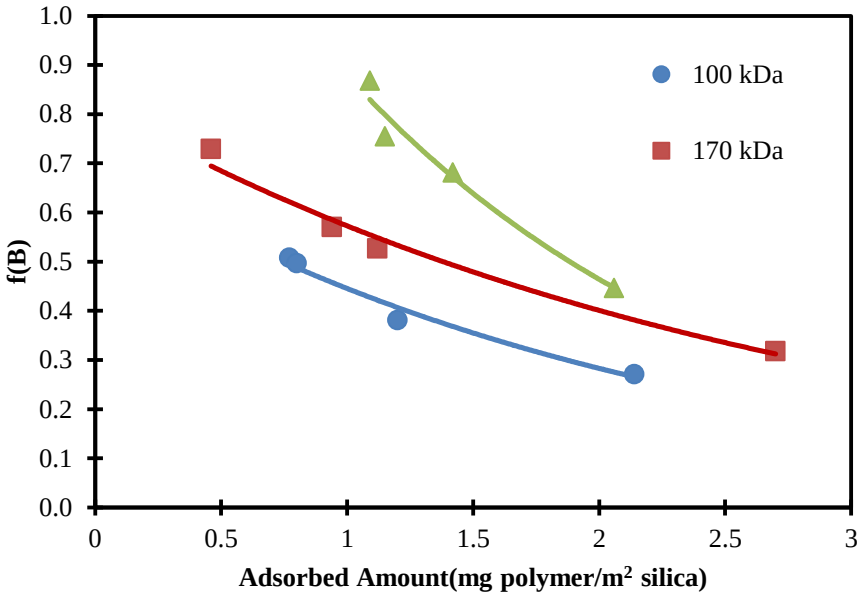

Figure 2.8 Bound fractions of PVAc on silica as a function of adsorbed amount from TMDSC for the 260 (triangles), 170 (squares), and 100 kDa (circles).

The molecular mass effect observed presumably involves the effect of polymer end groups; the low molecular mass polymer has more chain ends compared with those of higher mass. These free chain ends are more mobile and apparently not strongly binding on the surface.[83, 84]

On the basis of the model, the change in heat capacity is related to the molecular motion of polymers adsorbed on the surface. The ratios of heat capacity increments $\Delta C_{pA}/\Delta C_{pB}$ at T_g for the three different molecular masses 260, 170 and 100 kDa were roughly about 2.2, 1.2 and 0.8, respectively. Ratios greater than 1 indicate that the heat capacity is larger above T_g, consistent with more mobility of the polymer segments above that temperature. This suggests that the heat capacity increment at the T_g depends on the molecular mass.

5. Conclusion

TMDSC was used to probe the interaction of adsorbed PVAc on the surface of silica. Using a two-component model, with the assumption that the amount bound polymer would remain roughly constant regardless of the amount of polymer adsorbed, the amount of the tightly bound polymer was determined. According to our data, the amount of tightly bound PVAc for molecular mass of 260 and 170 kDa, respectively, appeared to be about 0.91and 0.66 mg/ m^2. These amounts were larger than those of the lower molecular mass, 100 kDa, which was about 0.53 mg/m^2. These amounts of tightly bound polymer corresponded to thicknesses of 9.1 Å, 6.6 and 4.0 Å, respectively. The relative mobility between loosely bound and tightly bound polymer was also seen from the ratios of heat capacity increments of $\Delta C_{pA}/\Delta C_{pB}$ at T_g, which were roughly about 2.2, 1.2 and 0.8 for all three different molecular masses of 260, 170 and 100 kDa, respectively. At the T_g, the loosely bound polymer seemed to be somewhat more mobile than the tightly bound polymer of the high and medium molecular masses. For the low molecular mass PVAc, the mobility changes at the T_g, of the loosely-bound and tightly-bound polymers was roughly the same probably due to the effect of the mobile chain ends.

CHAPTER III

PELLETS AND POWDERS OF MESOPOROUS SILICA FUNCTIONALIZED WITH TRIMETHYLCHLOROSILANE (TMCS) and ALKOXYSILANE GROUPS

3.1 Introduction

Mesoporous silica like MCM-41, due to its high surface area and large pores, has been a very promising candidate as catalysts, catalyst support, sensors, adsorption/separation, environmental pollution control, and stationary phases for different kind of chromatography.[49-58] Since the discovery of MCM-41 type materials, numerous studies on their synthesis and surface modifications in order to improve the bulk properties in various applications have been studied extensively.[85-88] Moreover, spherical mesoporous MCM-41 silica materials of tunable pore size provide a homogenous filling for chromatographic columns and are therefore superior in chromatographic applications.[49]

The idea of combining the properties of organic and inorganic building blocks within a single material is very interesting and attractive from the viewpoint of material scientists. The combination of organic and inorganic components can lead to materials with properties that are different from those of the individual components. For preparing inorganic-organic hybrid materials, surface modification of MCM-41 via silylation (using different silylating agents) has been carried out and this has been reviewed in by Wright and Davis.[89] There have been studies on the reaction of MCM-41 with

trimethylchlorosilanes to probe the surface hydroxyl groups of MCM-41 and also to study the reactivity of various silanol groups in the silylation reaction with trimethyl chlorosilane.[90,91] The molecular lengths of the silylating reagents play an important role in surface coverage. Due to steric hindrance, longer chains are assumed to bind primarily on the outer surface of the mesopores. Yasmin and Miller have studied the structural and surface properties of MCM-41 before and after surface modifications with alkyl silanes of different chain lengths.[61] Their main goal was to make new materials with improved HPLC performance by combining the pseudomorphic transformation route for synthesizing MCM-41 and surface modification. They found trifunctional silanes provide higher surface coverage because of their higher reactivity and higher cross-linking possibilities. They also found higher coverage is found for alkylsilanes with shorter chains because of their binding to the interior as well exterior of the mesopores. However they used alkyl silanes of only two different chain lengths, i.e., butyl and octyl silanes.

In this research we have synthesized mesoporous silica (OSU-6) with enhanced thermal and hydrothermal stabilities following the method described by Alothman and Apblett[60] and studied the structural and surface properties before and after surface modification with chlorine-based silylating agent and alkylsilanes of different alkyl chain lengths and functionalities ($CH_3(CH_2)_nSiR_3$, with n = 1,3,5,7; R =OCH_3, OEt). This work was performed by Materer and co-workers. Modification of the mesoporous surface with alkyl chains provides additional physical or chemical properties to the silica parent material e.g. increase the surface hydrophobicity, passivate the silanol groups to protect the framework against hydrolysis. The pore diameter can be progressively decreased by using alkyl chains of different lengths and functionalities.[61]

The attached functionalized species will react with the moisture and will produce silanol functional groups. This can lead to problems in the storage of functionalized

materials. The effect of moisture on the functionalized mesoporous silica has been studied earlier.[92,93] Although in certain cases when the amine containing adsorbents in mesoporous silica is used for CO_2 removal, the presence of moisture could be enhancing the CO_2 uptake,[94] there are cases where it could affect the efficiency of the functionalized material. Ken *et al*[92] noticed that the moisture can suppress the amorphization capacity of naphthalene but also can reverse an already-amorphized formulation in a drug delivery system. In this paper, we also studied the effect of moisture on functionalized silica for OSU-6 pellets functionalized with trimethylchlorosilanes; activated OSU-6 pellet functionalized with ethyltrimethoxysilane and activated OSU-6 pellet functionalized with hexyltrimethoxysilane.

The products were characterized using solid-state ^{13}C and ^{29}Si MAS NMR spectroscopy, total internal reflection infrared Fourier transform (TRIFT) spectroscopy, thermogravimetric analysis (TGA) and direct injection mass spectroscopy.

3.2 Material and Methods

3.2.1. Materials

The chemicals used in this work included: Tetraethylorthosilicate, 98% [TEOS, Aldrich] as the silica sources, 1-hexadecylamine, 90% [HDA,Aldrich] as the surfactant template and 1,3,5-trimethylbenzene 98% [mesitylene , TCI] as the organic additive during the mesoporous silica preparation. Other chemicals included are absolute ethyl alcohol [Pharmco, USA], isopropyl alcohol [HPLC-UV Grade, Pharmco, USA], hydrochloric acid [ACS reagent grade, Pharmco, USA], toluene 99.8% [HPLC grade], triethylamine (TEA) [reagent grade, Fisher Scientific] and acetone [HPLC-UV Grade, Pharmco, USA]. Functionalization agents were: trimethylsilylchloride [Aldrich],

ethyltrimethoxysilane [Aldrich], n-butyltrimethoxysilane [Gelest, INC.], hexyltrimethoxysilane [Gelest, INC.], n-octyltriethoxysilane [Gelest, INC.] Water was purified by reverse osmosis and deionization before use.

3.2.2 Synthesis of Modified Mesoporous Silica OSU-6

The modified mesoporous silica (here after referred as OSU-6) was synthesized following the reported literature procedure by Tuel and Gontier[95] with several alterations made by Al-Othman and Apblett.[60] A templating solution was prepared by dissolving 16 g of the neutral surfactant HDA in 65 ml of distilled H_2O at room temperature and sonicated until a foamy, uniform mixture persisted. HCl (1.0 M) was added to the first mixture until the pH of the mixture was approximately 4.5. A second solution was prepared by mixing 32.0 g of TEOS, 28 mL of ethanol, and 6 mL of isopropanol in a 250 mL closed Erlenmeyer flask under magnetic stirring at room temperature for about 30 minutes. This solution was then added to the reaction flask under mechanical stirring. After 5 minutes, 9.0 mL of mesitylene was added in the solution under stirring and the mixture was left stirring at room temperature for 25 minutes. Then the contents in the reaction flask were transferred to a 500 mL Erlenmeyer flask and then added 100 mL of water. The reaction mixture was mixed thoroughly by swirling and left to age for 7 days at room temperature. The resulting solid was recovered by filtration, washed with distilled water and ethanol (three times each with 30 mL) using a fine filter funnel, and was dried at room temperature for 48 h.

To removal of the organic template two different methods, calcination and extraction have been tried. The removal of the organic template was performed by calcination of the solid in the crucibles at 550 °C and 750 °C under air in an oven for 12 hours. The yield of OSU-6 was 9 g (~98%).

The removal of the organic template was performed by extraction with a hydrochloric acid/ethanol mixture. In the this process, 1.0 g of OSU-6 was washed five times with 50 mL of a hot solution of HCl–ethanol in order to remove the organic components.

As TGA results showed that weight loss of calcined OSU-6 was less than extracted OSU-6. (Figure 3.1)

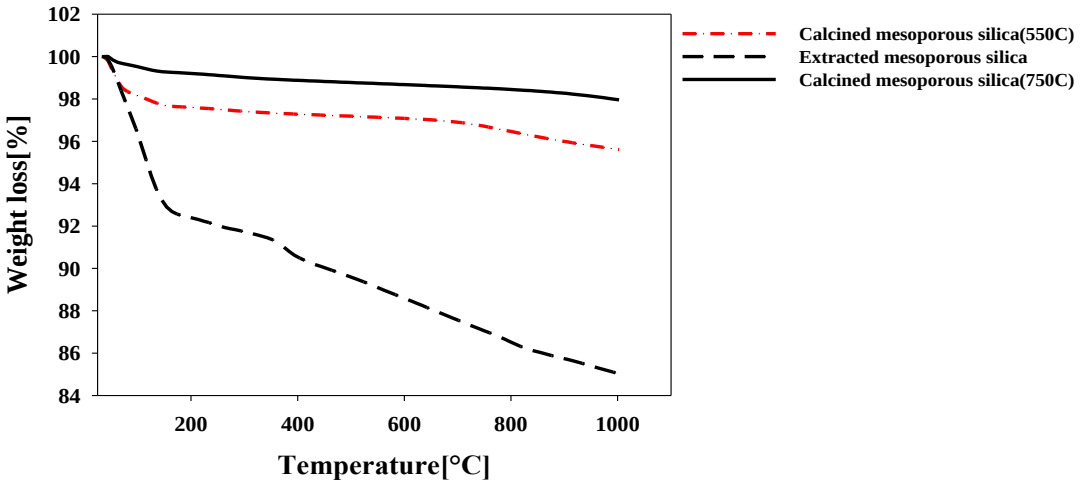

Figure 3.1 TGA curve of (-·-) Calcined mesoporous silica (550°C), (--) Extracted mesoporous silica, (−) Calcined mesoporous silica (750 °C) in nitrogen atmosphere from 25°C to 1000 °C at 10 °C/min

Figure 3.2 shows ^{13}C-NMR spectra of the calcined mesoporous silica. No carbon peak was observed for calcined OSU-6, indicating the complete removal of the organic surfactant template by calcination.

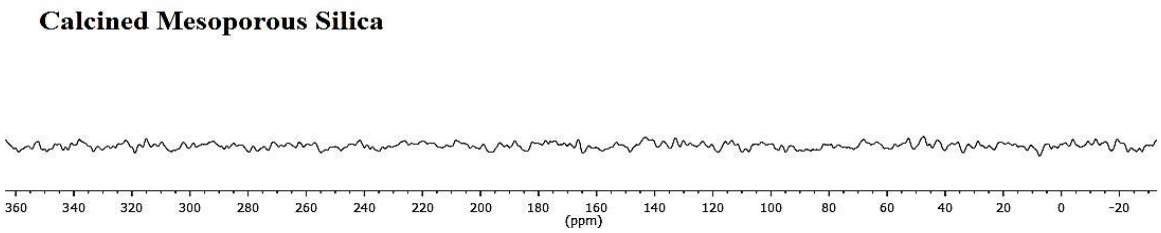

Figure 3.2 ^{13}C NMR CP/MAS Spectra of the calcined mesoporous silica

For special applications where a pellet form of mesoporous silica/activated mesoporous silica is needed, the powder will be subsequently pressed into pellets. For making each pellet, 0.200 g of the powder was pressed into 13 mm disks with clamping force of 2 tons pressure for 90 seconds using a Carver manual bench top standard unheated press. The clamping force of 2 tons was found to be the optimum to make the pellet without affecting the surface area.

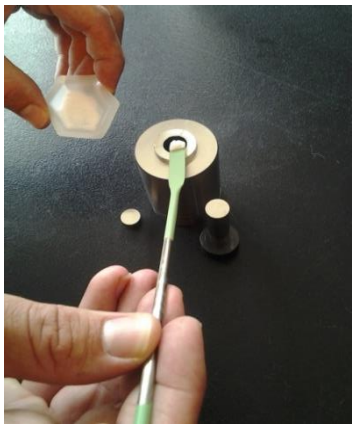

Figure 3.3 Pressing pellets of mesoporous silica

3.3 Functionalization of OSU-6

3.3.1 Functionalization of OSU-6 by trimethylchlorosilane

Any remaining organic template in the OSU-6 was removed by calcination at 550°C in air inside an oven for 12 hours before functionalization. In order to functionalize the OSU-6, first trimethylchlorosilane (TMCS) precursor was tried. A mixture of 0.56 g of OSU-6 and 0.7 mL of trimethylchlorosilane was refluxed at 70 °C for 4 hours in 14 mL of toluene under N_2. The resulting solid was then filtered, washed with toluene and then with acetone and dried overnight at 60 °C in oven. (Figure 3.4)

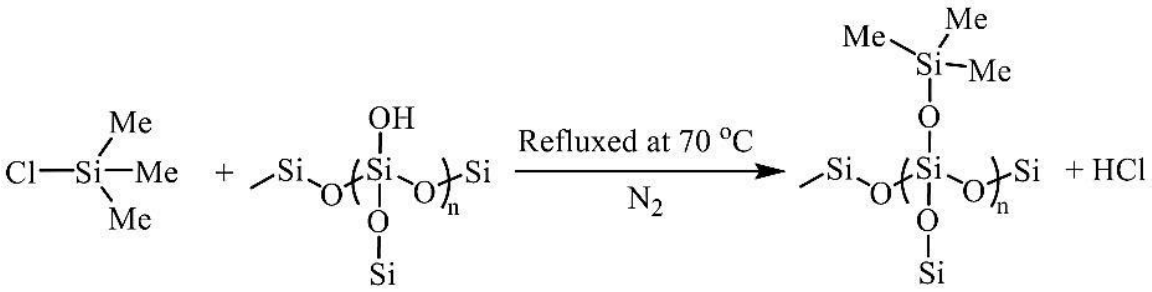

Figure 3.4 Functionalization of mesoporous silica with trimethylchlorosilane

For functionalizing OSU-6 pellets, following the similar procedure mentioned above for the powder, the OSU-6 pellets were refluxed with TMCS in toluene solution for the same time and temperature and then the TMCS and toluene solution was syringed out under N_2 instead of filtration. The pellets were then stirred with toluene followed by acetone. The toluene and acetone were syringed out under N_2 flow each time. Finally the pellets were dried overnight at 60 °C in oven.

3.3.2 Functionalization of OSU-6 by Alkylsilanes

The OSU-6 material was activated by refluxing 5.0 g of the mesoporous silica in 50 ml of dry toluene for 4 hours under a dry atmosphere, followed by washing with 50 mL dry toluene, and drying at 80 °C under vacuum. Next, the dried material was then reacted with a stirred solution of 10 mL of triethylamine in 50 mL of dry toluene and stirred for approximately 1 hour at room temperature. The resulting material was isolated by filtration with a medium filter funnel and was washed with dry toluene (3 x 25 mL) and dried again at 80°C under vacuum.[96] (Figure 3.5)

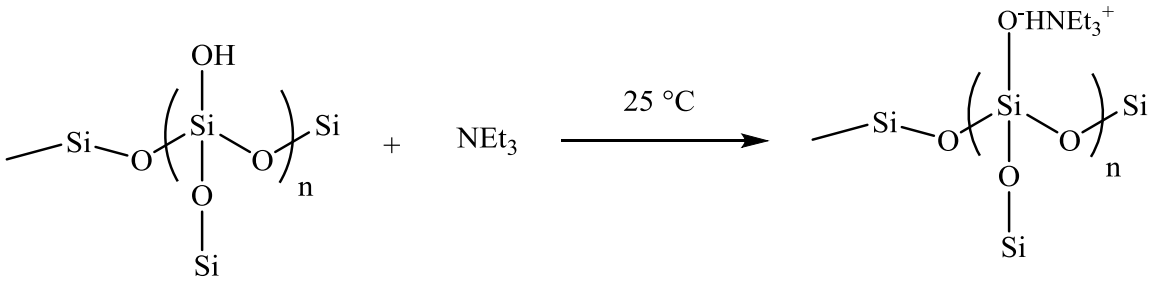

Figure 3.5 Activation of mesoporous silica

Triethylamine activated OSU-6 was than functionalized with the silylation agents namely, ethyltrimethoxysilane, n-butyltrimethoxysilane , hexyltrimethoxysilane, and n-octyltriethoxysilane. Functionalized activated OSU-6 was prepared by refluxing 1.0 g (~16.64 mmol) of the activated OSU-6 that has been outgassed at 150 °C, with 22.3 mmol of the silylation agent in 50 mL of toluene in a 250 mL round-bottomed flask for 4 hours at 110 °C under N_2. The resulting solid mixture was filtered off with a fine filter funnel, washed with toluene and then with ethanol (3×50 ml). The filtered powder was dried in oven at 60°C overnight. (Figure 3.6)

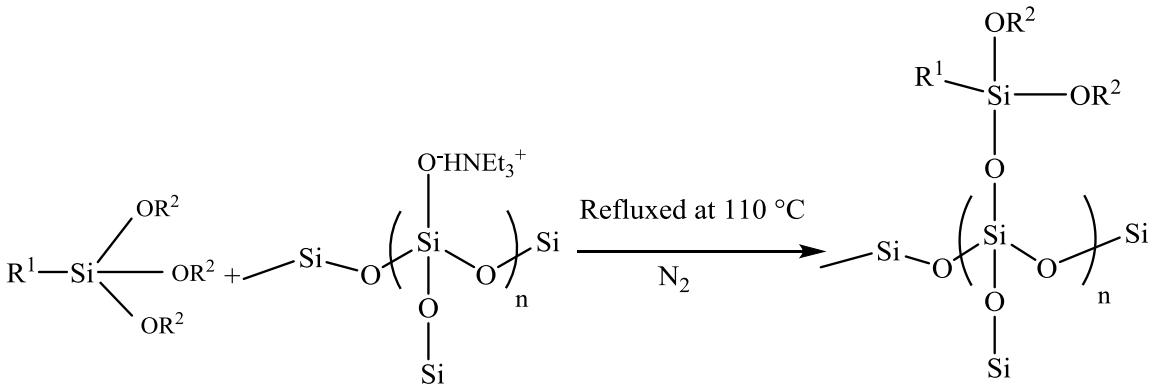

R^1: Ethyl, Butyl, Hexyl, Octyl

R^2: Methyl or Ethyl

Figure 3.6 Functionalization of mesoporous silica with alkoxylsilanes

The pellets of activated OSU-6 were functionalized as mentioned above. Instead of filtering the solution, the solution was syringed out under N_2 flow each time. The pellets were then dried in oven at 60 °C overnight.

3.4 Characterization

3.4.1 Characterization of the OSU-6 and Functionalized OSU-6

There are a wide variety of techniques available for the characterization of mesoporous silicas. Two of the most widely used spectroscopic techniques which have been used to characterize the silica surface and adsorbed species are vibrational spectroscopy and solid-state NMR spectroscopy. Vibrational spectroscopy can provide detailed information regarding hydrogen bonding, physical adsorption and chemisorption but it cannot give a quantitative measure of the number of adsorbed species of various

types without cumbersome calibrations to determine extinction coefficients which themselves can vary according to surface coverage. NMR can provide quantitative data relative to the absolute numbers of adsorbed species and it can provide information relative to the motional freedom of these species. Both methods yield qualitative data relative to the structure of adsorbed species, via the well-known group frequency concept in vibrational spectroscopy, and chemical shift data in NMR. This can be used to determine the nature of the functional groups present either on the surface of silica itself, or in adsorbed species. Although IR spectroscopy is admirably able to distinguish between hydrogen-bonded and free silanols, it is not able to differentiate between single and geminal hydroxyls; but NMR can make this distinction and this aspect will be discussed later in this chapter.

^{29}Si NMR was introduced as an important surface-chemical technique by the classic paper of Maciel and Sindorf[97] ^{29}Si NMR spectroscopy was employed for the determination of the surface species, amount of alkyl chain attachment. (Fig 3.7) Several signals are typically observed in the ^{29}Si NMR spectra which correspond to silicon atoms in different chemical environments. ^{29}Si CP/MAS NMR spectra of silicate show distinct resonances for siloxane [Q^n = $Si(OSi)_n(OH)_{4-n}$, n = 2–4] and organosiloxane [T^m = $RSi(OSi)_m(OH)_{3-m}$, m = 1–3] centers, such as siloxane Q^4 [(≡Si-O-)$_4$Si*] (*ca.* -110 ppm), single silanol Q^3 [(≡Si-O-)$_3$Si*-OH] (*ca.* -100 ppm), geminal silanol Q^2 [(≡Si-O-)$_2$Si*(-OH)$_2$] (*ca.* -90 ppm) or silicon from attached alkylsilane ligands – M [(≡Si-O)Si*(R)R'$_2$].

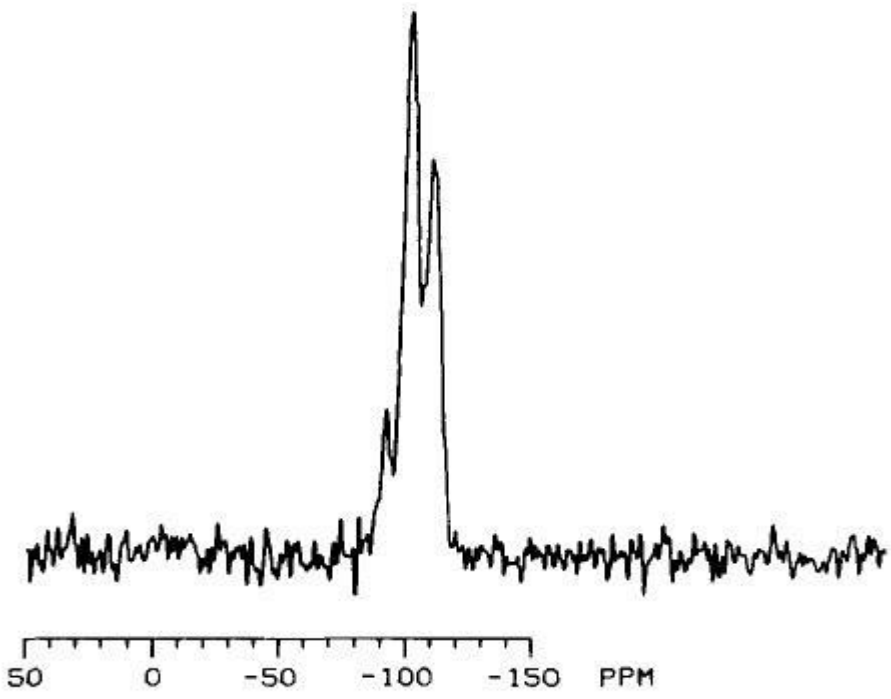

Figure 3.7 ^{29}Si CP/MAS spectrum of silica gel. Adapted from reference 98

^{13}C NMR spectroscopy was used to study the organic components after attaching alkylsilanes to the OSU-6 silica surface. At the beginning of the 1990s the thermogravimetric (TGA) technique was applied for investigation of thermal desorption of liquids from porous materials.[99] This technique is nondestructive and can provide details of the porous structure.

Solid-state ^{13}C and ^{29}Si nuclear magnetic resonance (NMR) were used for the characterization of the synthesized ordered mesoporous materials. Solid-state ^{13}C CP/MAS NMR spectra were obtained with a Chemagnetics CMX-II solid-state NMR spectrometer operating at 75.694 MHz for carbon-13, with a Chemagnetics 5 mm double resonance magic-angle spinning probe. ^{13}C cross polarization/magic-angle spinning

(CP/MAS) was carried out with a quasi-adiabatic ramped CP sequence[100] using two pulse phase modulation (TPPM) decoupling[101] at 55.6 kHz. Samples were packed in 5.0 mm zirconia rotors and spun at 6.0 kHz, maintained to within a range of ±5.0 Hz or less with a Chemagnetics speed controller. Spectra were collected with 18000 scans, using a 3.0 s pulse delay, a 5.0 ms contact time, and a 4.5 µs proton 90-degree pulse width. The ^{13}C CP contact pulse length was divided into 11 steps of equal length with ascending field strength, while the ^{1}H contact pulse had constant radiofrequency field strength. Solid-state ^{29}Si nuclear magnetic resonance (NMR) spectra were recorded with the same spectrometer and probe, operating at 59.800 MHz for the ^{29}Si nucleus, using the same pulse sequence given above. The ^{29}Si CP/MAS spectra were acquired with 6 kHz spinning speed, 5.0 s pulse delay, 17.0 ms contact time, 7.0 µs proton 90-degree pulse width, 35.7 kHz proton decoupling, and 2000 scans. Chemical shifts are given in ppm from external tetramethylsilane (0 ppm) for both ^{13}C and ^{29}Si. The total internal reflection infrared Fourier transform spectra were recorded on a Nicolet Magna nexus 670 FT-IR. The spectra were collected for all samples in the range from 400 to 4000 cm^{-1}. The samples were finely ground and a pinch of sample was placed on a germanium cell and IR spectra of the powders were taken. Thermal stability of the samples was measured by using STAR^{e} system TGA/DSC 1 Mettler Toledo under nitrogen flow (20 ml/min) with heating rate 10 °C/min from room temperature to 1000 °C. The hydrolysis study was carried out by analyzing the silanol peak (*m/z*=75) using a direct injection mass spectrometer HP 5989B where the sample holder was modified to handle solid samples.

3.5 Results and Discussion

The OSU-6, activated OSU-6 and the functionalized OSU-6 (using TMCS and alkylsilanes) in the powder form were characterized by NMR, FT-IR and TGA. The pellet form of the functionalized pellets was characterized by FT-IR and TGA to identify

the presence of the functional groups. Results for the alkyl silanes functionalized pellets only are presented. The pellets were crushed into powders for characterization.

3.5.1 Trimethylchlorosilane Reagents

3.5.1.1 Solid-State ^{29}Si CP/MAS NMR Spectroscopy

Solid-state ^{29}Si NMR measurements were performed in order to determine the surface structure of OSU-6 after modification.[96] The solid-state ^{29}Si NMR spectra of the mesoporous materials before and after silylation are shown in Figure 3.8 and the corresponding ^{29}Si chemical shifts are reported in table 3.1.

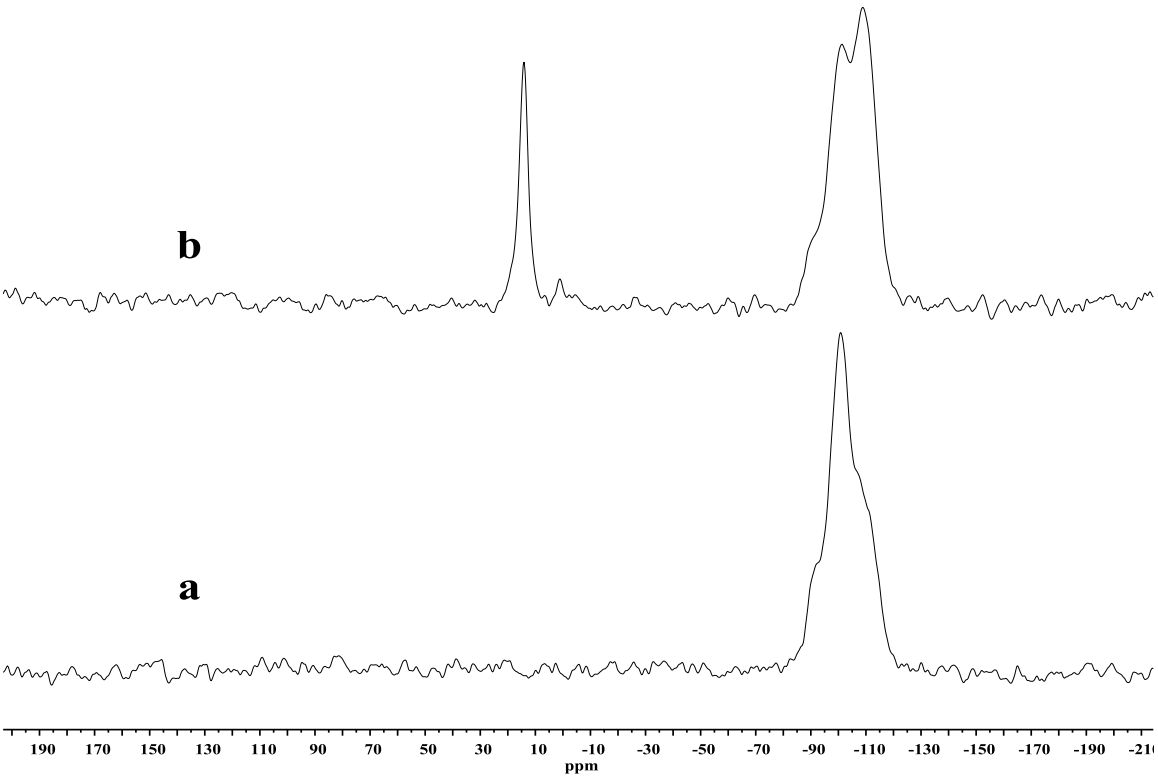

Figure 3.8 Solid-state ^{29}Si NMR CP/MAS spectra of the OSU-6 a) before and after functionalization

The OSU-6 calcined at 550 °C shows three ^{29}Si CP/MAS NMR peaks at ⁻110.3 and ⁻100.7 and -90.7 ppm which are related to the Q^4 , Q^3 , and shoulder Q^2 species (Q^n =

Table 3.1 ^{29}Si chemical shifts for OSU-6 materials before and after surface modification.

OSU-6 Sample	**Q^2 (ppm)**	**Q^3 (ppm)**	**Q^4 (ppm)**	**M (ppm)**
OSU-6	-90.7	⁻100.7	⁻110.3	
Functionalized with TMCS	-91.0	⁻100.3	⁻109.7	14.3

$Si(OSi)_n(OH)_{4-n}$, with n = 1–4)[61] while, after silylation with TMCS, shows three ^{29}Si CP/MAS NMR peaks at ⁻109.7 and ⁻100.3 and -91.0 ppm (Q^4, Q^3 and Q^2 environments) and one peak at 14.3 ppm M $(SiO)_3$*$Si(CH_3)_3$ [91] environments. R here represents the alkyl group belonging to TMCS. Zhao *et al* have observed in the solid-state ^{29}Si NMR spectra of trimethylchlorosilane treated MCM-41 sample a peak at 14 ppm besides the 3 peaks at -110, -101 and -92 ppm i.e., Q^4, Q^3 and Q^2 sites and attributed the peak at 14 ppm to the silicon atoms of the attached *Si $(CH_3)_3$ moiety.[91]

3.5.1.2 Solid-State ^{13}C CP/MAS NMR Spectroscopy

Solid state ^{13}C NMR spectra can enrich information about the attachment of the pendant groups.[102-103] Figure 3.9 shows ^{13}C-NMR spectra of the OSU-6 before and after functionalization.

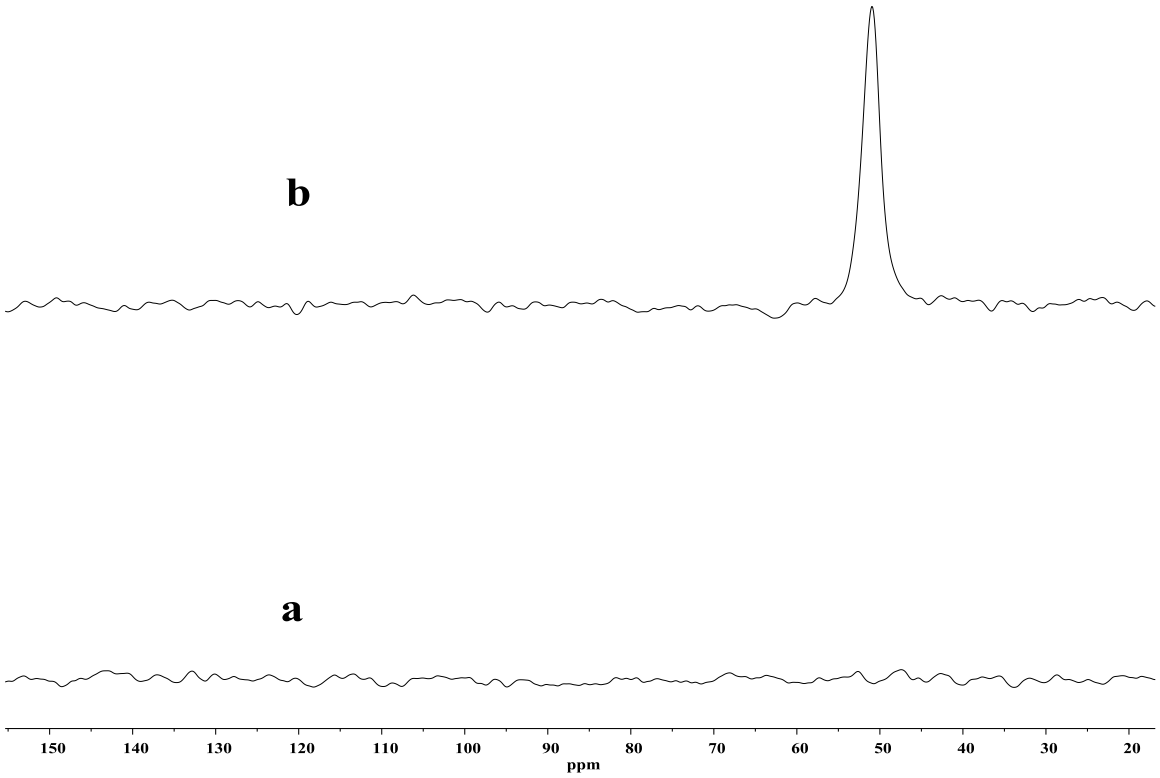

Figure 3.9 Solid-state ^{13}C NMR CP/MAS spectra of the OSU-6 a) before and b) after functionalization.

No carbon peak was observed for calcined OSU-6, indicating the complete removal of the organic surfactant template by calcination. Only a single sharp peak observed at 50.9 ppm in the spectrum of OSU-6 functionalized with TMCS corresponds the methyl group carbons in TMCS that is anchored on the silica surface of functionalized-OSU-6.[104, 105] The existence of one peak indicates that the local environment of the methyl carbons of TMCS is the same. The result of the ^{13}C CP/MAS NMR study has proved that trimethylsilyl groups have been successfully grafted onto the functionalized-OSU-6.[106] The ^{13}C chemical shifts are reported in Table 3.2.

Table 3.2 ^{13}C chemical shifts and assignment of surface modified OSU-6 materials.

OSU-6 Samples	**Carbon position**	**^{13}C shift (ppm)**
OSU-6	no carbon peak was observed for calcined OSU-6	-
Functionalized with TMCS	carbon of the methyl groups that anchored on the silica surface	50.9

3.5.1.3 Fourier Transform Infrared Spectroscopy (FT-IR)

The FTIR spectra of OSU-6 before and after silylation with Trimethylchlorosilane (TMCS) are illustrated in Figure 3.10. The symmetric stretching vibrations of Si-O at 806 cm^{-1} and asymmetric stretching vibration of the Si-O-Si band at around 1080 cm^{-1} are seen for both OSU-6 and functionalized OSU-6. The Si-O stretching of the surface silanols at around 960 cm^{-1} seen for OSU-6 almost vanished for functionalized OSU-6. The stretching mode of H_2O at 1608 and 1582 cm^{-1} is seen both for OSU-6 and functionalized OSU-6 (also seen in the TGA results). The stretching mode characteristics of Si-C stretching vibrations seen at 846 cm^{-1} and 757 cm^{-1} in the functionalized OSU-6 indicates the presence of methyl groups. The broad band around 3500 cm^{-1} corresponds to a hydrogen-bonded silanol group that perturbed by physically adsorbed water is seen for both the samples. The peak at 2966 cm^{-1} in functionalized OSU-6 corresponds to stretching band in the methylated OSU-6. This peak also appears in OSU-6 but it has less intensity.[106-107]

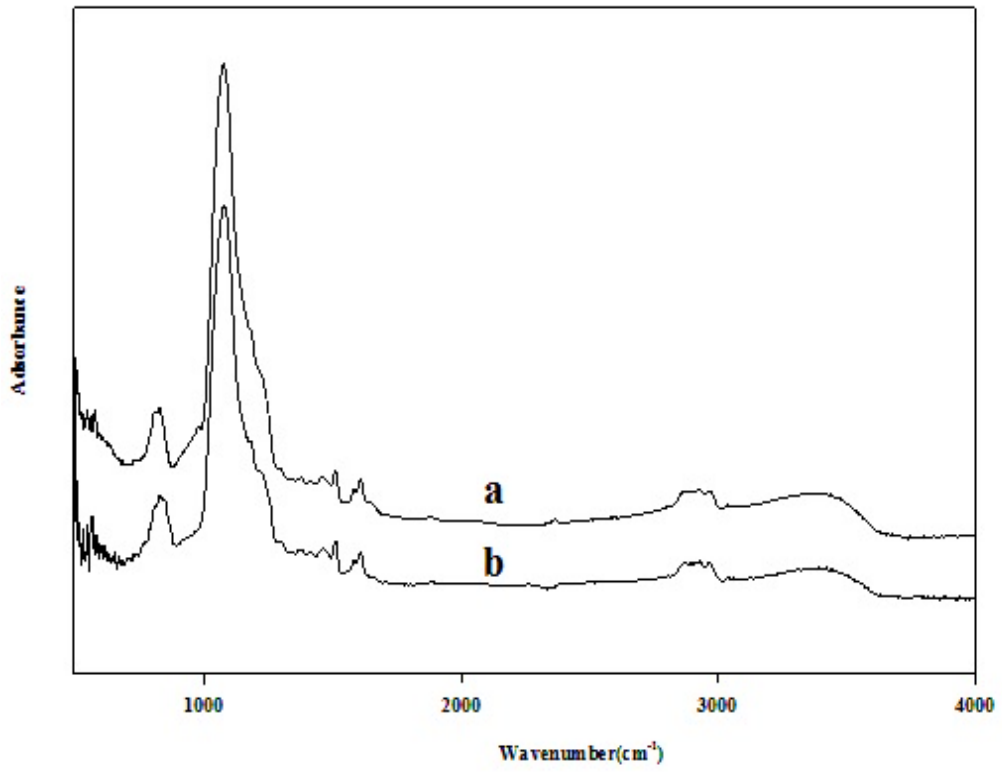

Figure 3.10 FTIR spectra of OSU-6 samples a) before and b) after functionalization

3.5.1.4 Thermogravimetric Analysis (TGA)

Figure 3.11 (a) shows the TGA profiles of the OSU-6 in nitrogen atmosphere showing three stages of weight loss. The first weight loss was observed at 46-186 ℃ about 2.14 % due to desorption of physisorbed water on the external surface of OSU-6.[108-109]

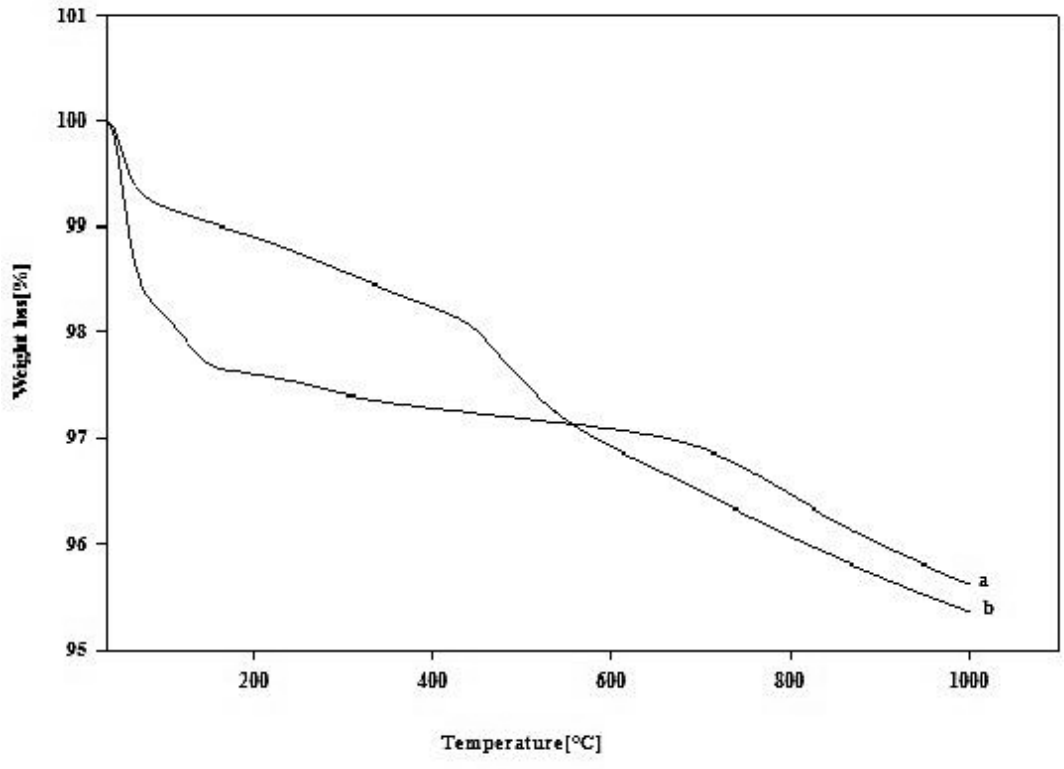

Figure 3.11 TGA curve of: (a) OSU-6; (b) OSU-6 functionalized with TMCS in nitrogen atmosphere from 25 °C to 1000 °C at 10 °C/min

Meanwhile, in the range of 186-640 °C a weight loss of about 0.59 % is attributed to the decomposition or removal of organic moieties.[110] In the temperature range 640-1000 °C the weight loss is due to residual surfactant decomposition and water loss from the condensation of adjacent silanol groups to form siloxane bonds and is about 1.42%. The total weight loss up to 1000s°C of this sample is 4.15%. Figure 3.11 (b) shows the TGA profiles of silylated OSU-6 which shows weight loss at 45-173 °C about 0.91% due to loss of physisorbed water molecules. The very gradual degradation rate observed at

temperatures over the range between 175 and 400 °C corresponds to hydroxyl dehydration and weight loss is about 0.73%. Meanwhile, further decomposition was observed after 400 °C due to the thermal dehydroxylation of internal un-functionalized surface silanol groups to form siloxane bridges and decomposition of attached TMCS groups and is about 2.89 %.

3.5.2. Alkylsilane Reagents

The solid samples were identified by solid-state ^{29}Si CP/MAS NMR spectroscopy, solid-state ^{13}C CP/MAS NMR spectroscopy, total reflectance infrared Fourier transform (TRIFT) spectroscopy and thermogravimetric analysis (TGA).

3.5.2.1 Solid-State ^{29}Si CP/MAS NMR Spectroscopy

Figure 3.12 shows ^{29}Si CP/MAS NMR spectra of activated OSU-6 and functionalized activated OSU-6. For the functionalized activated OSU-6 the peaks Q^2, Q^3, Q^4, T^1, and T^2 (T^n = $RSi(OSi)_n(OH)_{3-n}$, n = 1–3) [61] are present at around -94, -102, -112, -49 and -57 ppm.[111] The ^{29}Si chemical shifts are reported in Table 3.3.

Table 3.3 ^{29}Si chemical shifts for activated OSU-6 materials before and after surface modification.

OSU-6 Samples	**Q^2 (ppm)[111]**	**Q^3 (ppm)**	**Q^4 (ppm)**	**T^1 (ppm)**	**T^2 (ppm)**
Activated OSU-6	-94.2	-102.5	-112.0		
Functionalized with ethyltrimethoxysilane	-94.59	-102.6	-111.56	-49.78	-57.20
Functionalized with n-butyltrimethoxysilane [61]	-94.31	-102.23	-110.84	-49.45	-58.04
Functionalized with hexyltrimethoxysilane	-95.11	-103.43	-112.19	-50..55	-58.54
Functionalized with n-octyltriethoxysilane [61]	-94.42	-103.12	-111.96	-51.98	

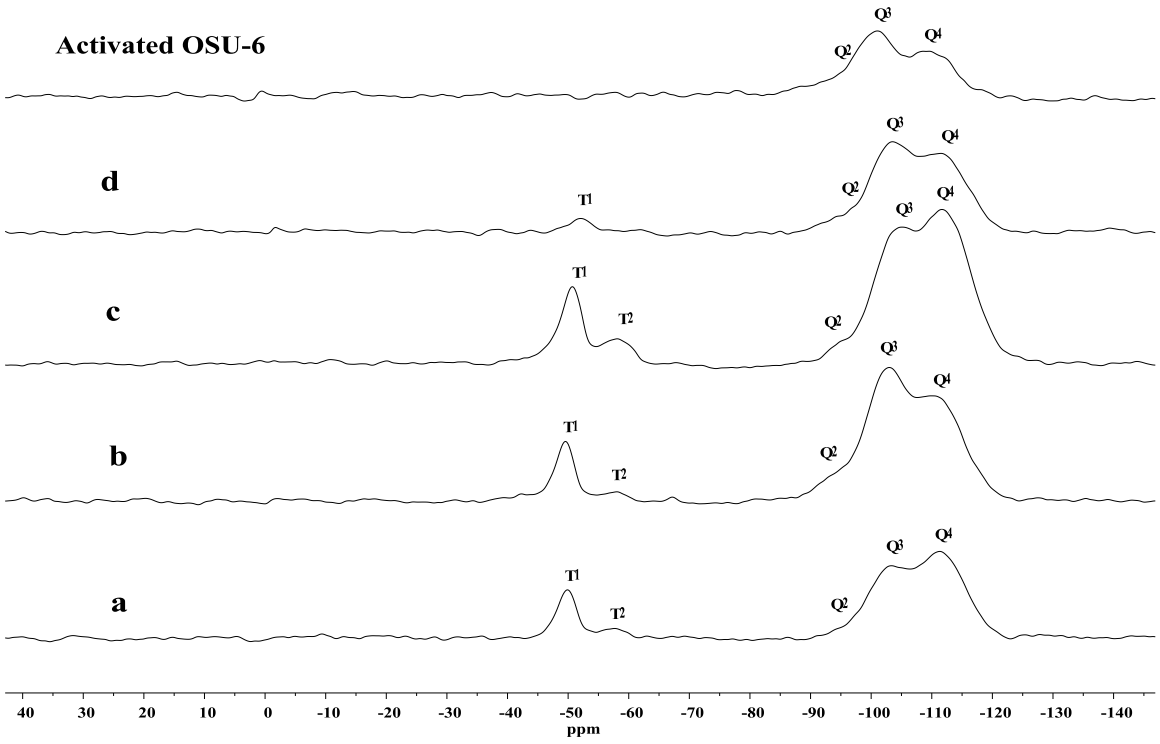

Figure 3.12 Solid-state ^{29}Si NMR CP/MAS spectra of the activated OSU-6 and functionalized activated OSU-6 a) ethyltrimethoxysilane b) n-butyltrimethoxysilane c) hexyltrimethoxysilane d) n-octyltriethoxysilane

Yasmin and Muller have observed the presence of T^1, T^2 and T^3 peaks at about -49 ppm, -57 ppm and -66 ppm for the MCM-41 samples treated with trifunctional alkylsilanes and attributed them to the attachment and cross-linking of the chains at the MCM-41 silica surface.[61] We do not see T^3 but T^1 and T^2 are present and that proves the attachment of silyl chains and cross-linking of these chains (although partial). Also the increase in intensity of both the peaks from ethyl to hexyl indicates the increase in the attachments of the chains. For octyl samples the peaks are very weak or absent.

Yasmin and Muller also observed that after the attachment of the silanes, the intensities of the Q^2 and Q^3 groups decrease (indicating the reduced surface hydroxyl groups) while the intensity of the Q^4 unit increases. The increase in the ratio of Q^4/Q^3 for the functionalized OSU-6 compared to the activated OSU-6 implies the presence of methyl groups, as seen in hexyltrimethoxysilane and ethyl trimethoxysilane.[61] The number of OH groups (**α**) can be calculated from these relative peak areas in the NMR data and is given by the formula:[91]

$$\alpha_{OH} = \frac{S \times (1+f+f_g^r)}{f} \text{ (number/nm}^2\text{)}$$

Where $f = \frac{I_s^r}{(I_{g+}^r I_l^r)}$, $f^r_g = \frac{I_g^r}{(I_{g+}^r I_l^r)}$. I^r_s denote the ^{29}Si peak areas at M in TMCS-OSU-6 and T^n in alkoxysilanes-OSU-6, I^r_g and I^r_l denote the ^{29}Si peak areas at Q^2 and Q^3, respectively; f is the ratio of attached silane silicons to the remaining silanol silicons in modified sample; f^r_g is the fraction of residual geminal silanols in the modified sample; S is the concentration of attached groups, which can be obtained by

$$S = \frac{\Delta W\% \times NA}{EMW \times S_{BET}} \times 10^{-20} \text{ (number/nm}^2\text{)}$$

where $\Delta W\%$ represents the weight gain after silylation (%), NA is Avogadro's number, EMW is the effective molar weight of the attached alkoxysilane groups, and S_{BET} is the BET surface area (m^2/g). Table 2.4 gives the number of OH groups and the ratio Q^4/Q^3 for these functionalized samples.

Table 3.4 Ratio of Q^4 to Q^3, area of the peaks T^1 and T^2 for alkylsilane functionalized OSU-6.

OSU-6 samples	α (number/nm^2) [91]	Q^4/Q^3 (area under the peak) [18]	Q^4/Q^3 (height ratio)	T^1 (area)	T^2 (area)
Activated OSU-6		0.99	0.76	13846.81	2222.52
Functionalized with ethyltrimethoxysilane	1.15	1.53	1.31	24531.24	
Functionalized with n-butyltrimethoxysilane	0.95	1.25	0.88	42183.62	7873.29
Functionalized with hexyltrimethoxysilane	0.27	2.00	1.40	4178.05	
Functionalized with n-octyltriethoxysilane	2.59	1.061	0.90		

3.5.2.2 Solid-State ^{13}C CP/MAS NMR Spectroscopy

The presence of different carbons in the functional groups is identified in the chemical shifts for all samples from the ^{13}C NMR spectra (Figure 3.13). ^{13}C chemical shifts and assignment of activated OSU-6 and surface modified activated OSU-6 materials are given in table 3.5.[61]

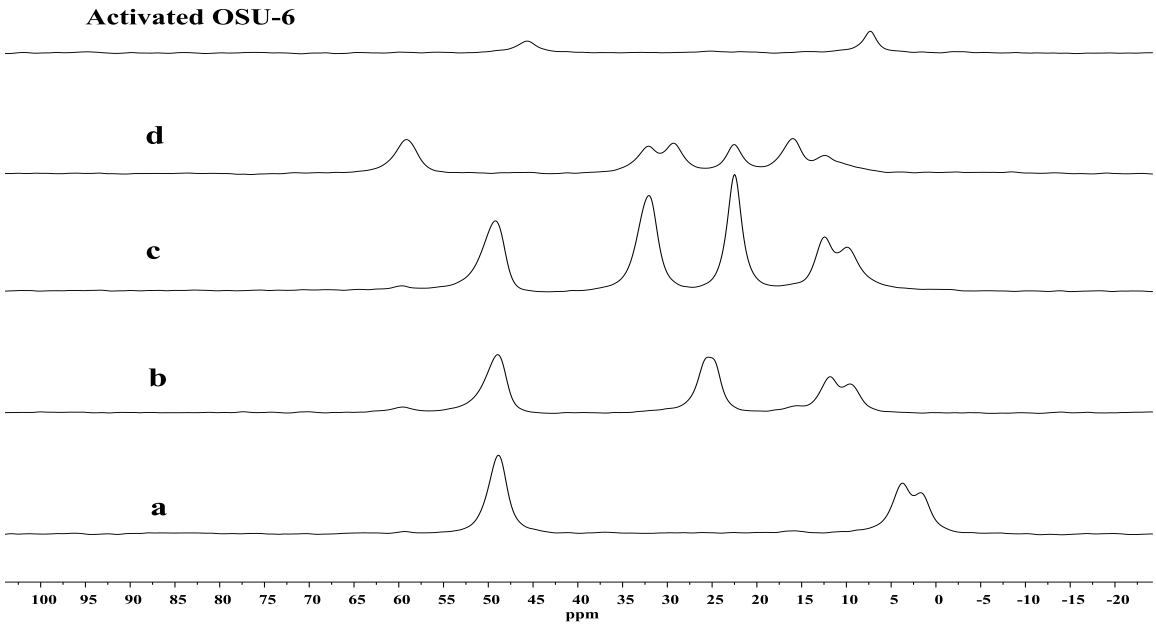

Figure 3.13 Solid-state ^{13}C NMR CP/MAS spectra of the activated OSU-6 and functionalized activated OSU-6: a) Ethyltrimethoxysilane; b) n-butyltrimethoxysilane; c) hexyltrimethoxysilane; d) n-octyltriethoxysilane

The chemical shifts for n-butyltrimethoxysilane closely match with those observed by Yasmin et al.[61] For other alkylation agents, we assigned the chemical shifts by comparison to the result of Yasmin and Muller.[61] For carbon-13 chemical shifts of amines, the data in Department of Chemistry, University of Wisconsin, by Hans J. Reich group was compared.[112, 113]

Table 3.5 ^{13}C chemical shifts and assignment of activated OSU-6 and surface modified activated OSU-6 materials.

OSU-6 Samples	Carbon position	^{13}C shift (ppm)
Activated	N-$\underline{C}H_2$-CH_3 *	45.65
	N-CH_2-$\underline{C}H_3$	7.33
Functionalized with ethyltrimethoxysilane	O-CH_3	48.87
	C2	3.73
	C1	1.71
Functionalized with n-butyltrimethoxysilane	N-$\underline{C}H_2$-CH_3	59.6
	O-CH_3	48.9
	C3	25.0
	C1	15.5
	C4	11.7
	N-CH_2-$\underline{C}H_3$	9.5
Functionalized with hexyltrimethoxysilane	N-$\underline{C}H_2$-CH_3	59.64(weak)
	O-CH3	49.17
	C2-C5	32.03
	C1	22.47
	C6	12.41
	N-CH2-$\underline{C}H_3$	9.89
Functionalized with n-octyltriethoxysilane	O-CH_3	59.14
	C3,C6	32.10
	C4,C5	29.31
	C2,C7	22.53
	C1	15.98

	C8	12.41

3.5.2.3 Fourier Transform Infrared Spectroscopy (FT-IR)

FTIR spectra of activated OSU-6 and functionalized activated OSU-6 are shown in Figure 3.14. The symmetric stretching vibrations of Si-O at 806 cm^{-1} and asymmetric stretching vibration of the Si-O-Si band at around 1080 cm^{-1} are seen for both OSU-6 and functionalized OSU-6. The stretching modes of H_2O at 1608 and 1582 cm^{-1} are seen both for activated OSU-6 and functionalized activated OSU-6 (also seen in the TGA results). The Si-C stretching vibrations are seen at 846 cm^{-1} for the functionalized OSU-6 indicating the presence of alkyl groups. The broad band around 3500 cm^{-1} corresponds to a hydrogen-bonded silanol group that perturbed by physically adsorbed water is seen for both the samples. The peak at 2966 cm^{-1} in functionalized OSU-6 corresponds to a stretching band in the alkylated OSU-6.

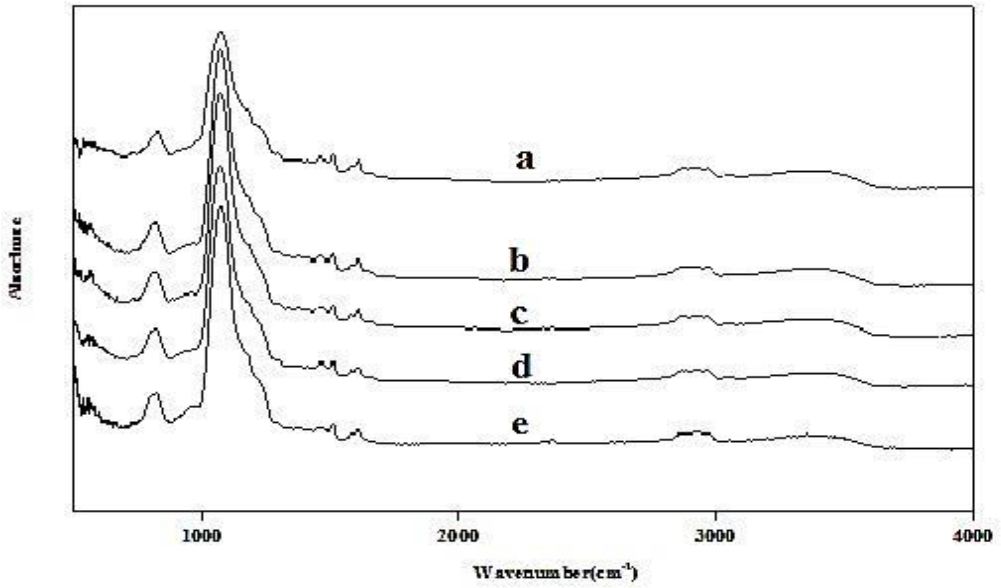

Figure 3.14 FTIR spectra of the: a) activated OSU-6 and functionalized activated OSU-6 b) Ethyltrimethoxysilane; c) n-butyltrimethoxysilane; d) Hexyltrimethoxysilane; e) n-octyltriethoxysilane

This peak also appears in OSU-6 but it has less intensity. Infrared absorption frequencies for OSU-6 functionalized with TMCS and activated functionalized OSU-6 are almost same but IR peaks show more intensities for functionalized OSU-6.[106-107]

3.5.2.4. Thermogravimetric Analysis (TGA)

Figure 3.15 shows the TGA results for the activated OSU-6 and functionalized activated OSU-6. The presence of adsorbed water that comes off below 200°C is seen in all samples. From 200 -1000°C the presence of hydroxyl group in the activated OSU-6 is seen and is about 8.5%.

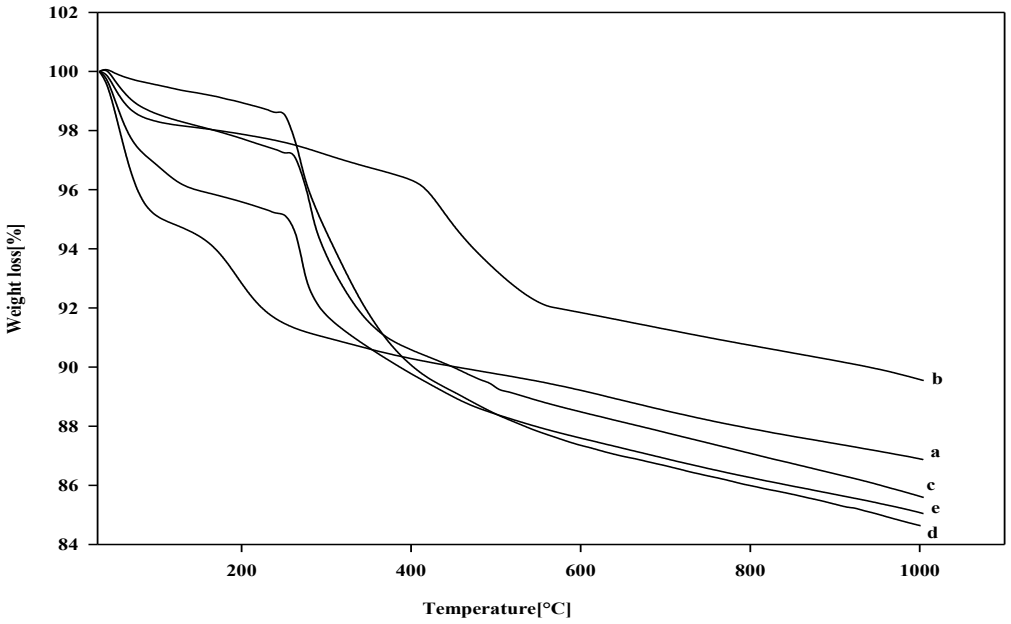

Figure 3.15 TGA curve of activated OSU-6 and activated functionalized OSU-6 samples in nitrogen atmosphere from 25 °C to 1000 °C at 10 °C/min. a) Activated OSU-6; b) OSU-6 functionalized with Ethyltrimethoxysilane; c) OSU-6 functionalized with n-butyltrimethoxysilane; d) OSU-6 functionalized with Hexyltrimethoxysilane; e) OSU-6 functionalized with n-octyltriethoxysilane.

The hydroxyl groups (that are not converted to functional group) and the functional groups are present in all the functionalized samples and are not clearly separated in the TGA and the hexyltrimethoxysilane sample showed the highest (about 15%) weight loss around 200-1000°C indicating the maximum coverage obtained (NMR shows the lowest number of hydroxyl groups for this sample).

3.6. Alkyl Functionalized Pellets

3.6.1. Fourier Transform Infrared Spectroscopy (FT-IR)

Figure 3.16 shows the FTIR results for activated OSU-6 and activated functionalized OSU-6 pellets. The symmetric stretching vibrations of Si-O at 806 cm^{-1} and asymmetric stretching vibration of the Si-O-Si band at around 1080 cm^{-1} are seen for both OSU-6 and functionalized OSU-6.

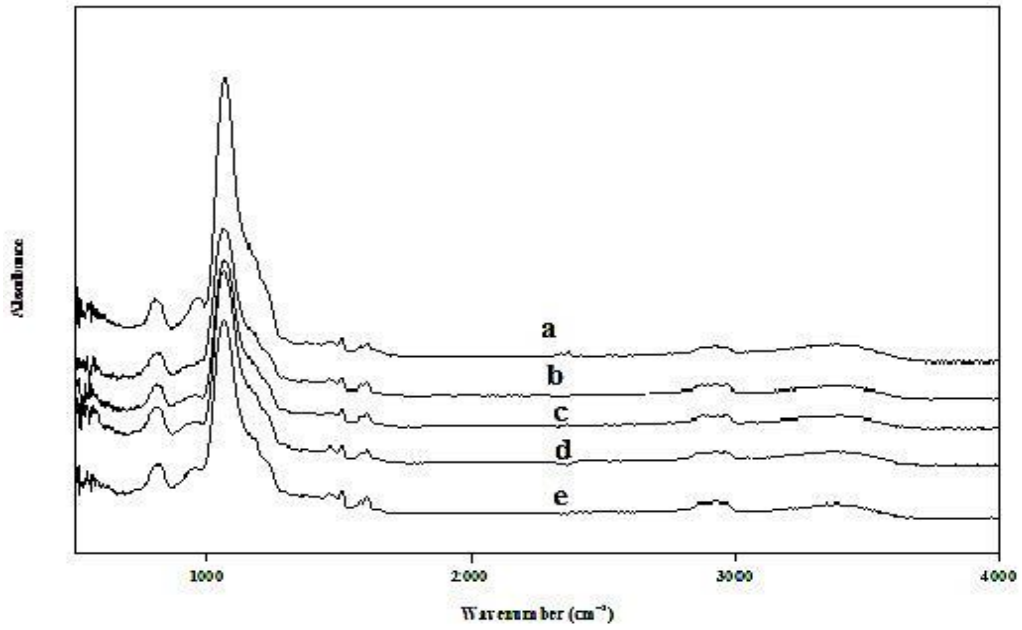

Figure 3.16 FTIR spectra of: a) activated OSU-6 and functionalized activated OSU-6; b) Ethyltrimethoxysilane; c) n-butyltrimethoxysilane; d) Hexyltrimethoxysilane; e) n-octyltriethoxysilane

The stretching modes of H_2O at 1608 and 1582 cm^{-1} are seen both for activated OSU-6 and functionalized activated OSU-6 (also seen in the TGA results). The stretching mode characteristics of Si-C stretching vibrations are seen at 846 cm^{-1} in the functionalized OSU-6 indicated the presence of alkyl group. The broad band around 3500 cm^{-1} corresponds to hydrogen-bonded silanol groups that are perturbed by physically adsorbed water are seen for both the samples. The peak at 2966 cm^{-1} in functionalized OSU-6 corresponds to a stretching band in the alkylated OSU-6. This peak also appears in OSU-6 but it has less intensity. The Si-O stretching of the surface silanols at around 960 cm^{-1} seen for OSU-6 almost vanished for TMCS-OSU-6 and functionalized activated OSU-6

powder but it appears in functionalized activated OSU-6 pellets. Infrared absorption frequencies for TMCS-OSU-6 and activated functionalized OSU-6 powder and pellets are almost same but IR peaks show more intensities for functionalized activated OSU-6 powders and pellets.

3.6.2. Thermogravimetric Analysis (TGA)

TGA curves of activated OSU-6 and activated functionalized OSU-6 pellets are shown in Figure 3.17. The results show that the presence of adsorbed water that comes off below 200 °C is seen in all samples. From 200-1000 °C the presence of hydroxyl group and the organic remains in the activated OSU-6 is seen and is about 10.18 %. The hydroxyl groups (that are not functionalized) and the functional groups are present in all the functionalized samples and are not clearly separated in the TGA and the hexyltrimethoxysilane [d] sample showed the highest (about 13.51 %) weight loss around 200-1000°C indicating the maximum coverage obtained. The next samples that showed higher loading are n-octyltriethoxysilane [e] (about 12.86 %), n-butyltrimethoxysilane [c] (about 10.14 %) and ethyltrimethoxysilane [b] (about 9.68 %).

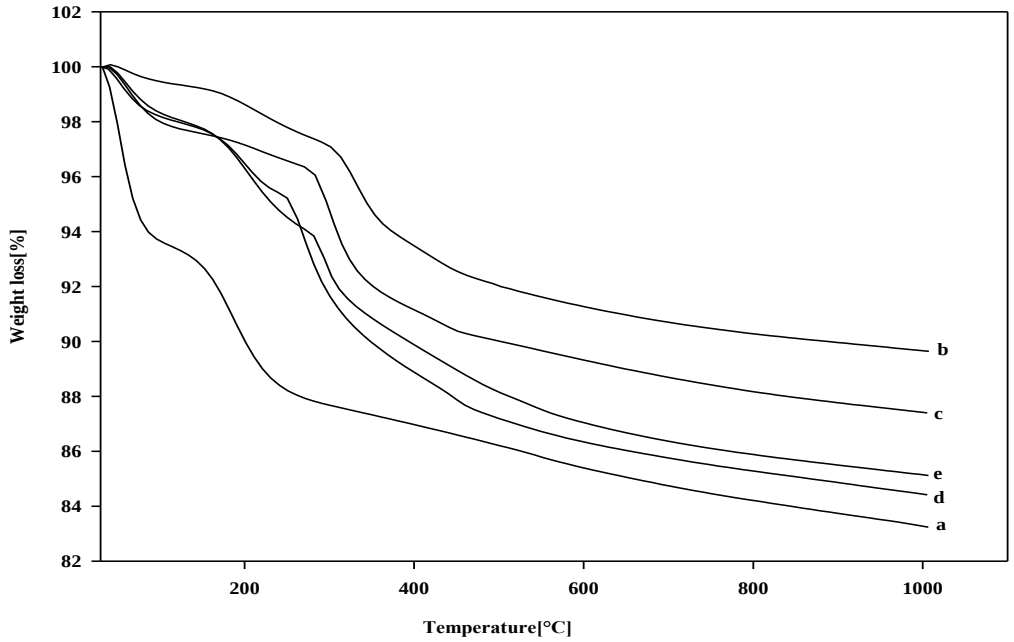

Figure 3.17 TGA curve of activated OSU-6 and activated functionalized OSU-6 pellets in nitrogen atmosphere from 25 °C to 1000°C at 10 °C/min. a) activated OSU-6 b) activated OSU-6 pellet functionalized with ethyltrimethoxysilane c) activated OSU-6 pellet functionalized with n-butyltrimethoxysilane d) activated OSU-6 pellet functionalized with hexyltrimethoxysilane e) activated OSU-6 pellet functionalized with n-octyltriethoxysilane.

3.7 Hydrolysis Study

Direct injection mass spectroscopy was used to look at the stability of silylation agents in OSU-6 pellets functionalized with Trimethylchlorosilane; activated OSU-6 pellets functionalized with ethyltrimethoxysilane, and activated OSU-6 pellet

functionalized with hexyltrimethoxysilane. A functionalized pellet was broken to several pieces and kept in an open vial at the room temperature, exposed to room humidity.

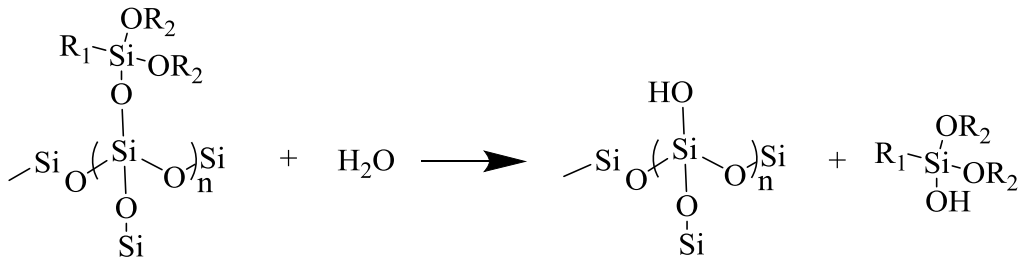

(a)

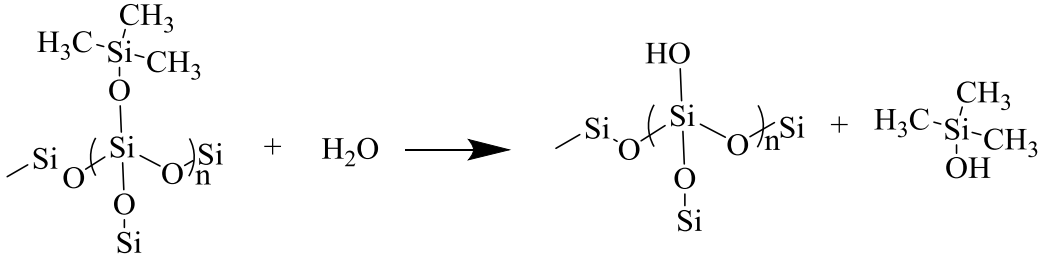

(b)

Figure 3.18 Hydrolysis reaction of functionalized OSU-6 a) Functionalized OSU-6 pellets by alkoxysilanes b) OSU-6 pellet functionalized with trimethylchlorosilane.

The intensity of the silanol peak (peak at *m/z*=75) was given in counts/mg. Hydrolysis occurs by the nucleophilic attack of the oxygen contained in the water on the silicon atom. Organotrialkoxysilanes and diorganodialkoxysilanes hydrolyze upon exposure to water vapor.[114] It is generally argued that hydrolysis proceeds by bimolecular

nucleophilic displacement reactions involving pentacoordinate intermediates or transition states (Figure 3.19).[115-117]

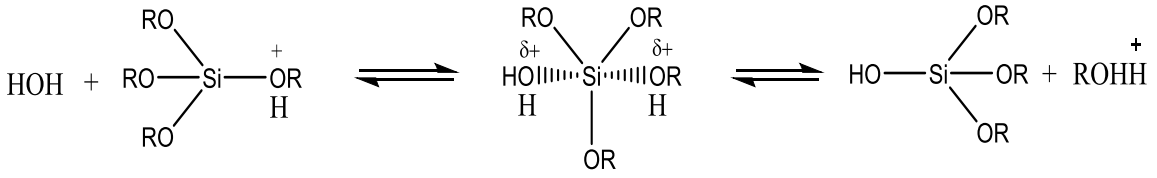

Figure 3.19 Hydrolysis mechanism with SN2 type character transition state.

Several investigators have proposed hydrolysis mechanisms involving flank-side attack without inversion of the silicon tetrahedron (Figure 3.20).[118,119]

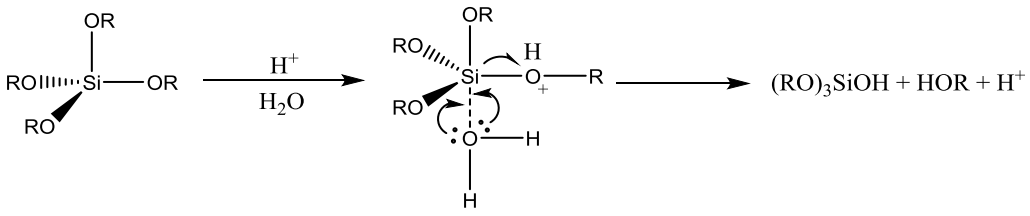

Figure 3.20 Hydrolysis mechanism with involving flank-side attack without inversion of silicon tetrahedron.

Figure 3.21 shows that only for the OSU-6 functionalized with Trimethylchlorosilane, the increase in intensity peak at 75 in the first 2 weeks indicates that the silyl species on the surface are hydrolyzed at a faster rate in the first week and remains the same for 2 weeks and then starts to decrease but still remain significantly higher than that noted for other silylation agents such as those functionalized

ethyltrimethoxysilane and hexyltrimethoxysilane pellets where the hydrolysis does not seem to affect the silylation agents on the surface.

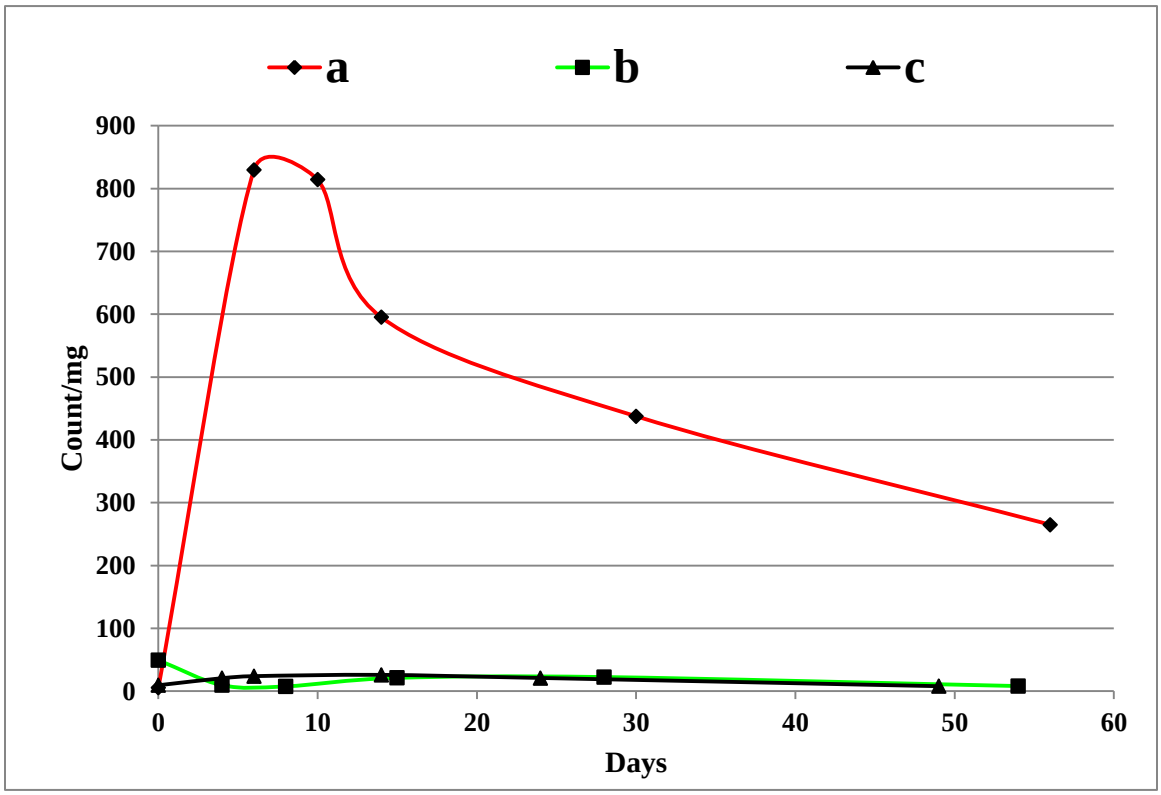

Figure 3.21 Hydrolysis rates of OSU-6 pellet functionalized with a) trimethylchlorosilane; b) Ethyltrimethoxysilane; and c) hexyltrimethoxysilane.

The functionalized OSU-6 with ethyltrimethoxysilane and hexyltrimethoxysilane could be used for impregnating inorganic species that are sensitive to moisture and OSU-6 functionalized with trimethtylchlrosilane can be used for impregnating inorganic species where the presence of moisture can be a beneficial factor.

3.8 Conclusion

Functionalized hexagonal mesoporous silica, in powder and pellet forms, were prepared by chemical modification of surfactant free mesoporous silica (OSU-6) with a chlorine-based silylating agent as well as long alkyl chain silylating agents of different chain lengths. The FT-IR, NMR and TGA results show that TMCS and alkoxysilanyl groups have been chemically bonded to silicon atoms on the surface of mesoporous silica. Based on NMR and TGA better loading of organic moieties were found when hexyltrimethoxysilane was used. A hydrolysis study for OSU-6 functionalized with TMCS shows that silyl species on the surface were hydrolyzed at a faster rate. We have also shown that the functionalized silica can be made in a pellet form that allows for easier and safer handling in certain applications.

CHAPTER IV

SPECTROSCOPIC DETERMINATION OF ENTHALPIES OF EVAPORATION AND SUBLIMATION OF VOLATILE ORGANIC COMPOUNDS ADSORBED ON FUNCTIONALIZED MESOPOROUS SILICA

4.1 Introduction

Volatile organic compounds (VOCs) are one of the most common air pollutants that need to be controlled according to increasingly stringent environmental regulations. The presence of VOCs in the air presents a number of harmful effects associated with their toxicity and their contribution to photochemical smog, acting as precursors in the generation of photochemical ozone. One of the main sources of VOCs is the use of fossil fuels. The quantity of VOCs emitted in the processes of distribution and storage of gasoline accounts for about 5% of the total amount of VOCs released to the atmosphere.[64] As discussed in the introduction, a number of technologies have been developed and applied commercially for VOC abatement.[120]

Activated carbons are the most common adsorbent applied for VOCs removal, although their use involves a number of problems, mainly related to the fact that activated carbons are flammable materials with difficult regeneration.[68,69] Zeolites and ordered mesoporous materials have been proposed as alternative adsorbents to replace activated carbons in VOC recovery processes due to their organophilicity and high hydrothermal

and chemical stability.[121] In 1992, a novel mesoporous materials family, MCM-41, was discovered by scientists at the Mobil Corporation.[122] Due to its high surface area and large pores mesoporous silica like MCM-41 was a very promising candidate for the removal of VOCs present in high-humidity gas streams or wastewater. Functionalization of the mesoporous silica with alkyl chains provides a method to change the absorption properties of these materials.

Accurate values of enthalpies of sublimation/evaporation in the vapor phase are crucial in evaluating environmental transport properties, polymorphism, enthalpy of formation, and predictions of molecular packing and their persistence.[123]

Enthalpies of sublimation/evaporation are usually determined in the condensed phase and then used to correct those values determined in the vapor phase.[124] Enthalpies of sublimation can be determined using ‘‘static or direct’’ and ‘‘dynamic or indirect’’ methods. Direct techniques are based on the determination of the heat associated with the sublimation by using heat flux[125,126] or differential scanning calorimety (DSC).[127] Indirect determination of enthalpies of sublimation utilizes vapor pressure measurements with complex experimental systems such as the Knudsen effusion technique[128], temperature drop microcalorimetry[129], gas saturation techniques.[130] From these reults, the heat of sublimation can be determined using the Clausius–Clapeyron equation. Gas saturation and effusion are generally considered the most accurate indirect experimental methods for determination of enthalpies of sublimation of materials with vapor pressure lower than ~1 Pa.[131,132] However, these methods are often complicated; time consuming, and susceptible to certain types of systematic errors such as leaks that can be difficult to detect. Thermogravimetric analysis (TGA) is the most widely used indirect technique in determining thermodynamic parameters in the bulk form of materials.[133-136] However, the mass change detectable by TGA is on the order of few nanograms, thereby limiting the

usefulness to samples larger than a few milligrams, depending on the sensitivity of the balance.

W.M. Hikal, *et al.* recently reported the successful use of optical absorbance spectroscopy for the accurate determination of the sublimation rates and enthalpies of sublimation of low volatile materials in the form of continuous nanofilms when operated isothermally for 2,4,6-trinitrotoluene (TNT), cyclotrimethylenetrinitramine (RDX), and PETN[137-139] at relatively low temperatures (55-100 °C), and nonisothermally for TNT[140] below their melting points. The elegance of this method is its simplicity and the accuracy of the determined sublimation rates and thermodynamic parameters. It is based on monitoring the change in absorbance of a material at a specific wavelength (absorbance peaks) as a function of time as the temperature of the film is changed This work targets the development of a simple optical methodology to determine the latent heats of sublimation and evaporation of volatile materials at equilibrium for volatile materials, powders and liquids form. Thus, we report the use of absorbance spectroscopy in the UV region of the electromagnetic spectrum to determine the latent heats of sublimation and evaporation of toluene, nitrobenzene, and naphthalene.

4.2 Material and Methods

4.2.1 Materials

The chemicals used in this work included: mesoporous silica, toluene 99.8% [Pharmco-AAPER, HPLC grade], nitrobenzene [Aldrich, ACS reagent], naphthalene [Aldrich, scintillation grade], ethyl alcohol [Pharmco, USA]. The functionalization agent is hexyltrimethoxysilane [Gelest, INC.].

Absorbance spectra for toluene, nitrobenzene, and naphthalene were recorded *in situ* using a Varian Cary 5000 UV/Visible/Near Infrared spectrophotometer with temperature control and software to perform kinetic studies. The spectrometer is equipped with a temperature controller allowing for *in situ* temperature-dependent absorbance measurements with an accuracy of 0.05 °C for both the sample and reference. The material was added to a cuvette which was then hermetically sealed with a special cap provided with the cuvette by the supplier. Each material was then heated *in situ* and the prominent absorbance peaks of their gas phase were determined. The temperature was manually changed to the desired values using the temperature controller attached to the spectrometer. The absorbance was simultaneously recorded every second and the temperature was changed every 10 minutes after each sample was scanned twice at the same temperature. The first scan (absorbance) of the gas started 5 minutes after each temperature change. To eliminate the possible absorption of air (N_2 and O_2), before the first scan the cuvette's cap was opened for 5 seconds to let the air come out. After the first scan, we will wait for 5 more minutes and scan it again. The cuvette's cap would not be open for the second scan. Temperature can be measured inside the cuvette with the optional temperature probe accessory or the temperature of the multicell block can be used. Temperature data is stored with the data file. The user can specify the temperature at which the sample is held after the data collection is complete. We repeated the UV absorption experiment three times for each sample to check the reproducibility of data.

4.2.2 Manufacturing of Mesoporous OSU-6 Pellet

The modified mesoporous silica (here referred as OSU-6)/activated mesoporous silica (here after referred as act-OSU-6) was synthesized following the reported literature procedure by Tuel and Gontier[95] with several alterations that have been made by Alothman and Apblett.[60] For special applications where the pellet form of mesoporous

silica/activated mesoporous silica is needed, the powder was subsequently pressed into pellets. For making each pellet, 0.200 g of the powder was pressed into 13 mm disks with a clamping force of 2 tons pressure for 90 seconds by Carver manual bench top standard unheated press. The clamping force of 2 tons was found to be the optimum to make the pellet without affecting the surface area.

4.3 Absorption of Organic Materials (Toluene, Nitrobenzene, and Naphthalene) in the Vapor Phase on OSU-6

A special vial (Figure 4.1) was designed for this purpose. One OSU-6 pellet was placed inside the pellet holder and the organic material at the bottom of vial. The vial was then sealed with a special cap. The pellet was weighed at certain time intervals.

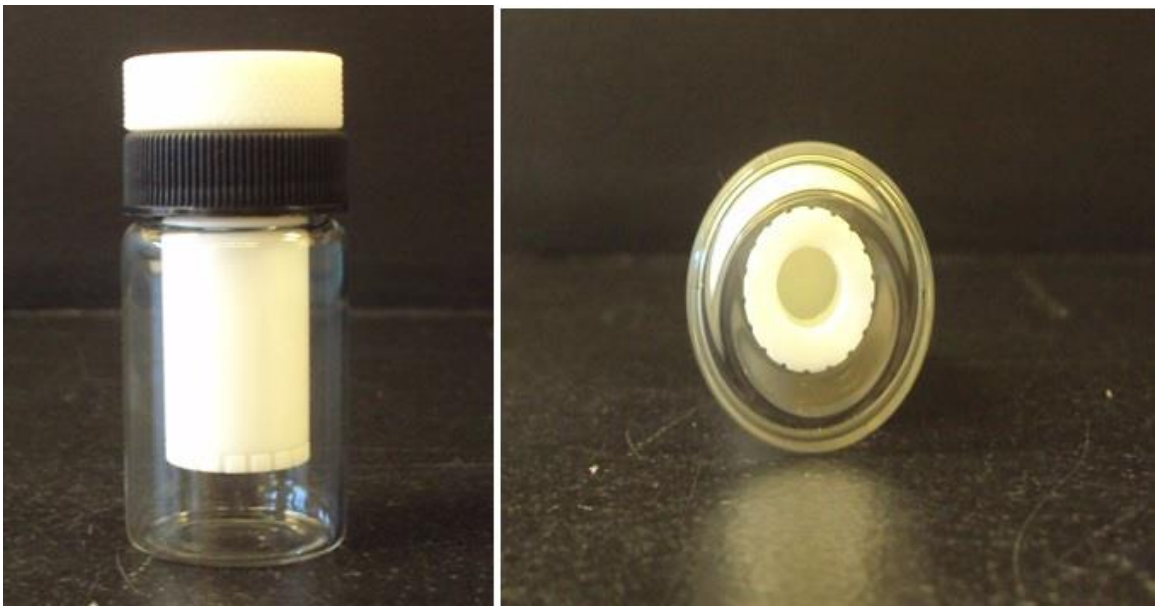

Figure 4.1 Experiments vial.

Figure 4.2 shows the number of moles versus time (in hours). As it was shown in Figure 3.2, OSU-6 pellet exposed to toluene reached to saturation after 120 hours; however the weight of OSU-6 pellet loaded with nitrobenzene (Figure 4.3) or naphthalene (Figure 4.4) kept increasing.

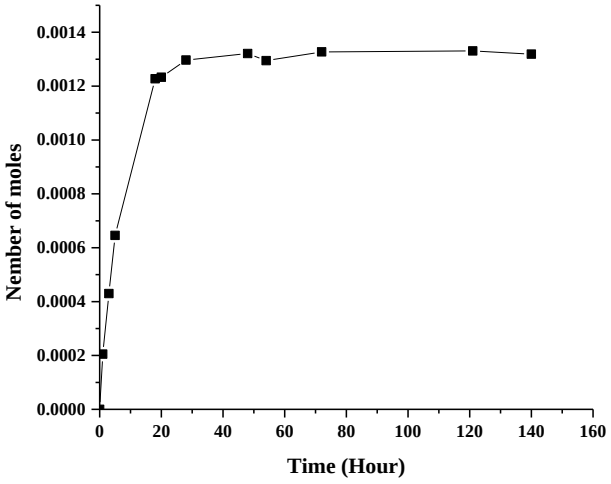

Figure 4.2 Number of moles versus time (hours) of OSU-6 pellet loaded with toluene.

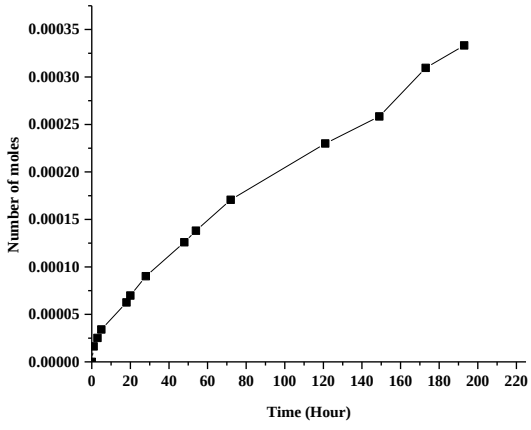

Figure 4.3 Number of moles versus time (hour) of OSU-6 pellet loaded with nitrobenzene

Directly after OSU-6 reaches to saturation with toluene, the pellet was broken to the pieces. One piece will be weighed and placed in the cuvette for a UV absorption experiment.

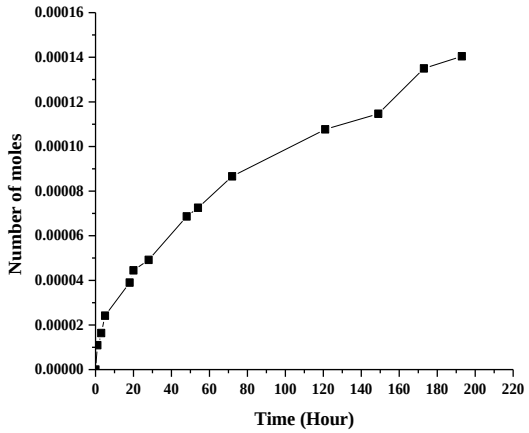

Figure 4.4 Number of moles versus time (hours) of OSU-6 pellet loaded with naphthalene.

An OSU-6 pellet loaded with nitrobenzene and naphthalene was removed from the vial after 200 hours and studied using the same protocol described for the OSU-6 pellet loaded with toluene.

4.4. Manufacturing a Functionalized Mesoporous Silica Pellet

4.4.1 Functionalization of OSU-6 Pellets by hexyltrimethoxysilane

The procedure of functionalization of OSU-6 pellets was described in Chapter III.

4.5 Absorption of Organic Materials (Toluene, Nitrobenzene, and Naphthalene) in the Vapor phase by the Activated OSU-6 Pellets Functionalized with hexyltrimethoxysilane

One activated OSU-6 pellet functionalized with hexyltrimethoxysilane was placed in the pellet holder and the organic material was placed at the bottom of a vial. The vial was then sealed with a special cap. A pellet mass was checked after a series of time intervals. As shown in Figure 4.5, the activated OSU-6 pellet functionalized with hexyltrimethoxysilane loaded with toluene reaches mass saturation after 144 hours, but nitrobenzene (Figure 4.6) and naphthalene uptake requires an extended time (Figure 4.7).

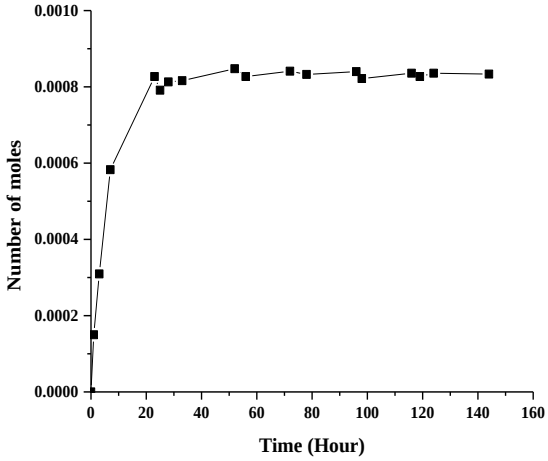

Figure 4.5 Number of moles versus time (hours) of activated OSU-6 pellet functionalized with hexyltrimethoxysilane loaded with toluene.

After OSU-6 pellets reached saturation, the pellet was broken into pieces. One piece was weighed and placed in the cuvette for UV absorption experiment. The OSU-6 pellet functionalized with hexyltrimethoxysilane loaded with nitrobenzene and the OSU-6

pellet functionalized with hexyltrimethoxysilane loaded with naphthalene were removed from the corresponding vials after 168 and 195 hours respectively and the same procedure was repeated for those pellets.

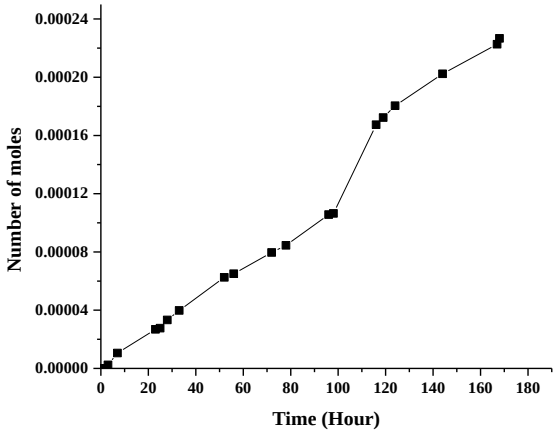

Figure 4.6 Number of moles versus time (hours) of OSU-6 pellet functionalized with hexyltrimethoxysilane loaded with nitrobenzene.

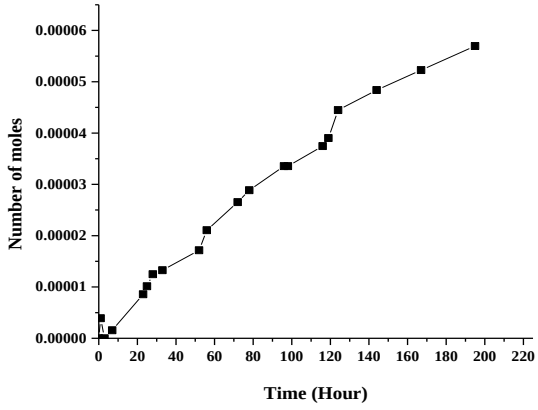

Figure 4.7 Number of moles versus time (hours) of OSU-6 pellet functionalized with hexyltrimethoxysilane loaded with naphthalene.

4.6 Results and Discussion

Figure B1-B3 represents the UV-absorbance spectra of the vapor phase of toluene in three different temperatures. Toluene exhibited one prominent absorbance peak located at 260 nm with two shoulders at 253 nm and 266 nm. As the temperature increaseed the peaks became more intense and observable. At 60 and 70 °C, a slight shift in the prominent absorbance peak location was observed with heating the toluene.

Figure B4-B6 represents the UV-absorbance spectra of the vapor phase of OSU-6 loaded with toluene in three different temperatures. The absorbance peaks were similar to toluene but the intensity is lower in comparison to toluene.

Figure B7-B9 represents the UV-absorbance spectra of the vapor phase of OSU-6 functionalized with hexyltrimethoxysilane loaded with toluene in three different temperatures. The absorbance amount was lower than toluene and OSU-6 loaded with toluene.

Figure B10-B12 represents the UV-absorbance spectra of the vapor phase of nitrobenzene at three different temperatures. Nitrobenzene exhibited one prominent broad absorbance peak located at 240 nm. As the temperature increased the absorbance increases.

Figure B13-B15 represents the UV-absorbance spectra of the vapor phase of OSU-6 loaded with nitrobenzene at three different temperatures. At 20 °C no peak was observed but as temperature was increased the prominent peak has appeared at 240 nm.

Figure B16-B18 represents the UV-absorbance spectra of the vapor phase of OSU-6 functionalized with hexyltrimethoxysilane loaded with nitrobenzene in three different temperatures. The absorbance amount was lower than nitrobenzene and higher than OSU-6 loaded with nitrobenzene.

Figure B19-B21 represents the UV-absorbance spectra of the vapor phase of naphthalene at three different temperatures. Naphthalene exhibited a prominent sharp absorbance peak at 211 nm that at 60 and 70 °C became very broad with a shoulder located at 206 nm. This shoulder, at 60 and 70 °C disappears. Another prominent broad absorbance peak was observed at 221 nm. There were three other peaks at 259, 268 and 279 nm above 40 °C.

Figure B22-B24 represents the UV-absorbance spectra of the vapor phase of OSU-6 loaded with naphthalene at three different temperatures. Naphthalene exhibited a prominent absorbance peak at 211 nm with a shoulder located at 206 nm. Another broad absorbance peak was observed at 220 nm. No shift in the absorbance peaks locations was observed upon heating the three materials up to 70 °C.

Figure B25-B27 represents the UV-absorbance spectra of the vapor phase of OSU-6 functionalized with hexyltrimethoxysilane loaded with naphthalene at three different temperatures.

Peak broadening at 211 did not occur for OSU-6 loaded with naphthalene or OSU-6 functionalized with hexyltrimethoxysilane loaded with naphthalene. The absorbance amount of OSU-6 functionalized with hexyltrimethoxysilane loaded with naphthalene was lower than naphthalene and higher than OSU-6 loaded with naphthalene. The absorbance amount of OSU-6 loaded with naphthalene was (much)

lower than both naphthalene and OSU-6 functionalized with hexyltrimethoxysilane loaded with naphthalene. UV-absorbance spectra are in Appendix B.

In the vapor phase of a substance, the absorbance is related to the concentration of the saturated gas via Beer–Lambert law given by:[141]

$$A(\lambda) = \alpha(\lambda)l = \sigma(\lambda)N_s l \quad (1)$$

where A(λ) is the absorbance at a specific wavelength (λ), α is the absorbance coefficient, σ(λ) is cross section of light absorption by a single particle at a specific wavelength, and N_s is the density (number per unit volume) of absorbing particles at equilibrium/saturation. Thus for a constant path length (l), the absorbance is directly proportional to the concentration of the gas molecules.

Assuming an ideal gas, when a gas reaches saturation at a constant temperature the saturation pressure of the gas is given by the universal gas law:

$$P_s = N_s k_B T \quad (2)$$

where k_B is the Boltzmann's constant and T is the absolute temperature.
Substituting Eq. (1) in Eq. (2) yields:

$$P_s = \frac{k_B}{\sigma(\lambda)l} A(\lambda)T \quad (3)$$

Equation (3) represents a linear proportionality between the saturated vapor pressure P_S and the absorbance of the gas multiplied by the absolute temperature when monitored at a specific wavelength. Thus, the quantity A(λ)T can be used as a physical quantity

associated with the temperature-dependent saturation pressure values of the gas. Hence, the enthalpy of sublimation and evaporation can be determined using the Clausius–Clapeyron equation which is in the form:

$$lnP = lnk - \frac{\Delta H}{k_B T} \tag{4}$$

where k is a constant and ΔH is the enthalpy of sublimation. Substituting Eq. (3) in Eq. (4) yields:

$$ln[A(\lambda)] = ln\left[\frac{k\sigma(\lambda)l}{k_B}\right] - \frac{\Delta H}{k_B} \cdot \frac{1}{T} \tag{5}$$

To determine the enthalpies of sublimation of each sample we chose 5 different wavelengths including the λ_{max}, and then the logarithm of the absorbance corresponding to the gas saturation multiplied by the absolute temperature in Kelvin is plotted versus the inverse of the absolute temperature. In Figure 4.8 such a plot for toluene first scan at 260 nm (λ_{max}) is shown giving the corresponding evaporation enthalpy of 30 $kJmol^{-1}$.

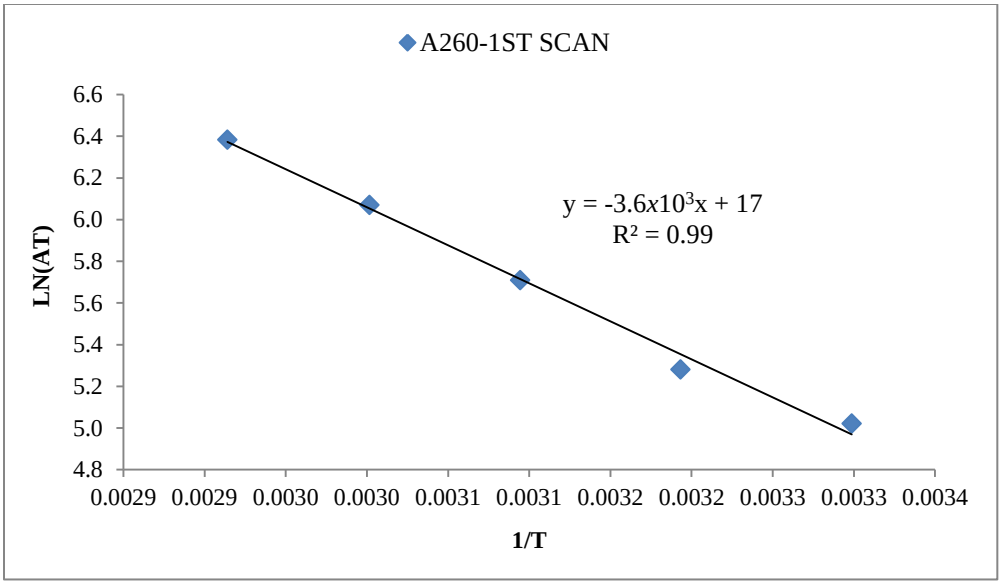

Figure 4.8 Plot of the logarithm of A(λ)T of toluene versus the inverse of the absolute temperature.

Enthalpies of sublimation of organic and organometallic compounds compendium[130] is a compendium of sublimation enthalpies, published within the period 1910–2001 (over 1200 references). A brief review of the temperature adjustments for the sublimation enthalpies from the temperature of measurement to the standard reference temperature, 298.15 K, is included, as are recently suggested values for several reference materials. Examination of the data in this compendium will reveal some large discrepancies in reported enthalpies of sublimation. It is likely that some of the discrepancies reported by different laboratories are due to measurements made on different polymorphic modifications.[142]

Phase transition enthalpy measurements of organic and organometallic compounds compendium[143] is a compendium of phase change enthalpies including

fusion, vaporization, and sublimation are included for organic, organometallic, and a few inorganic compounds from 1880 to 2010. This compendium is a combination of three previous series focusing on phase change enthalpies updated to 2009.

Table 4.1 contains a listing of the acronyms that are used in these two tables.

	Acronyms used in tables
A	calculated from the vapor pressure data reported by the method of least squares
B	calculated from the sum of the enthalpy of vaporization at temperature T and the enthalpy of fusion at the melting point
C	calorimetric determination
GC	gas chromatography
CGC–DSC	combined correlation gas chromatography–differential scanning calorimetry
DM	diaphragm manometer
DSC	differential scanning calorimeter
GS	gas saturation, transpiration
LE	Langmuir evaporation
HSA	head space analysis
KG	Knudsen gauge
ME	Mass effusion–Knudsen effusion
TE	torsion effusion
TSGC	temperature scanning gas chromatography
QF	quartz fiber
V	viscosity gauge

Table 4.2, 4.3 and 4.4 contains sublimation enthalpy data for naphthalene, toluene and nitrobenzene. The first entry is the range of temperatures studied. For measurements performed at a constant temperature or when not specified, this entry is left blank. ΔH_{sub} (T_m) is the next entry followed by the mean temperature (K), an acronym briefly describing the type of measurement, and the reference to the original work. If the authors of the work have adjusted their results to 298.15 K, then this information along with the reference is entered on the third column. This information is repeated for multiple measurements. The measurements are arranged in reverse chronological order.

Table 4.2 Reported enthalpies of sublimation of naphthalene.

Temperature range (K)	ΔH_{sub}/kJ mol^{-1}	(T_m /K)	Method	Reference
	70.4	298	CGC-DSC	[144]
313-353	71.7	333	GS	[145]
337-352	78.2±1		GC	[146]
	70.9±0.4	323	DSC	[147]
	72.6±0.1	298	TE,ME,DM	[148,149]
	72.4±0.7	298	C	[150]
303-329	74.35±1.7		TSGC	[151]
263-298	67.8±3.5	280	HSA	[152]
281-290	64±0.5		LE	[153]
230-260	72.7±0.3		KG	[154,155]
276-283	66.3		V	[156]
237-276	76.6		QF	[157]
	57.876			[158]
	83.5			[159]
267–303	88.0±2.5		ME	[160]

Table 4.3 Reported enthalpies of vaporization for toluene:

Temperature range (K)	ΔH_{vap}/kJ mol^{-1}	(T_m /K)	Method	Reference
	33.2			[161]
210–279	40.6	264	A	[162]
	33.18			[163]
	24.0±0.1	505	C	[164]
	27.1±0.1	470	C	[164]
	29.4±0.1	441	C	[164]
	32.1±0.1	403	C	[164]
	33.5±0.1	380	C	[164]
	39.20			[165]
	43.1	298	B	[166]

Table 4.4 Reported enthalpies of vaporization for nitrobenzene.

Temperature range (K)	ΔH_{vap}/kJ mol^{-1}	(T_m /K)	Method	Reference
313–353	54.5	298	CGC	[167]
279–296	54.7	287	A	[168]
288–318	54.3	303	CGC	[169]
291–305	56.1±1.7	298	ME	[170]
	55.0	298	ME	[171]
283–303	52.5	293	ME	[172, 173]
407–483	48.5	422	ME	[174,175]
369–481	48.9	425	ME	[176,177]

Average of enthalpy of all 5 wavelengths was reported as the enthalpy of sublimation and evaporation for each single experiment. For each experiment, we will have two enthalpies because each sample was scanned twice. We ran the UV experiment 3 times for each

sample, so overall 6 enthalpies will be reported for each single sample. Enthalpies are reported in Table C1 to C9 in Appendix C.

Enthalpy of evaporation of toluene, OSU-6 loaded with toluene, and OSU-6 functionalized with hexyltrimethoxysilane loaded with toluene are 29±1, 31±1 and 32±1 $kJmol^{-1}$ respectively.

Enthalpy of evaporation of nitrobenzene, OSU-6 loaded with nitrobenzene, and OSU-6 functionalized with hexyltrimethoxysilane loaded with nitrobenzene are 48±1, 54±1 and 46±1 $kJmol^{-1}$ respectively. The nitrobenzene binding energy in hydroxylated OSU-6 is higher in comparison to functionalized OSU-6. This is presuming because the polarity of nitrobenzene increases its affinity to hydroxyl groups of OSU-6.

Enthalpy of evaporation of naphthalene, OSU-6 loaded with naphthalene, and OSU-6 functionalized with hexyltrimethoxysilane loaded with naphthalene are 56±1, 34±1 and 47±1 $kJmol^{-1}$ respectively. Naphthalene binding energy in functionalized OSU-6 is higher in comparison to hydroxylated OSU-6. Naphthalene has hydrophobic properties and thus has a good affinity to hexyltrimethoxysilane.

REFERENCES

(1) http://scifun.chem.wisc.edu/chemweek/polymers/polymers.html.

(2) Hetayothin, B. *EFFECT OF STRUCTURE AND PLASTICIZER ON THE GLASS TRANSITION OF ADSORBED POLYMER* **2010**.

(3) Dan, N. *Langmuir* **2000**, *16*, 4045.

(4) Fleer, G. J.; Cohen Stuart, M. A.; Scheutjens, J. M. H. M.; Cosgrove, T.; Vincent, B. *Polymers at Interfaces; Chapman and Hall: London, U.K.*, **1993**.

(5) J., F. W.; Munro, H. S. *Polymer Surfaces and Interfaces; Wiley, NY* **1987**.

(6) Kajiyama, T.; Tanaka, K.; Takahara, A. *Macromolecules* **1997**, *30*, 280.

(7) Moddel, M. B., M.; Janke, W. *J. Phys. Chem. B* **2009**, *113*, 3314.

(8) Reiter, G. *Macromolecules* **1994**, *27*, 3046.

(9) Soga, I. *J. Coat. Technol.* **2003**, *75*, 53.

(10) Wicks, Z. W.; Jones, F. N.; Pappas, S. P.; Wicks, D. A. *Wiley Interscience, New Jersey* **2007**.

(11) Hobden, J. F.; Jellinek, H. H. G. *J. Polym. Sci* **1953**, *11*, 365.

(12) Howard, G. J.; McConnell, P. *J. Chem. Phys.* **1967**, *71*, 2974.

(13) Herd, M. J.; Hopkins, A. J.; Howard, G. J. *J. Polym. Sci* **1971**, *34*, 211;ibid. 1971 A.

(14) White, J. L.; Sadakne, G. S. *J. Appl. Polym. Sci.* **1973**, *17*, 453.

(15) Silberberg, A. *J. Chem. Phys.* **1968**, *48*, 2835.

(16) Stuart, C. M. A.; Scheutjens, J. M. H. M.; J., F. G. *J. Polym. Sci.* **1980**, *18*, 559.

(17) Roe, R. J. *J. Chem. Phys.* **1974**, *60*, 4192.

(18) Andrade, J. D. *Polymer Surface Dynamics; Plenum Press: New York* **1988**.

(19) Porter, C. E.; Blum, F. D. *Macromolecules* **2002**, *35*, 7448.

(20) Kulkeratiyut, S.; Kulkeratiyut, S.; D., B. F. *J. Polym. Sci Part B* **2006**, *44*, 2071.

(21) Blum, F. D.; Young, E. Y.; Smith, G.; C., S. O. *Langmuir* **2006**, *22*, 4741.

(22) Khatiwada, B. K.; Blum, F. D. *Polymer Preprints 2011, 52(2), 326* **2011**, *52*, 326.

(23) Plastics *Differential scanning calorimetry (DSC) Part 2: Determination of glass transition temperature* **1999**, *ISO 11357-2*.

(24) Seyler, R. J. **1994**.

(25) Painter, P. C.; Coleman, M. M. *Fundamentals of Polymer Science 2nd ed; CRC Press: Boca Raton* **1997**.

(26) Reading, M.; Hourston, D. J. *Modulated Temperature Differential Scanning Calorimetry, Theoretical and Practical Applications in polymer Characterisation. Springer: Dordrecht. The Netherlands* **2006**.

(27) Annighofer, F.; Gronski, W. *Makromol. Chem.* **1984**, *185*, 2231.

(28) Roe, R. J. *J. Appl. Crystallogr.* **1982**, *15*, 18.

(29) Vesely, D. *Folkes, M. J.; Hope, P. S., Eds.; Blackie Academic & Professional: London* **1993**.

(30) Thomas, D. A. *In advances in preparation and characterization of multi-polymer systems, Ambrose, R. J.; Aggarwal, S. L., Eds.; John Wiley and Sons: N.Y.* **1978**.
(31) Dubault, A. B., L.; Gandin, E.; Halary, J. L. *Polym. Int.* **2003**, *52*, 1108.
(32) O'Reilly, J. M. *Journal of Applied Physics* **1977**, *48*, 4043.
(33) Biliaderis, C. G.; Page, C. M.; Maurice, T. J.; Juliano, B. O. *Journal of Agricultural and Food Chemistry* **1986**, *34*, 6.
(34) Russell, P. L.; Oliver, G. *Journal of Cereal Science* **1989**, *10*, 123.
(35) Hutchinson, J. M. *Journal of Thermal Analysis and Calorimetry* **2003**, *72*, 619.
(36) Jin, Y.; Bonilla, J.; Lin, Y.-G.; Morgan, J.; McCracken, L.; Carnahan, J. *Journal of thermal analysis* **1996**, *46*, 1047.
(37) Cao, J. *Thermochimica Acta* **1999**, *325*, 101.
(38) Verdonck, E.; Schaap, K.; Thomas, L. C. *International Journal of Pharmaceutics* **1999**, *192*, 3.
(39) Mortazavian, H.; Alizadeh-Bazazi, S.; Blum, F. D. *To be submitted.*
(40) Yanagisawa, T.; Schimizu, T.; Kiroda, K.; Kato, C. *Bull. Chem. Soc. Jpn.* **1990**, *63*, 988.
(41) Zhao, X. S.; Lu, G. Q.; Millar, G. J. *Ind. Eng. Chem. Res.* **1996**, *35*, 2075.
(42) Kresge, C. T. L., M. E.; Roth; W. J.; Vartulli, J. C.; Beck, J. S. *Nature* **1992**, *359*, 710.
(43) Borman, S.; Dagani, R.; Rawls, R. L. a.; Zurer, P. S. *Chemical & Engineering News* **January 12, 1998**.
(44) Beck, J. S.; Calabro, D. C.; McCullen, S. B.; Pelrine, B. P.; Schmitt, K. D.; Vartuli, J. C. *US Patent* **1993**, *101*, 220.
(45) Gibson, L. T. *Chem. Soc. Rev.* **2014**, *43*, 5163.
(46) Beck, J. S. *U.S. Patent 5, 057* **1991**, *296*.
(47) McCusker, L. B.; Baerlocher, E. J.; Bulow, M. *Zeolites* **1991**, *11*, 308.
(48) Papirer, E. *Adsorption on silica surfaces* **2000**, *Taylor & Francis*, 666.
(49) Galarneau, A.; Iapichella, J.; Brunel, D.; Fajula, F.; Bayram-Hahn, Z.; Unger, K.; Puy, G.; Demesmay, C.; Rocca, J. *Journal of Separation Science* **2006**, *29*, 844.
(50) Kurganov, A.; Unger, K.; Issaeva, T. *Journal of Chromatography A* **1996**, *753*, 177.
(51) Raimondo, M.; Perez, G.; Sinibaldi, M.; De Stefanis, A.; Tomlinson, A. A. G. *Chem. Commun.* **1997**, *1997*, 1343.
(52) Thoelen, C.; Van de Walle, K.; Vankelecom, I. F. J.; Jacobs, P. A. *Chem. Commun.* **1999**, *1999*, 1841.
(53) Martin , T.; Galarneau , A.; Di Renzo , F.; Brunel , D.; Fajula, F.; Heinisch , S.; Crétier , G.; Rocca, J. L. *Chem. Mater.* **2004**, *16*, 1725.
(54) Deschler, U.; Kleinschmit, P.; Panster, P. *Angewandte Chemie International Edition in English* **1986**, *25*, 236.
(55) Bluemel, J. *Inorg. Chem.* **1994**, *33*, 5050.
(56) Zhao, X. S.; Lu, G. Q.; Millar, G. *J. Ind. Eng. Chem. Res.* **1996**, *35*, 2075.
(57) Raman, N. A.; Anderson, M. T.; Brinker, C. J. *Chem. Mater.* **1996**, *8*, 1682.
(58) Galarneau, A.; Iapichella, J.; Bonhomme, K.; Di Renzo, F.; Kooyman, P.; Terasaki, O.; Fajula, F. *Advanced Functional Materials* **2006**, *16*, 1657.

(59) Al-othman, Z. A. Synthesis, modification, and application of mesoporous materials based on MCM-41 **2006**, 44.
(60) AlOthman, Z. A.; Apblett, A. W. *Applied Surface Science* **2010**, *256*, 3573.
(61) Yasmina, T.; Müller, K. *Journal of Chromatography A* **2010**, *1217*, 3362.
(62) Jobson, B. T.; Berkowitz, C. M.; Kuster, W. C.; Goldan, P. D.; Williams, E. J.; Fesenfeld, F. C.; Apel, E. C.; Karl, T.; Lonneman, W. A.; Riemer, D. *J. Geophys. Res.* **2004**, *D 109*, D24305.
(63) Latella, A.; Stani, G.; Cobelli, L.; Duane, M.; Junninen, K.; Astorga, C.; Larsen, B. R. *J. Chromatogr., A* **2003**, *2005*, 29.
(64) Serrano, D. P.; Calleja, G.; Botas, J. A.; Gutierrez, F. *J. Ind. Eng. Chem. Res.* **2004**, *43*, 7010.
(65) Khan, F. K.; Ghosal, A. K. *Journal of Loss Prevention in the Process Industries* **2000**, *13*, 527.
(66) Guillemot, M.; Mijoin, J.; Mignard, S.; Magnoux, P. *Ind. Eng. Chem. Res.* **2007**, *46*, 4614.
(67) Hu, X.; Qiao, S.; Zhao, X.; Lu, G. *Ind. Eng. Chem. Res.* **2001**, *40*, 862.
(68) Fajula, F.; D., P. *Stud. Surf. Sci. Catal.* **1994**, *85*, 633.
(69) Zhao, X. Z.; Ma, Q.; Lu, G. Q. *Energy Fuels* **1998**, *12*, 1051.
(70) Zhao, X. S.; Lu, G. Q.; Hu, X. *Colloids Surf. A* **2001**, *179*, 261.
(71) Zhao, X. S.; Ma, Q.; Lu, G. Q. *Energy Fuels* **1998**, *12*, 1051.
(72) Choudhary, V. R.; Mantri, K. *Langmuir* **2000**, *16*, 7031.
(73) Trouvé, A.; Batonneau-Gener, I.; Valange, S.; Bonne, M.; Mignard, S. *Journal of hazardous materials* **2012**, *201*, 107.
(74) Zhao, X. S.; Lu, G. Q.; Whittaker, A. J.; Millar, G. J.; Zhu, H. Y. *J. Phys. Chem. B* **1997**, *101*, 6525.
(75) Zhao, X. S.; Lu, G. Q.; Zhu, H. Y. *Proceedings of the 24th Australia and New Zealand Chemical Engineering Conference and Exhibition* **1996**, *4*, 39.
(76) Feng, X.; Fryxell, G. E.; Wang, L.-Q.; Kim, A. Y.; Liu, J.; Kemner, K. M. *Science* **1997**, *276*, 923.
(77) Pyda, M.; Wunderlich, B. *Macromolecules* **1999**, *32*, 2044.
(78) Pyda, M. *Macromolecules* **2002**, *35*, 4009.
(79) B., H.; Blum, F. D. *Polymer Preprints* **2008**, *49*.
(80) Pezzin, S. *http://slideplayer.com.br/slide/363854/*.
(81) Instruments., T. *Modulated DSC Compendium, Basic Theory & Experimental Considerations.*
(82) Hetayothin, B.; Blum, F. D. *Polymer Preprints* **2010**, *51*, 480.
(83) Metin, B.; Blum, F. D. *J. Chem. Phys.* **2006**, *125*, 054707/054701.
(84) Damme, H. S.; van Hogt, A. H.; Feijen, J. *J. Colloid Interface Sci.* **1986**, *114*, 167.
(85) Kresge, C. T.; Leonowicz, M. E.; Roth, W. J.; Vartuli, J. C.; Beck, J. S. *Nature* **1992**, *359*, 710
(86) Tanev, P. T.; Chibwe, M.; Pinnavaia, T. J. *Nature* **1994**, *368*, 321.
(87) Wu, C. G.; Bein, T. *Science* **1994**, *264*, 1757.
(88) Wu, C. G.; Bein, T. *Science* **1994**, *266*, 1013.
(89) Wright, A. P.; Davis, M. E. *Chem. Rev.* **2002**, *102*, 3589.

(90) Wouters, B. H.; Chen, T.; Dewilde, M.; Grobet, P. J. *Micro. Meso. Mater.* **2001**, *44-45*, 453.
(91) Zhao, X. S.; Lu, G. Q.; Whittaker, A. K.; Millar, G. J.; Zhu, H. Y. *J. Phys. Chem. B* **1997**, *101*, 6525.
(92) Qian, K. K.; Wurster, D. E.; Bogner, R. H. *Pharmaceutical Research* **2012**, *29*, 2698.
(93) Sayari, A.; Belmabkhout, Y. *J.Am.Chem.Soc.* **2010**, *132*, 6312.
(94) Harlick, P. J. E.; Sayari, A. *Ind. Eng. Chem. Res.* **2007**, *46*, 446.
(95) Tuel, A. a.; Gontier, S. *Chem. Mater.* **1996**, *8*, 114.
(96) Alothmana, Z. A.; Apblettb, A. W. *Chemical Engineering Journal* **2009**, *155*, 916.
(97) Maciel, G. E.; Sindorf, D. W. *J Am Chem Soc* **1980**, *102*, 7606.
(98) Papirer, E. *Adsorption on silica surfaces* **2000**, *Taylor & Francis*, 26.
(99) Papirer, E. *Adsorption on Silica Surfaces* **2000**, 29.
(100) Bennett, A. E.; Rienstra, C. M.; Auger, M.; Lakshmi, K. V.; Griffin, R. G. *Journal of Chemical Physics* **1995**, *103*, 6951.
(101) Zhang, S.; Czekaj, C.; Ford, W. T. *Journal of Magnetic Resonance, Series A* **1994**, *111*, 87.
(102) Jal, P. K.; Patel, S.; Mishra, B. K. *Talanta* **2004**, *62*, 1005.
(103) Lin Y; Fiskum SK; Yantasee W; Wu H; Mattigod SV; Vorpagel E; Fryxell GE; Raymond KN; J., X. *Environ Sci Technol.* **2005**, *39*, 1332.
(104) Sutra, P.; Fajula, F.; Brunel, D.; Lentz, P.; Daelen, G.; Nagy, J. B. *Colloids and Surfaces A: Physicochemical and Engineering Aspects* **1999**, *158*, 21.
(105) Bu, J.; Rhee, H.-K. *Catalysis Letters* **2000**, *65*, 141.
(106) Taib, N. I.; Endud, S.; Katun, M. N. *International Journal of Chemistry* **2011**, *3*, 2.
(107) Li, X.-D.; Zhai, Q.-Z. *J. Iran. Chem. Soc.* **2011**, *8*, S1.
(108) Selvaraj, M.; Pandurangan, A.; Seshadri, K. S.; Sinha, P. K.; Lal, K. B. *Applied Catalysis A: General* **2003**, *242*, 347.
(109) Chu, P. P.; Reddy, M. J.; H.M., K. *Solid State Ionics* **2003**, *156*, 141.
(110) Guo, W.; Huang, L.; Deng, P.; Xue, Z.; Li, Q. *Microporous and Mesoporous Materials* **2001**, *44-45*, 427.
(111) Lafon, O.; Thankamony, A.; Kobayashi, T.; Carnevale, D.; Vitzthum, V.; Slowing, I.; Kandel, K.; Vezin, H.; Amoureux, J.; Bodenhausen, G.; and Pruski, M. *J. Phys. Chem. C* **2013**, *117*, 1375.
(112) Unverferth, K.; Engel, J.; Hofgen, N.; Rostock, A.; Gunther, R.; Lankau, H.; Menzer, M.; Rolfs, A.; Liebscher, J.; Muller, B.; Hofmann, H. *J. Med. Chem.* **1998**, *41*, 63.
(113) http://www.chem.wisc.edu/areas/reich/handouts/nmr-c13/cdata.htm.
(114) Brinker, C. J. *Journal of Non-Crystalline Solids* **1988**, *100*, 31.
(115) McNeil , K. J.; DiCaprio , A.; Walsh , D. A.; Pratt, R. F. *J. Am. Chem. Soc.* **1980**, *102*, 1859.
(116) Hatsuo, I.; Ganesh, K. *Molecular Characterization of Composite Interfaces* **1985**, *27*, 453.
(117) Pope, E. J. A.; Mackenzie, J. D. *Journal of Non-Crystalline Solids* **1986**, *87*, 185.
(118) Brinker , C. J.; Clark , D. E.; Ulrich, D. R. *New York: Elsevier Science* **1984**, 15.

(119) Brinker , C. J.; Clark , D. E.; Ulrich, D. R. *New York: Elsevier Science* **1984**, 59.
(120) Khan, F. K. G.; Ghoshal, A. K. *Journal of Loss Prevention in the Process Industries* **2000**, *13*, 527.
(121) Seo, H. K.; Oh, J. W.; Choung, S. J. *Stud. Surf. Sci. Catal.* **2001**, *135*, 328.
(122) Kresge, C. T.; Leonowicz, M. E.; Roth, W. J.; Vartuli, J. C.; Beck, J. S. *Nature* **1992**, *359*, 710.
(123) Shiu, W.-Y.; Ma, K.-C. *J. Phys. Chem. Ref. Data* **2000**, *29*, 41.
(124) Chickos, J. S.; Acree Jr., W. E. *J. Phys. Chem. Ref. Data* **2002**, *31*, 537.
(125) Eusébio, M. E.; Lopes Jesus, A. J.; Cruz, M. S. C.; Leitão, M. L. P.; Simões Redinha, J. *J. Chem. Thermodyn.* **2003**, *35*, 123.
(126) Sabbah, R.; Antipine, I.; Coten, M.; Davy, L. *Thermochim. Acta* **1987**, *115*, 153.
(127) Rojas-Aguilar, A.; E. Orozco-Guareño, E.; Martinez-Herrera, M. *J. Chem. Thermodyn.* **2001**, *33*, 1405.
(128) Ribeiro da Silva, M. A. V.; Monte, M. J. S.; Ribeiro, J. R. *J. Chem. Thermodyn.* **2011**, *33*, 23.
(129) Hoch, M.; Johnston, H. L. *J. Phys. Chem. B* **1961**, *65*, 855.
(130) Chickos, J. S.; Acree Jr., W. E. *J. Phys. Chem. Ref. Data* **2002**, *31*, 537.
(131) Bilde, M.; Svenningsson, B.; Mønster, J.; Rosenørn, T. *Environ. Sci. Technol.* **2003**, *37*, 1371.
(132) Cappa, C. D.; Lovejoy, E. R.; Ravishankara, A. R. *J. Phys. Chem. A* **2008**, *112*, 3959.
(133) Czarnecki, J.; Sestak, J. *J. Therm. Anal. Calorim.* **2000**, *60*, 759.
(134) Hajimirsadeghis, S. S.; Teimouri, M. R.; Rahimi-Nasrabadi, M.; Dehghanpour, S. *J. Therm. Anal. Calorim.* **2009**, *98*, 463.
(135) Hikal, W. M.; Bhattacharia, S. K.; Peterson, G. R.; Weeks, B. L. *Thermochem. Acta* **2012**, *536*, 63.
(136) Hobbs, M. L.; Nakos, J. T.; Brady, P. D. J. *J. Therm. Anal. Calorim.* **2011**, *103*, 543.
(137) Hikal, W. M.; Paden, J. T.; Weeks, B. L. *J. Phys. Chem. B* **2011**, *115* 13287.
(138) Hikal, W. M.; Paden, J. T.; Weeks, B. L. *Talanta* **2011**, *87*, 290.
(139) Hikal, W. M.; Weeks, B. L. *J. Therm. Anal. Calorim.* **2012**, *110*, 955.
(140) Hikal, W. M.; Paden, J. T.; Weeks, B. L. *Chem. Phys. Chem.* **2012**, *13*, 2729.
(141) Ingle, J. D. J.; Crouch, S. R. *Spectrochemical Analysis, Prentice Hall, New Jersey* **1988**.
(142) Griesser, U. J.; Szelagiewicz, M.; Hofmeier, U. C.; Pitt, C.; Cianferani, S. J. *Therm. Anal. Calorimetry* **1999**, *57*, 45.
(143) Acree Jr., W.; Chickos, J. S. *Journal of Physical and Chemical Reference Data* **2010**, *39*.
(144) Chickos, J. S.; Hesse, D. G.; Hosseini, S.; Nichols, G.; Webb, P. *Thermochim. Acta* **1998**, *313*, 101.
(145) Nass, K.; Lenoir, D.; Kettrup, A. *Angew. Chem. Int. Ed. Engl.* **1995**, *34*, 1735.
(146) Khudyakov, V. L. *Russ. J. Phys. Chem. A* **1988**, *62*, 1743.
(147) Torres-Gomez, L. A.; Barreiro-Rodriguez, G.; Galarza-Mondragon, A. *Thermochim. Acta* **1988**, *124*, 229.

(148) DeKruif, C. G.; Kuipers, T.; van Miltenburg, J. C.; Schaake, R. C. F.; Stevens, G. J. *J. Chem. Thermodyn.* **1981**, *13*, 1081.

(149) Van Ekeren, P. J.; Jacobs, M. H. G.; Offringa, J. C. A.; DeKruif, C. G. *J. Chem. Thermodyn.* **1983**, *15*, 409.

(150) Murata, S.; Sakiyama, M.; Seki, S. *J. Chem. Thermodyn.* **1982**, *14*, 723.

(151) McEachern, D. M.; Sandoval, O.; Iniguez, J. C. *J. Chem. Thermodyn.* **1975**, *7*, 299.

(152) Chickos, J. S. *J. Chem. Educ.* **1975**, *52*, 134.

(153) McEachern, D. M.; Sandoval, O. *J. Phys. E.* **1973**, *6*, 155.

(154) Miller, G. A. *J. Chem. Eng. Data* **1963**, *8*, 69.

(155) Cox, J. D.; Pilcher, G. *Thermochemistry of Organic and Organometallic Compounds ~Academic, NewYork* **1970**.

(156) Aihara, A. *Bull. Chem. Soc. Jpn.* **1959**, *32*, 1242.

(157) Andrews, M. R. *J. Phys. Chem. A* **1926**, *30*, 1497.

(158) Dreisbach, R. R. *Physical Properties of Chemical Compounds, Adv. Chem. Ser. 15 ~American Chemical Society, Washington, D.C.* **1955**.

(159) Osborn, A. G.; Douslin, D. R. *J. Chem. Eng. Data 20*, 229.

(160) Boller, A.; Wiedemann, H. G. *J. Therm. Anal. Calorim.* **1998**, *53*.

(161) Dean, J. A. *Lange's Handbook of Chemistry, 14th ed. McGraw-Hill, New York, N.Y.* **1992**.

(162) Stephenson, R. M.; Malanowski, S. *Handbook of theThermodynamics of Organic Compounds _Elsevier: NewYork* **1987**.

(163) Riddick, J. A.; Bunger, W. B.; Sakano, T. K. *Organic Solvents: Physical Properties and Methods of Purification, 4th ed. Wiley, New York* **1986**.

(164) Natarajan, G.; Viswanath, D. S. *J. Chem. Eng. Data* **1985**, *30*.

(165) Weast, R. *Handbook of Chemistry and Physics, 63rd. ed. CRC, Boca Raton, FL* **1982–83**.

(166) Lenchitz, C.; Velicky, R. *J. Chem. Eng. Data* **1970**, *15*, 401.

(167) Chickos, J. S.; Hosseini, S.; Hesse, D. G. *Thermochim.Acta* **1995**, *249*.

(168) Stephenson, R. M.; Malanowski, S. *Elsevier, New York* **1987**.

(169) Zaraiskii, A. P. *Zh. Fiz. Khim.* **1985**, *59*.

(170) Lebedeva, N. D.; Katin, Y. A.; Akhmedova, G. Y. *Russ. J. Phys. Chem. A* **1971**, *45*.

(171) Kusano, K.; Wadso, I. *Bull. Chem. Soc. Jpn.* **1971**, *44*, 1705.

(172) Sklyarenko, S. I.; Markin, B. I.; Belyaeva, L. B. *Zh. Fiz. Khim.* **1958**, *32*.

(173) Sklyarenko, S. I.; Markin, B. I.; Belyaeva, L. B. *Chem. Abstr.* **1959**, *53*.

(174) Oliver, G. D.; Grisard, J. W. *J. Am. Chem. Soc.* **1952**, *74*.

(175) Boublik, T.; Fried, V.; Hala, E. *The Vapour Pressures of Pure Substances: Selected Values of the Temperature Dependence of the Vapour Pressures of Some Pure Substances in the Normal and Low Pressure Region, 2nd ed. Elsevier, Amsterdan* **1984**.

(176) Toral, M. T.; Moles, E. *An. R. Soc. Esp. Fis. Quim.* **1933**, *31*.

(177) Toral, M. T.; Moles, E. *Chem. Abstr.* **1934**, *28*.

APPENDICES

APPENDIX A – *Temperature-Modulated Calorimetry (TMDSC) Thermograms for Adsorbed Polymers on Silica*, **Chapter II**

This appendix includes supporting Figures for the work done on TMDSC experiments. The area integrations of adsorbed PVAc on silica at various adsorbed amounts for three different molecular masses (100 kDa, 170 kDa, and 260 kDa) are shown in Figures A1-A15.

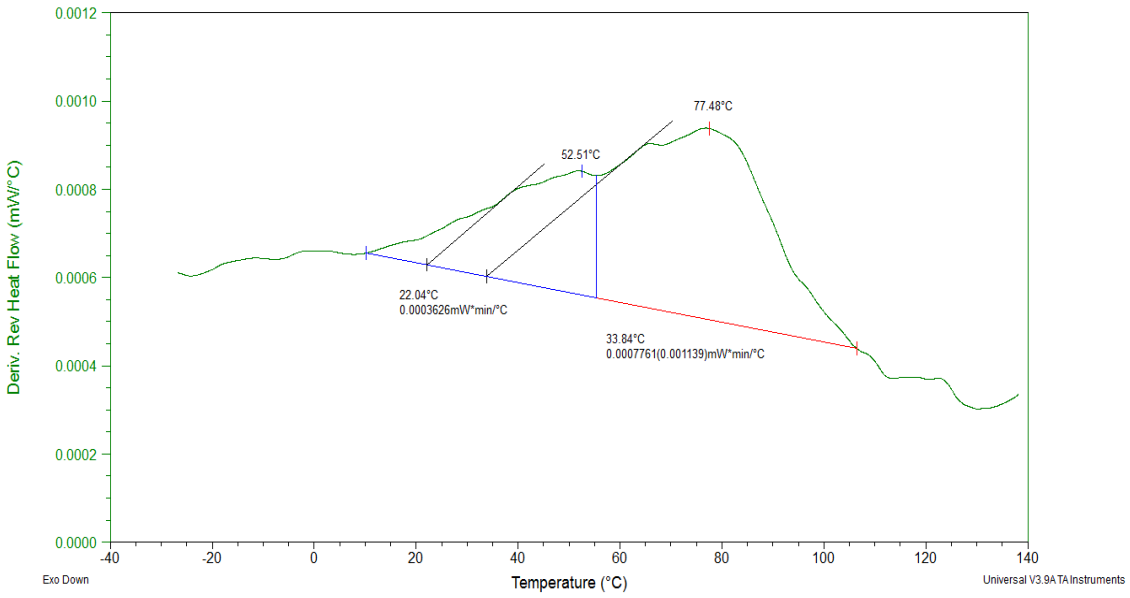

Figure A1. TMDSC thermogram of 100 kDa adsorbed PVAc on silica, 0.3 mg/m^2.

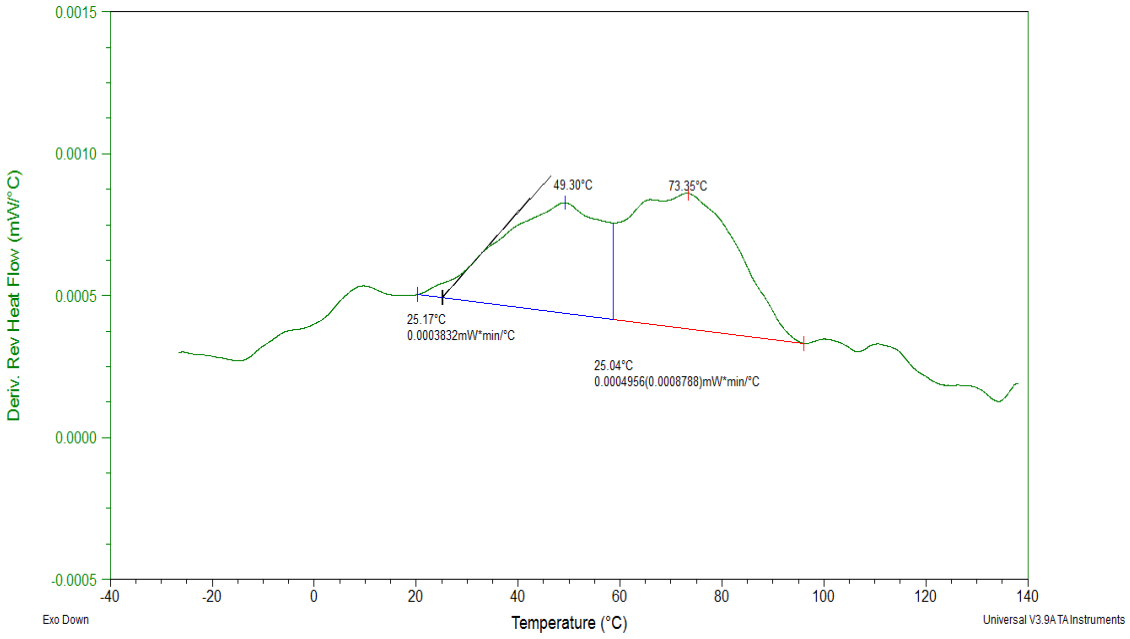

Figure A2. TMDSC thermogram of 100 kDa adsorbed PVAc on silica, 1.02 mg/m^2.

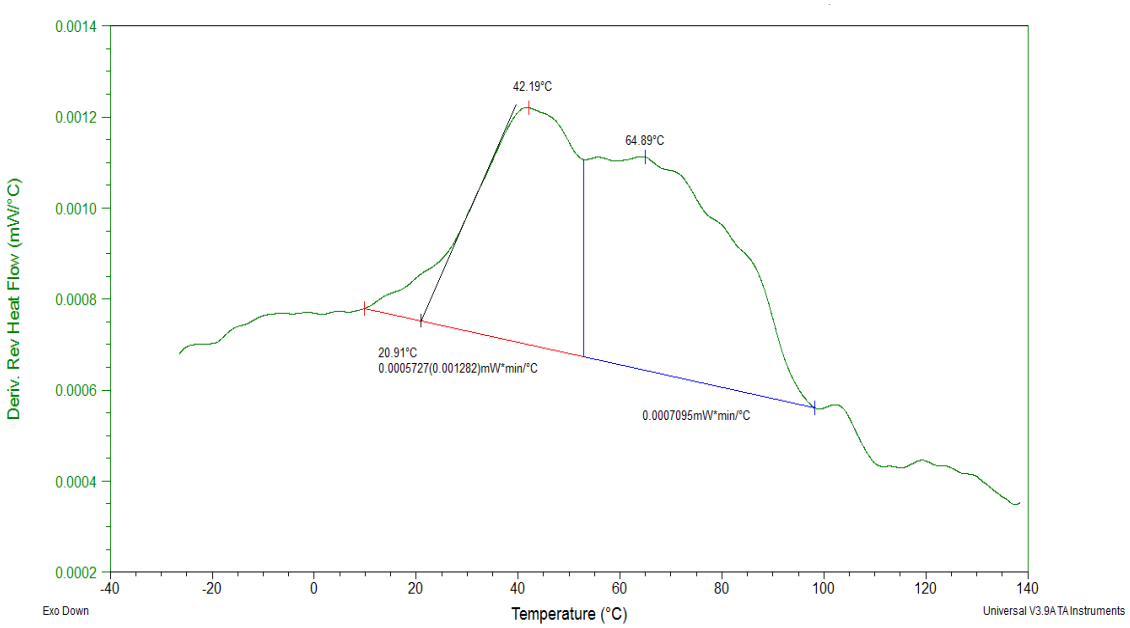

Figure A3. TMDSC thermogram of 100 kDa adsorbed PVAc on silica, 1.11 mg/m^2.

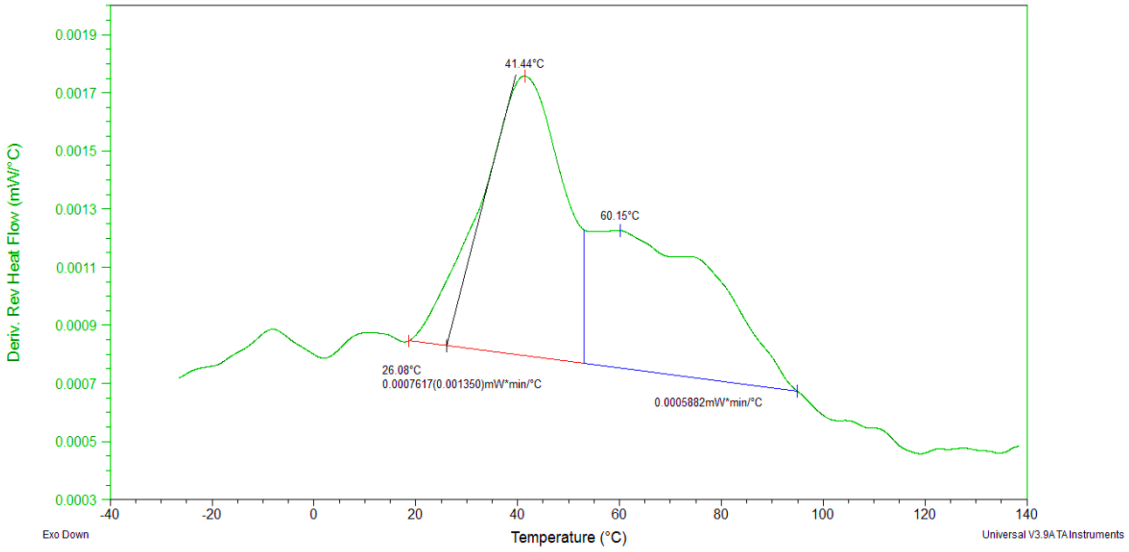

Figure A4. TMDSC thermogram of 100 kDa adsorbed PVAc on silica, 1.41 mg/m^2.

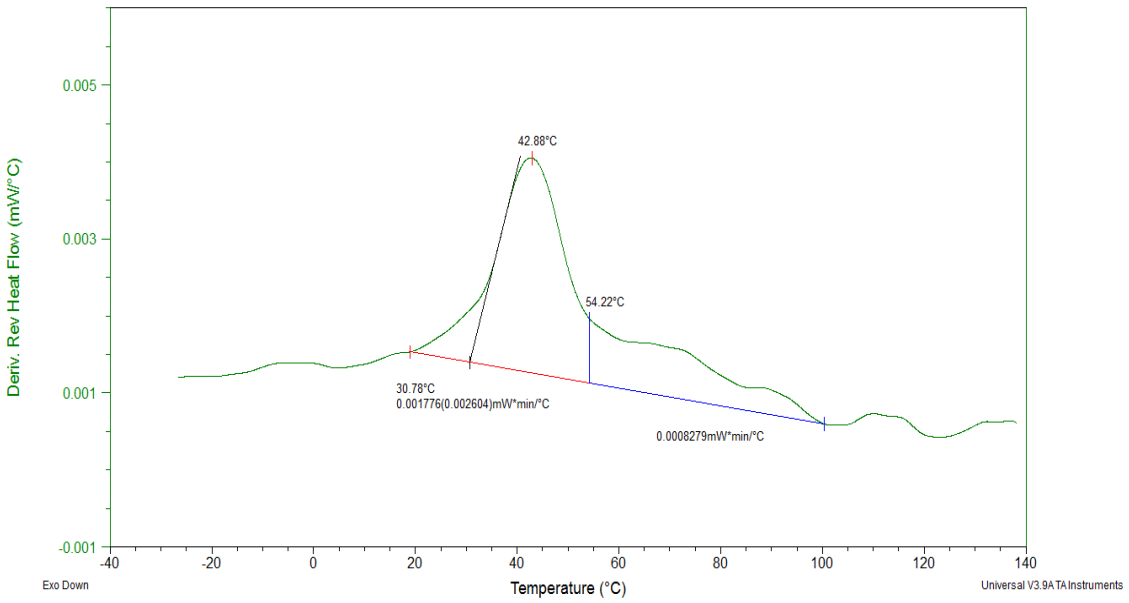

Figure A5. TMDSC thermogram of 100 kDa adsorbed PVAc on silica, 1.98 mg/m^2.

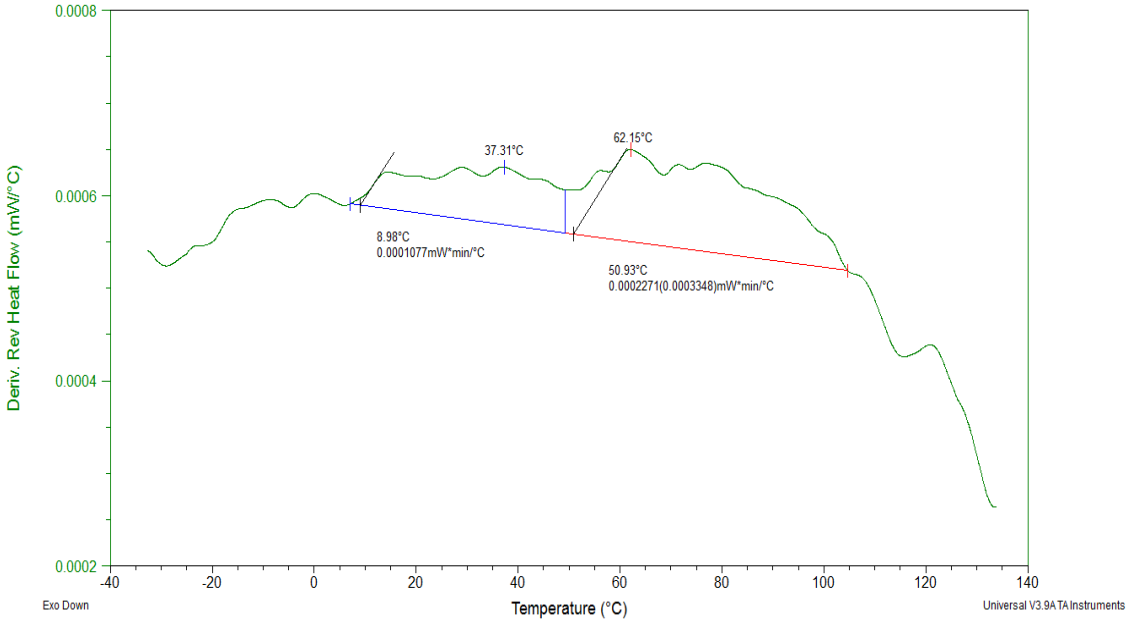

Figure A6. TMDSC thermogram of 170 kDa adsorbed PVAc on silica, 0.46 mg/m^2.

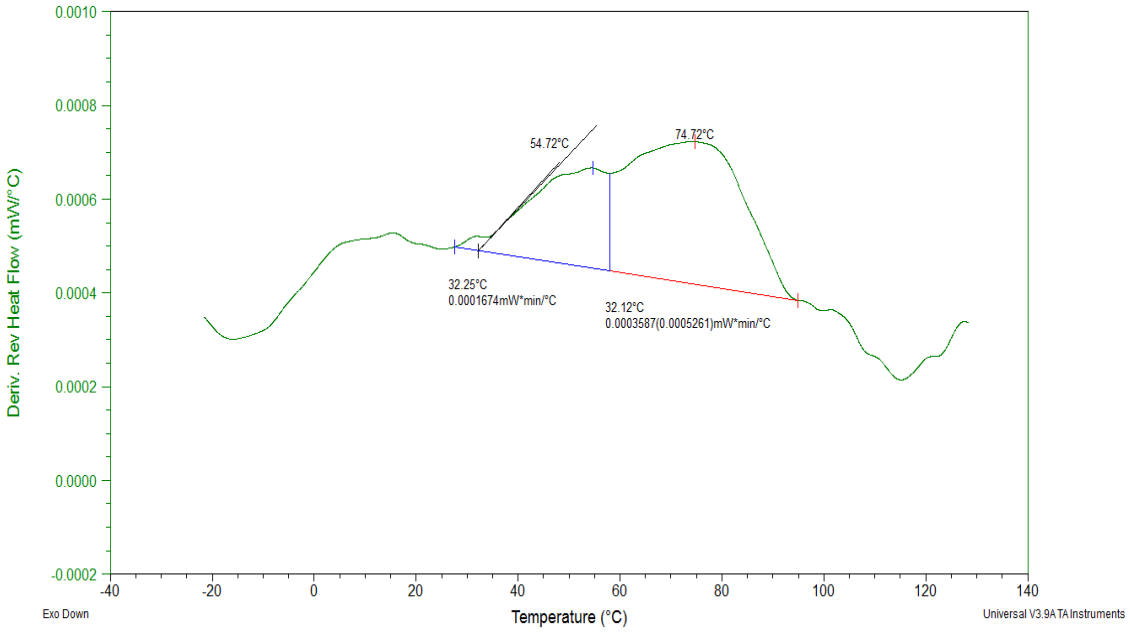

Figure A7. TMDSC thermogram of 170 kDa adsorbed PVAc on silica, 0.99 mg/m^2.

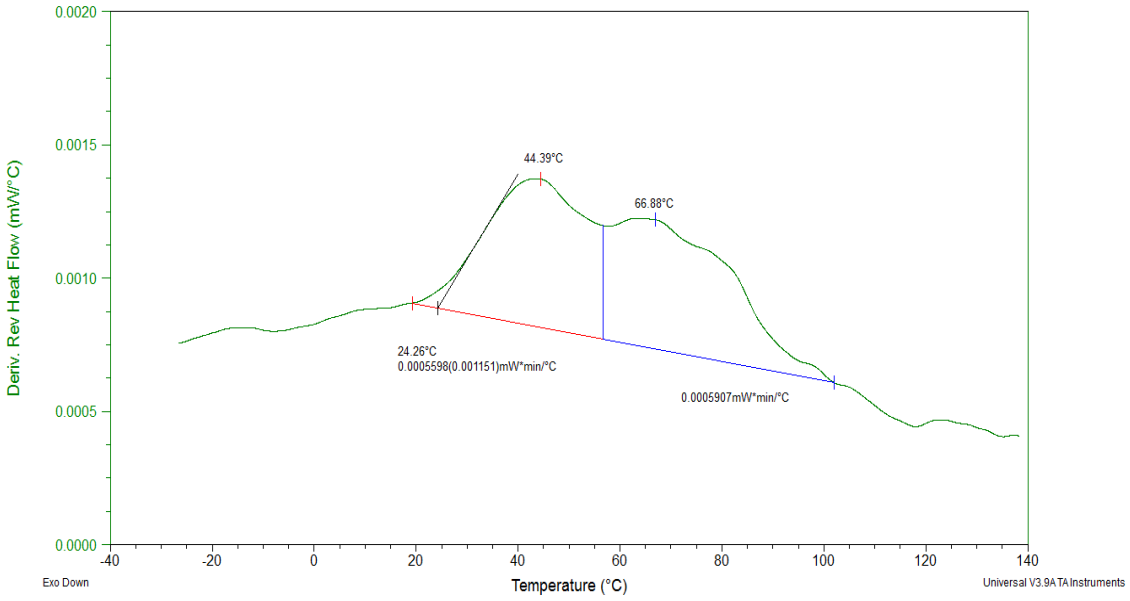

Figure A8. TMDSC thermogram of 170 kDa adsorbed PVAc on silica, 1.09 mg/m^2.

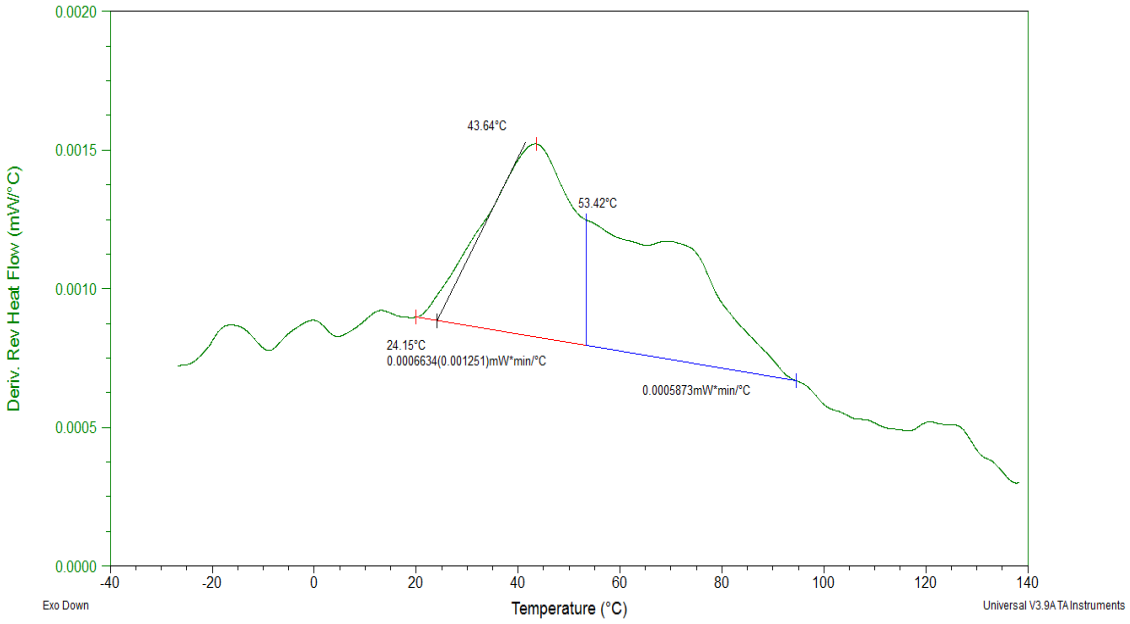

Figure A9. TMDSC thermogram of 170 kDa adsorbed PVAc on silica, 1.25 mg/m^2.

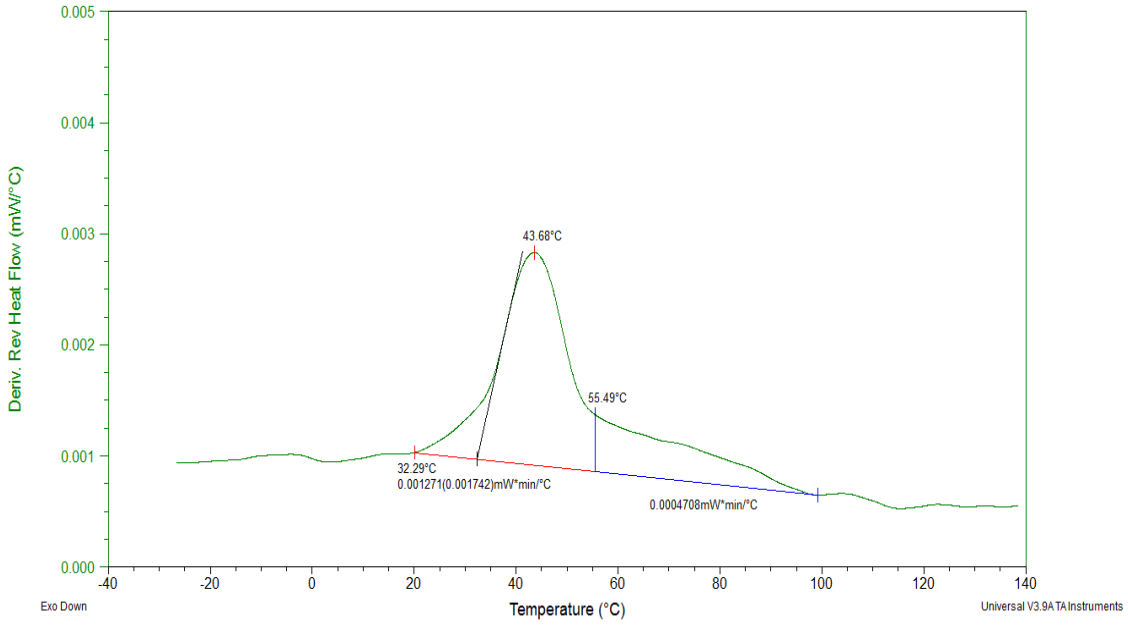

Figure A10. TMDSC thermogram of 170 kDa adsorbed PVAc on silica, 2.11 mg/m^2.

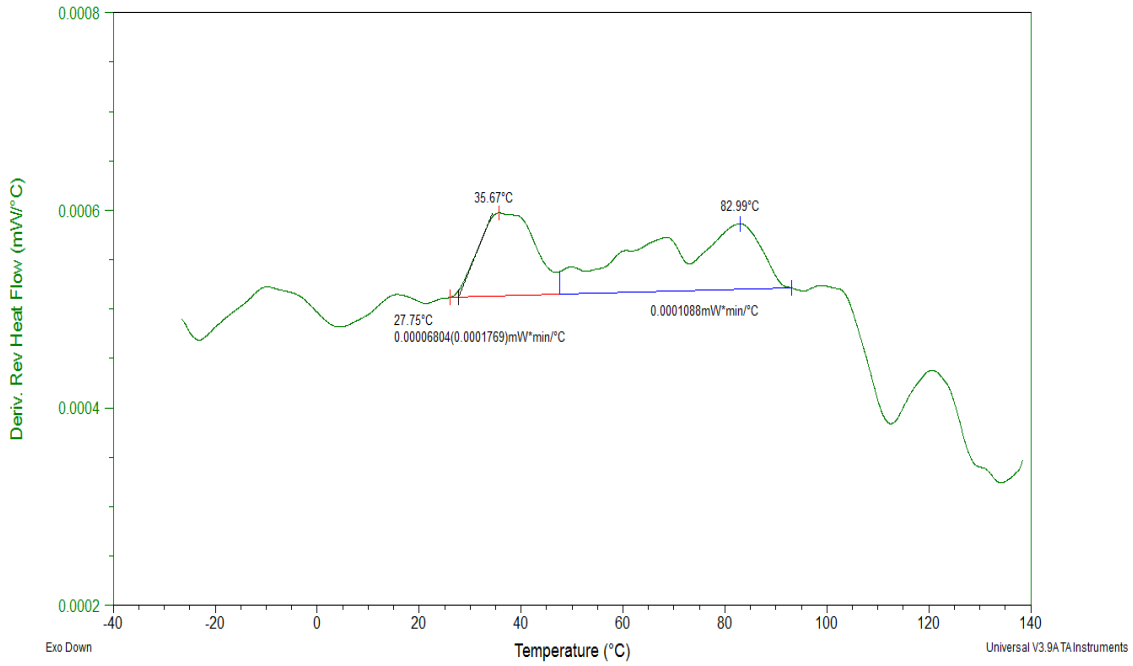

Figure A11. TMDSC thermogram of 260 kDa adsorbed PVAc on silica, 0.71 mg/m^2.

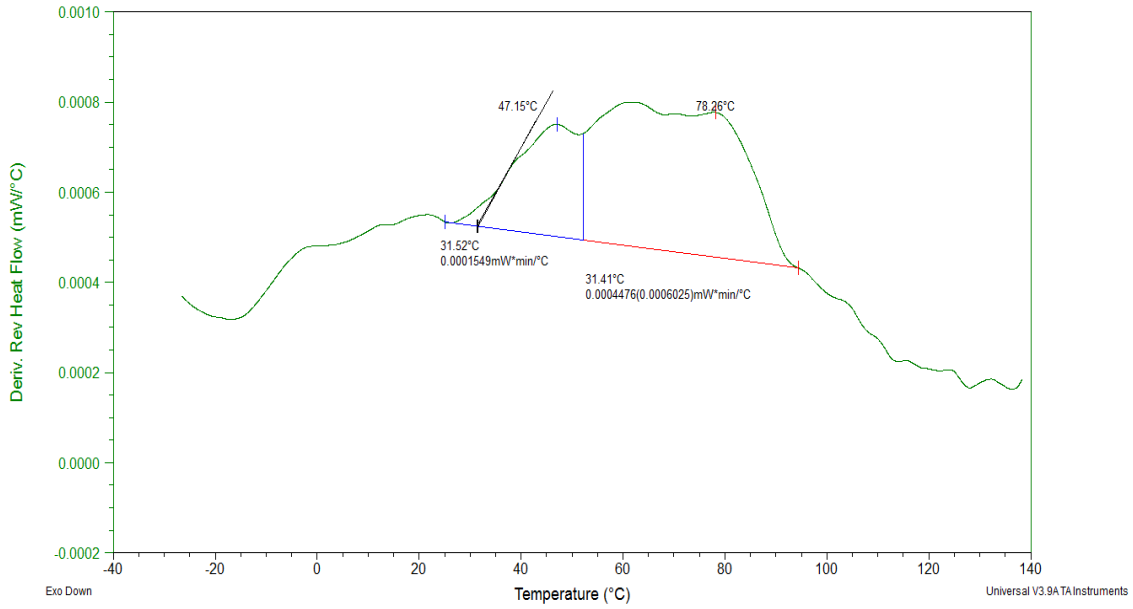

Figure A12. TMDSC thermogram of 260 kDa adsorbed PVAc on silica, 1.09 mg/m^2.

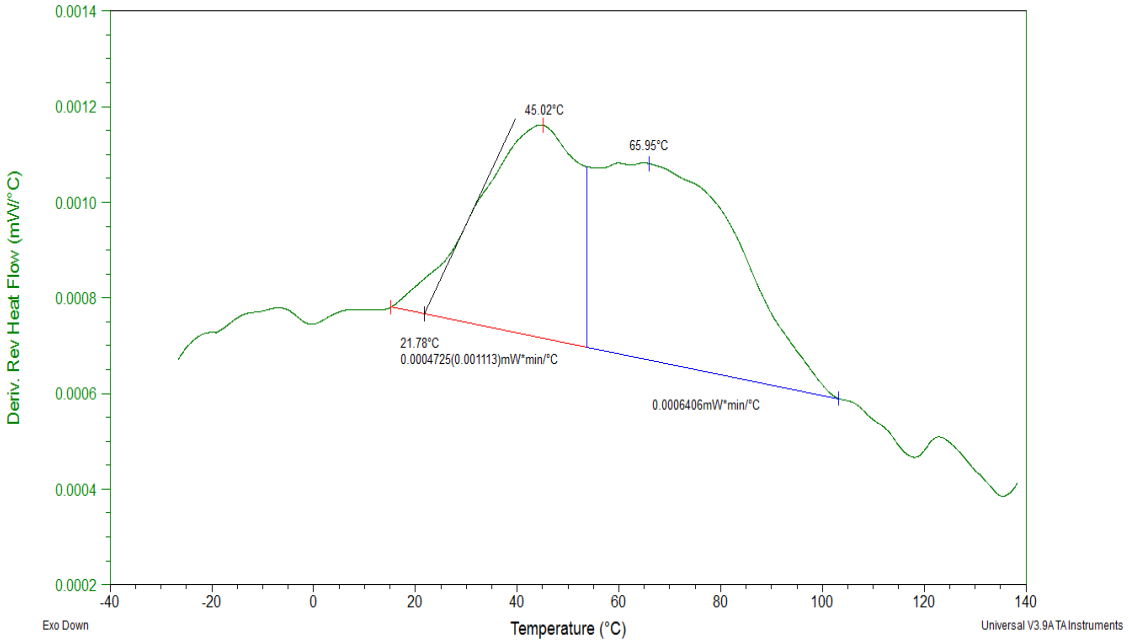

Figure A13. TMDSC thermogram of 260 kDa adsorbed PVAc on silica, 1.15 mg/m^2.

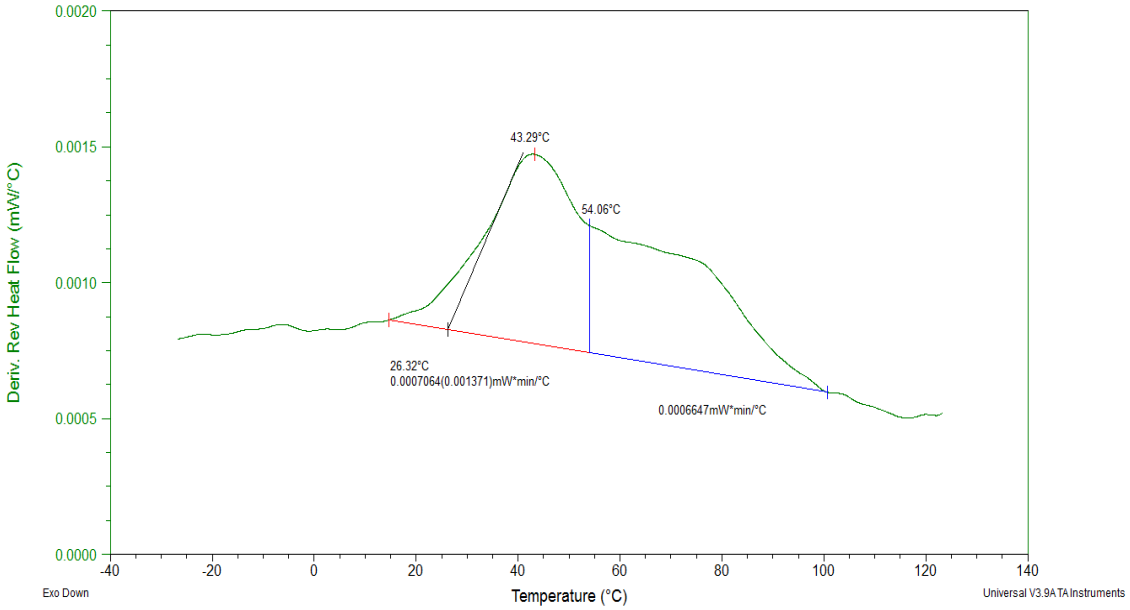

Figure A14. TMDSC thermogram of 260 kDa adsorbed PVAc on silica, 1.42 mg/m^2.

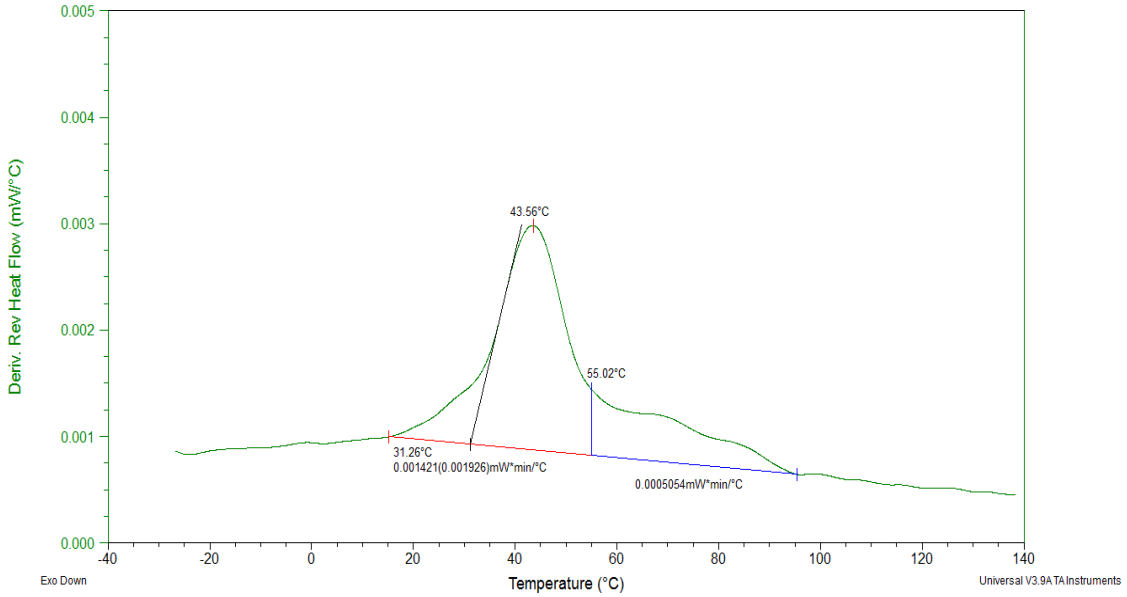

Figure A15. TMDSC thermogram of 260 kDa adsorbed PVAc on silica, 2.06 mg/m^2.

APPENDIX B – *UV-absorbance spectra of the vapor phase*, **Chapter IV**

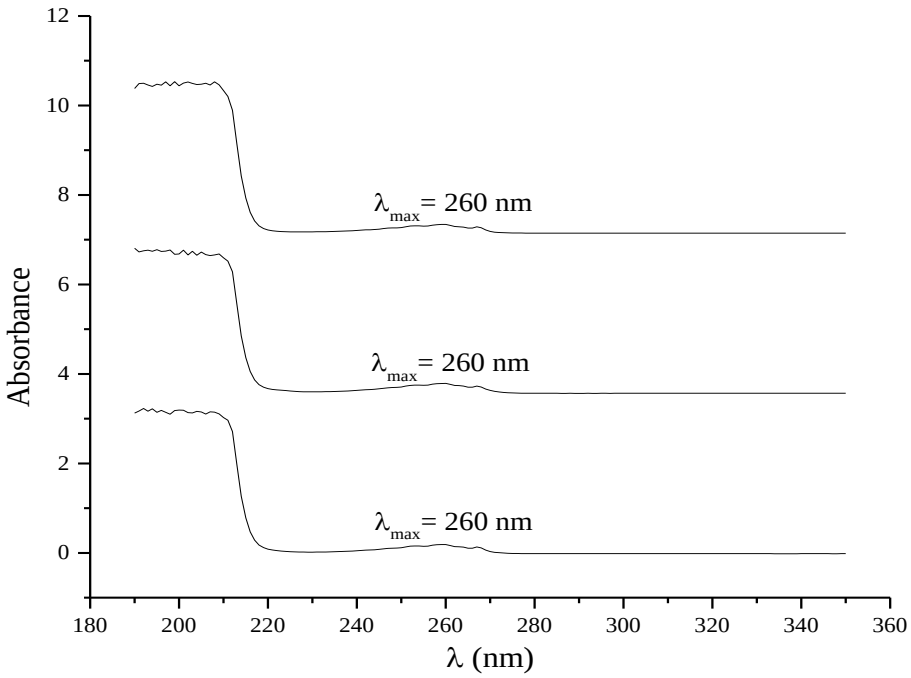

Figure B1. UV-absorbance spectra of the vapor phase of toluene at 20 °C.

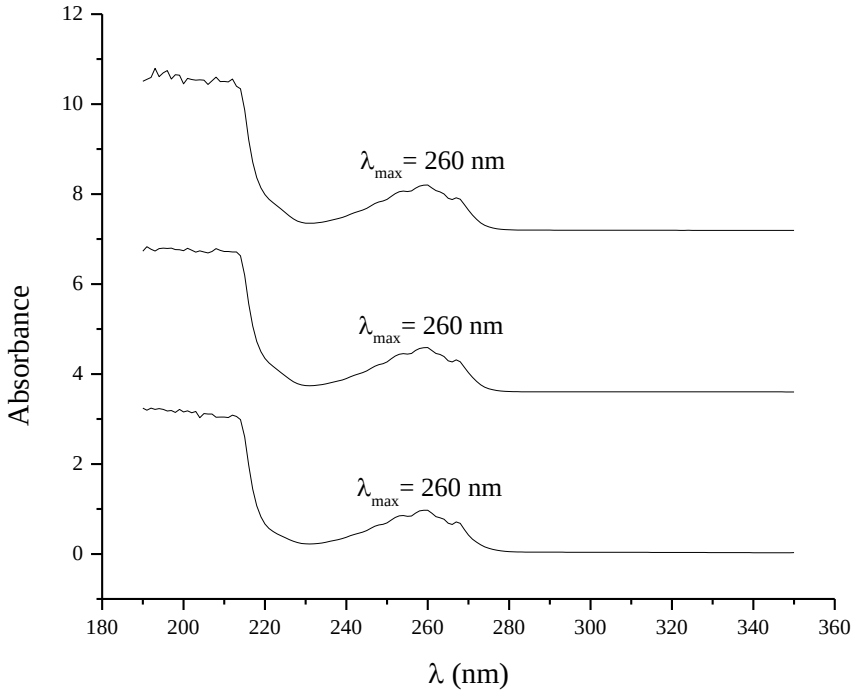

Figure B2. UV-absorbance spectra of the vapor phase of toluene at 50 °C.

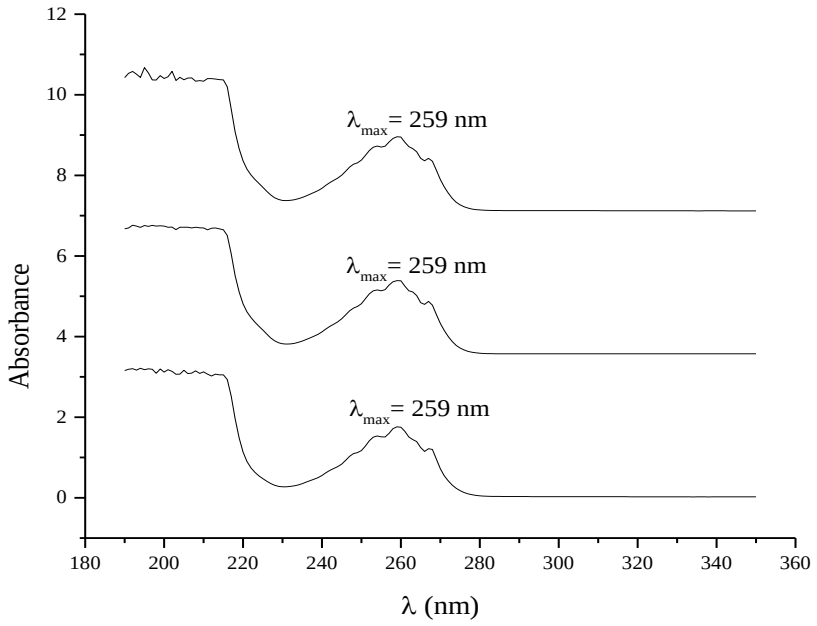

Figure B3. UV-absorbance spectra of the vapor phase of toluene at 70 °C.

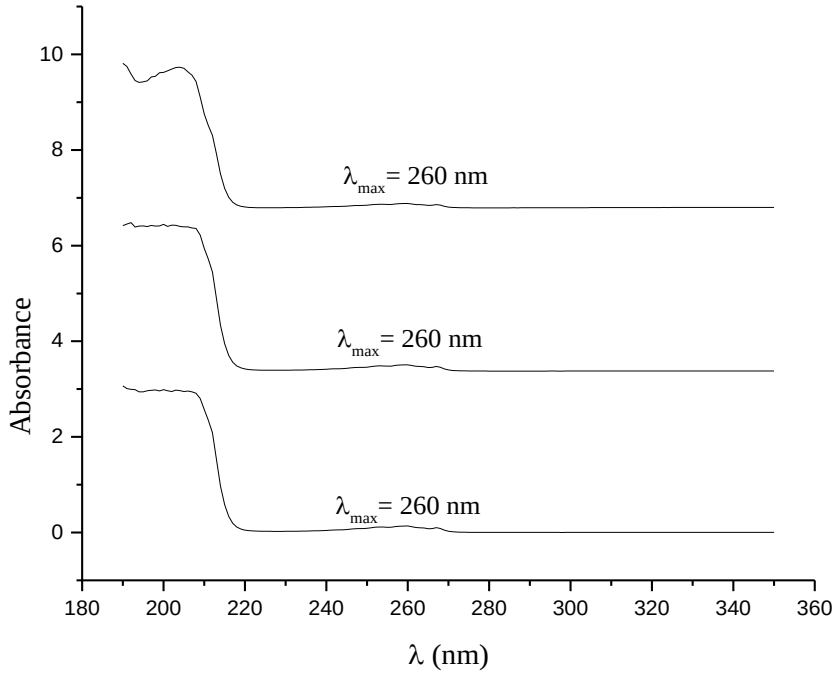

Figure B4. UV-absorbance spectra of the vapor phase of OSU-6 loaded with toluene at 20 °C.

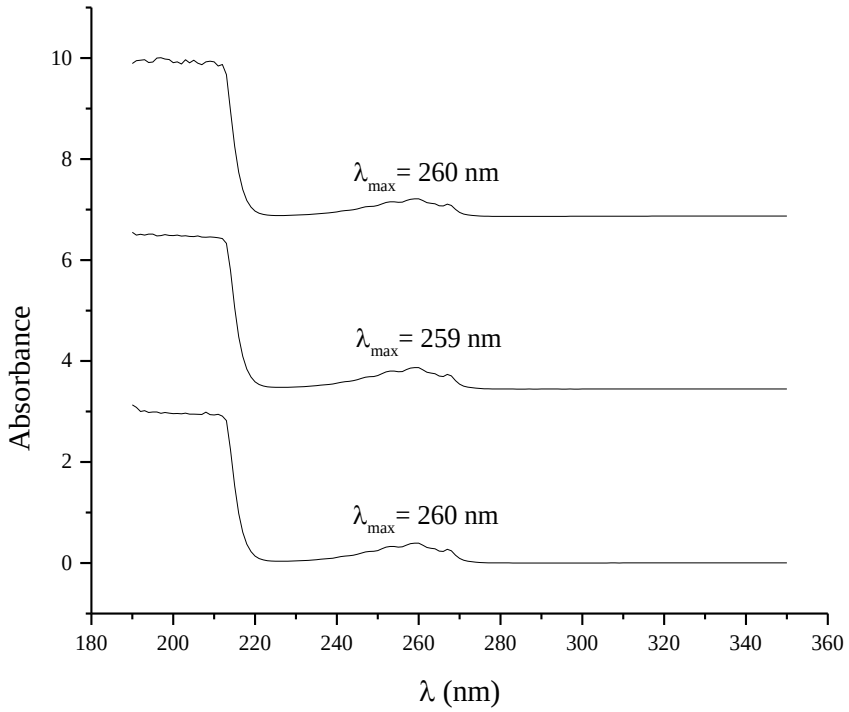

Figure B5. UV-absorbance spectra of the vapor phase of OSU-6 loaded with toluene at 50 °C.

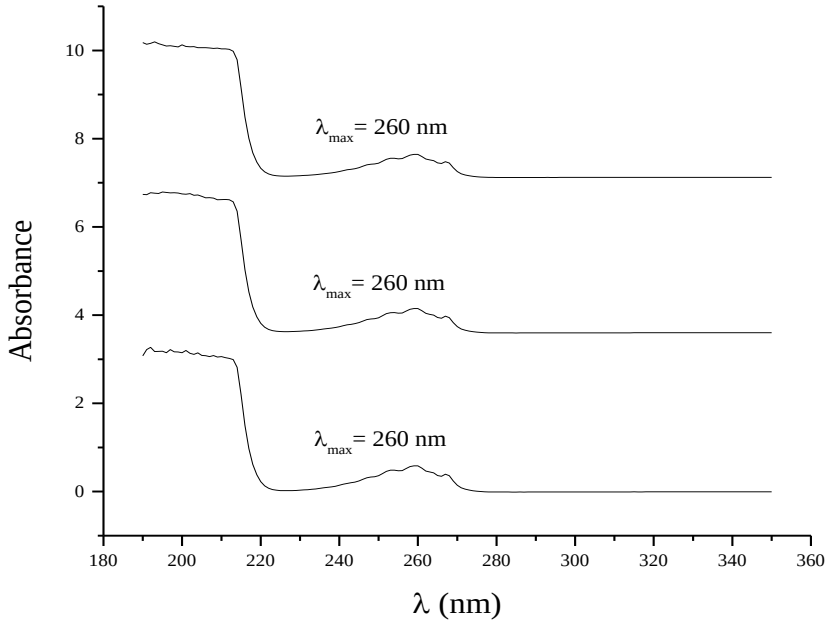

Figure B6. UV-absorbance spectra of the vapor phase of OSU-6 loaded with toluene at 70 °C.

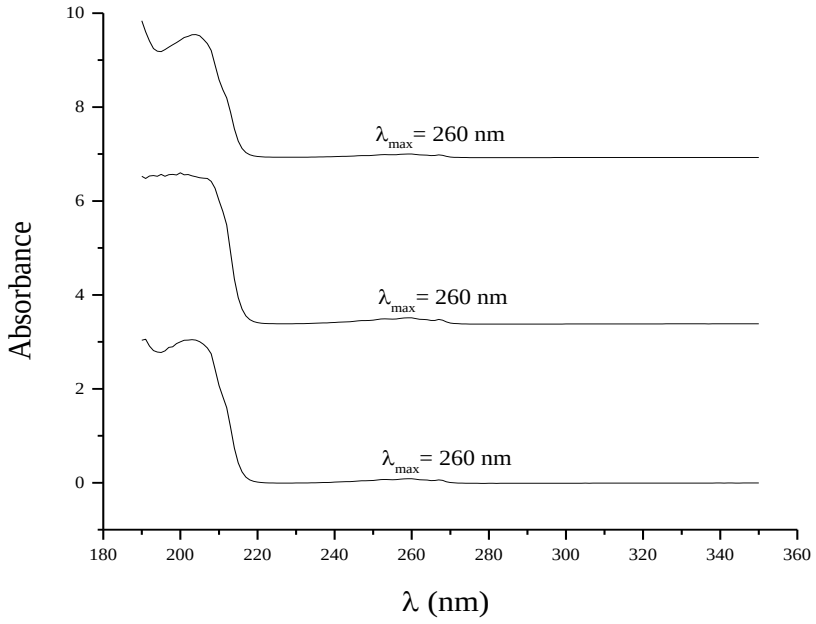

Figure B7. UV-absorbance spectra of the vapor phase of OSU-6 functionalized with hexyltrimethoxysilane loaded with toluene at 20 °C.

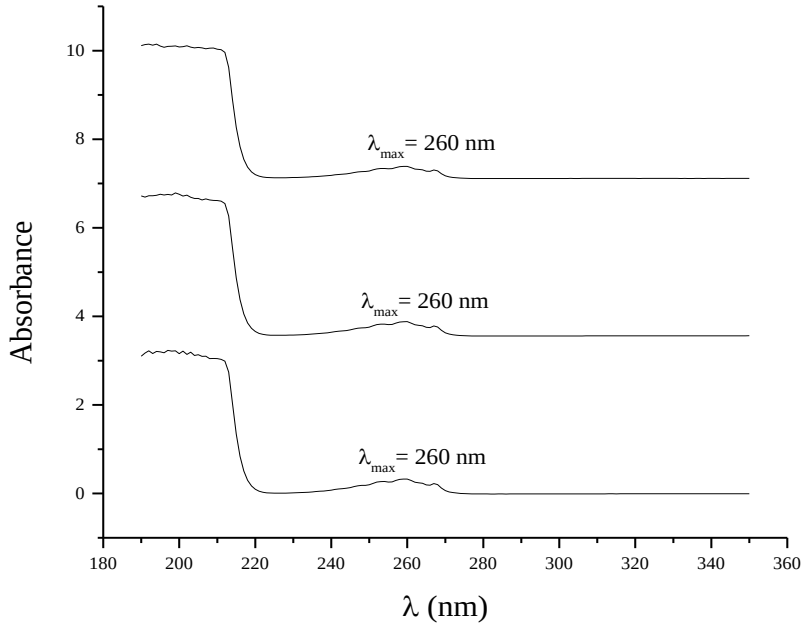

Figure B8. UV-absorbance spectra of the vapor phase of OSU-6 functionalized with hexyltrimethoxysilane loaded with toluene at 50 °C.

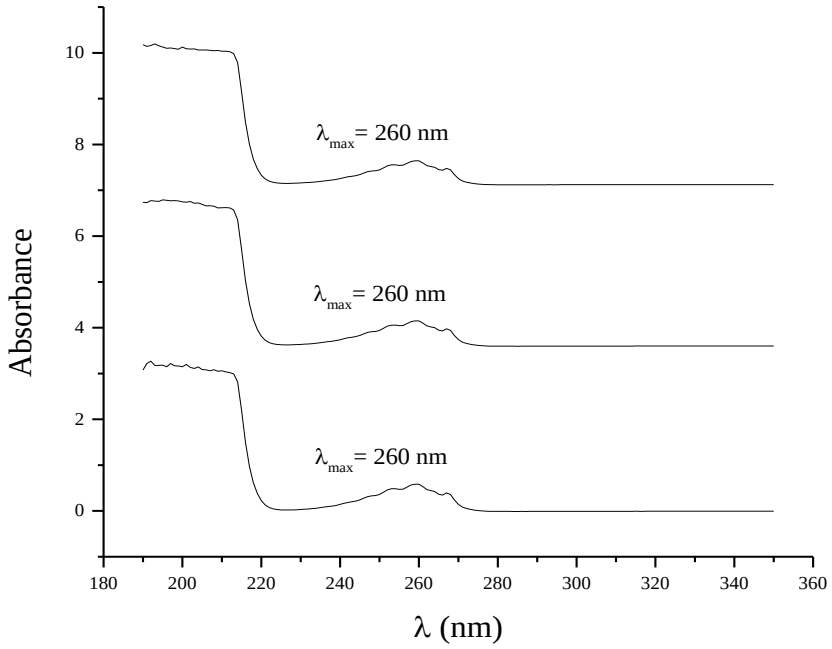

Figure B9. UV-absorbance spectra of the vapor phase of OSU-6 functionalized with hexyltrimethoxysilane loaded with toluene at 70 °C.

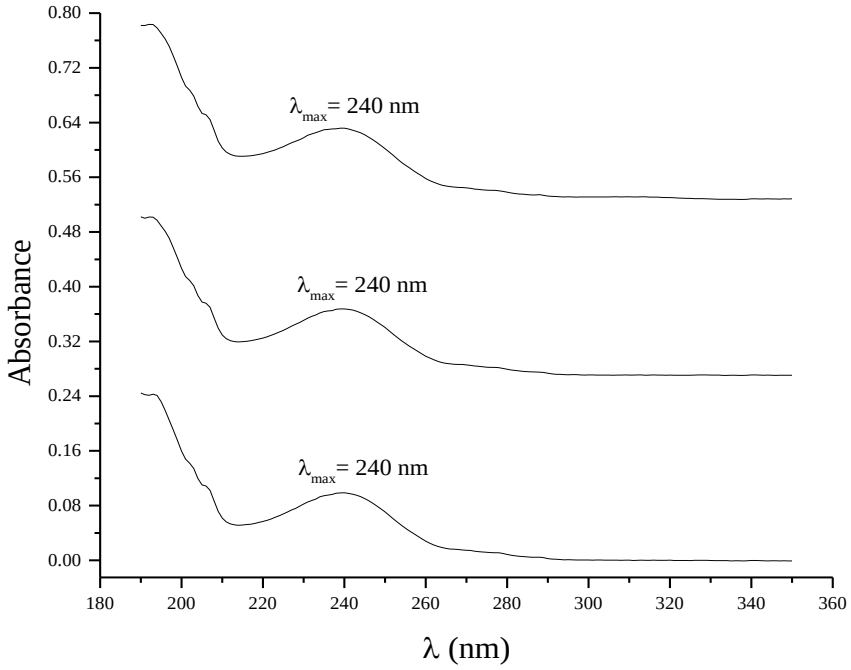

Figure B10. UV-absorbance spectra of the vapor phase of nitrobenzene at 20 °C.

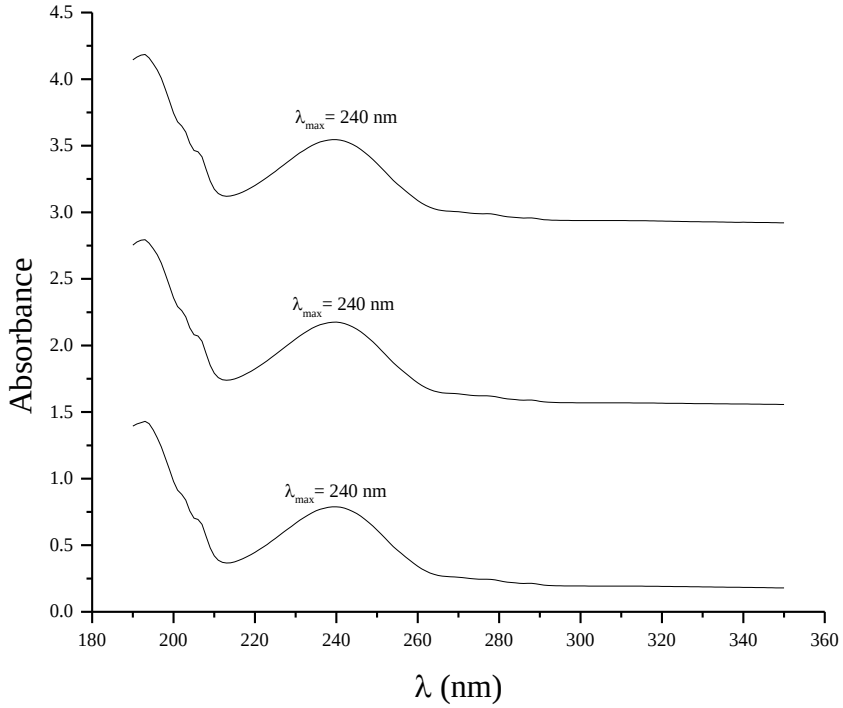

Figure B11. UV-absorbance spectra of the vapor phase of nitrobenzene at 50 °C.

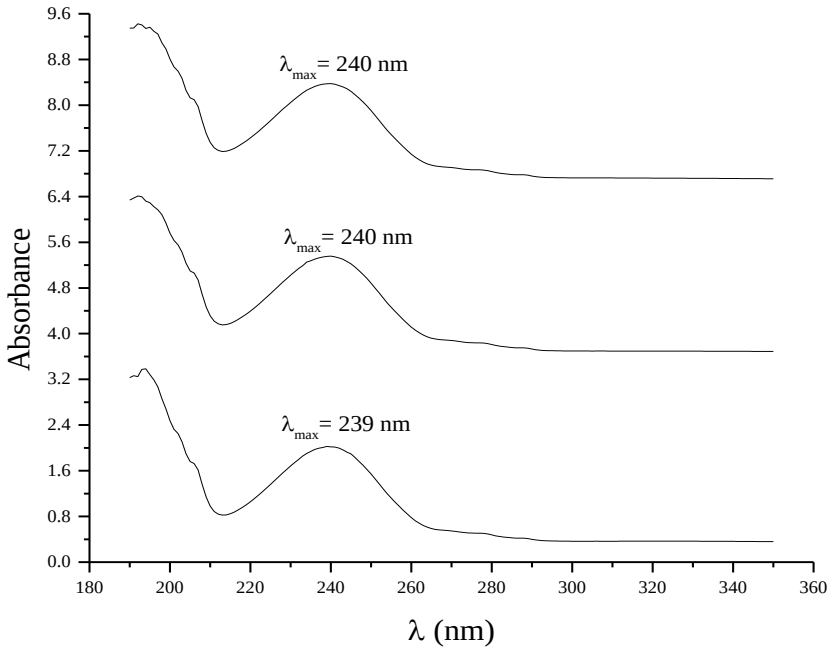

Figure B12. UV-absorbance spectra of the vapor phase of nitrobenzene at 70 °C.

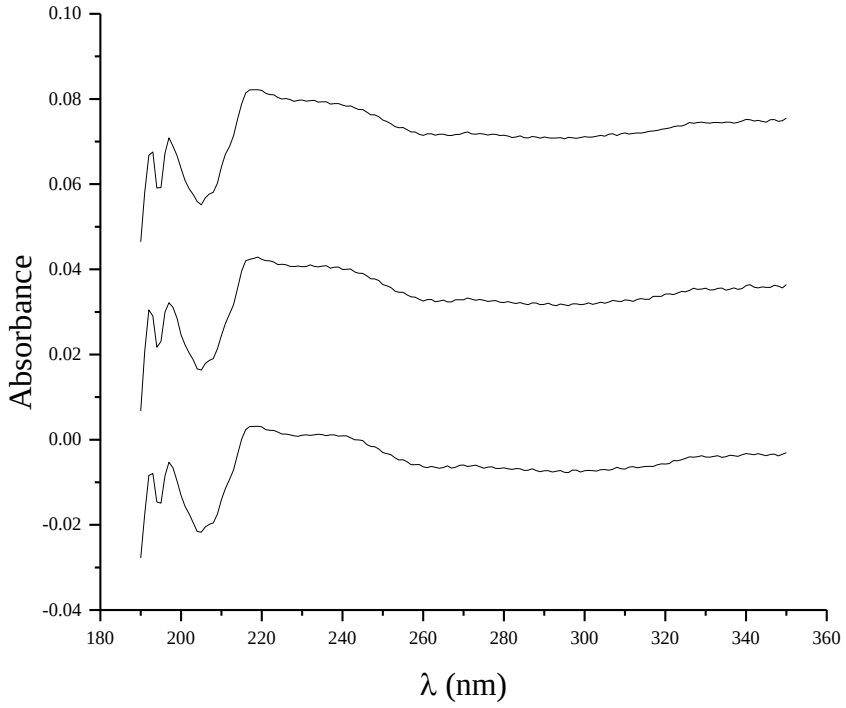

Figure B13. UV-absorbance spectra of the vapor phase of OSU-6 loaded with nitrobenzene at 20 °C.

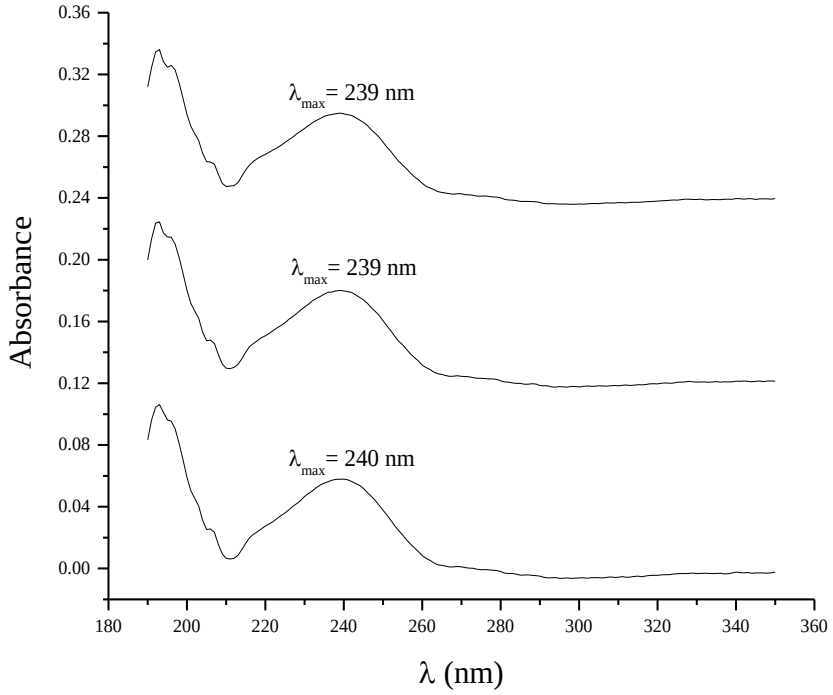

Figure B14. UV-absorbance spectra of the vapor phase of OSU-6 loaded with nitrobenzene at 50 °C.

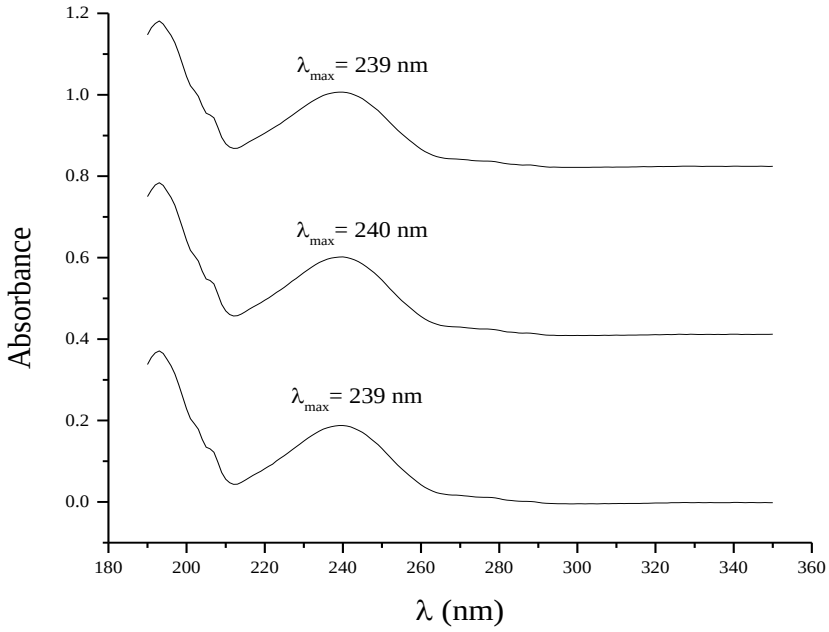

Figure B15. UV-absorbance spectra of the vapor phase of OSU-6 loaded with nitrobenzene at 70 °C.

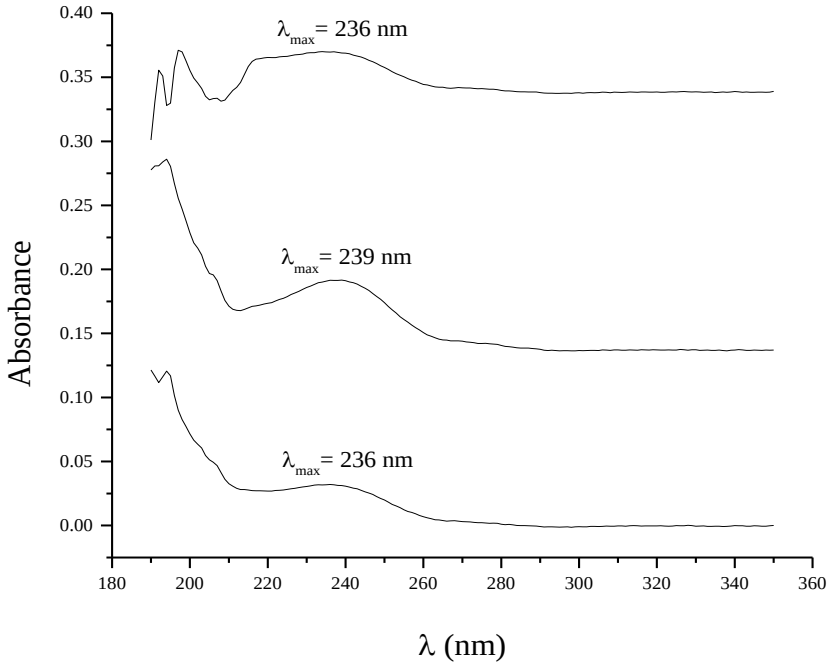

Figure B16. UV-absorbance spectra of the vapor phase of OSU-6 functionalized with hexyltrimethoxysilane loaded with nitrobenzene at 20 °C.

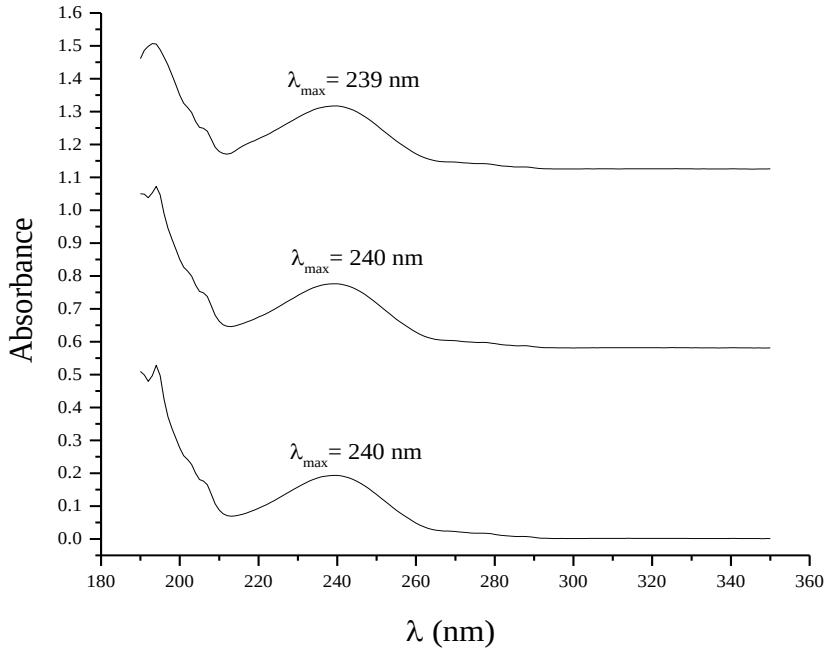

Figure B17. UV-absorbance spectra of the vapor phase of OSU-6 functionalized with hexyltrimethoxysilane loaded with nitrobenzene at 50 °C.

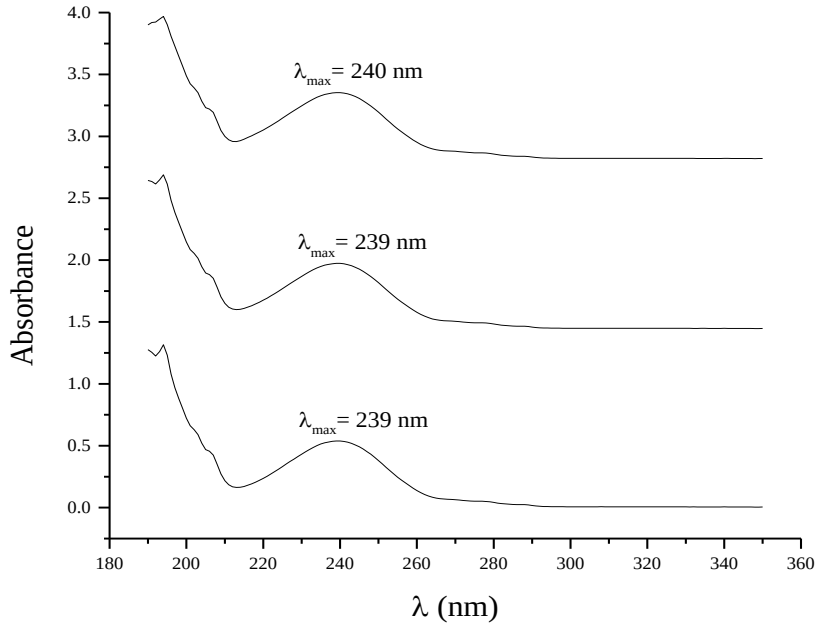

Figure B18. UV-absorbance spectra of the vapor phase of OSU-6 functionalized with hexyltrimethoxysilane loaded with nitrobenzene at 70 °C.

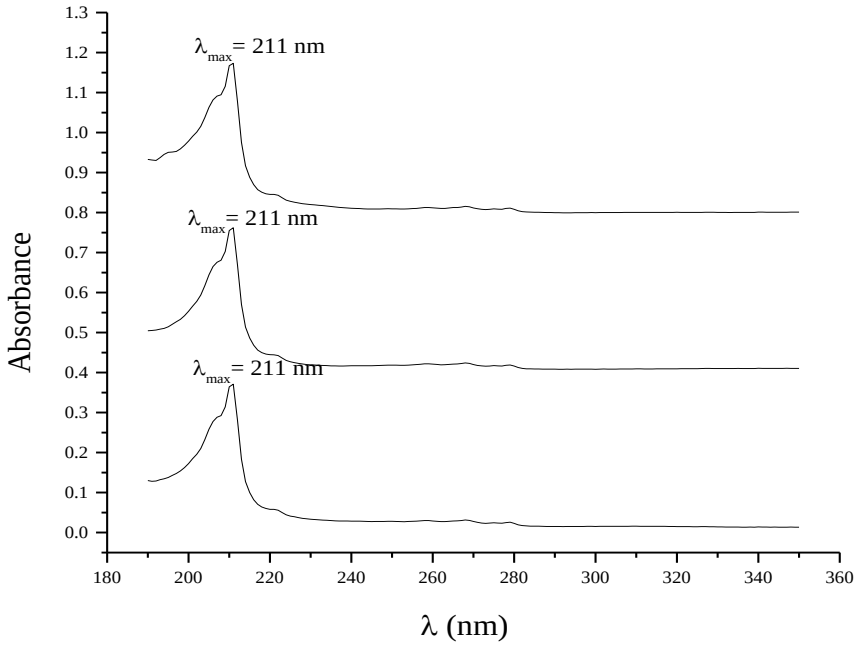

Figure B19. UV-absorbance spectra of the vapor phase of naphthalene at 20 °C.

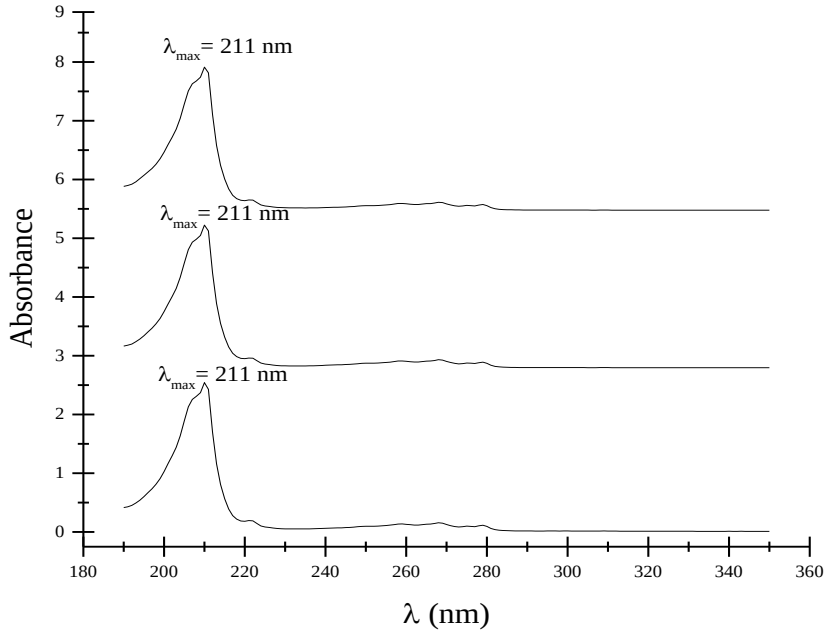

Figure B20. UV-absorbance spectra of the vapor phase of naphthalene at 50 °C.

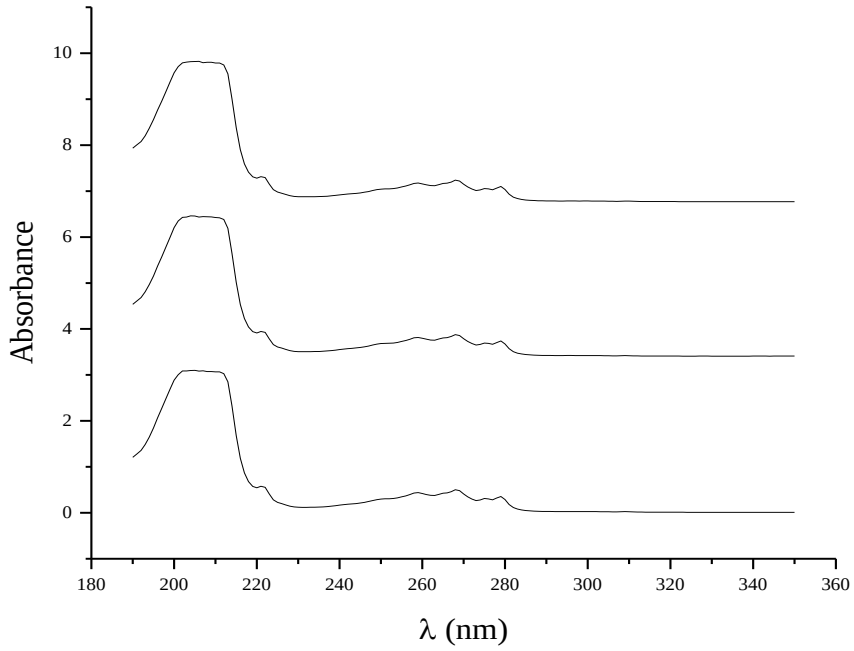

Figure B21. UV-absorbance spectra of the vapor phase of naphthalene at 70 °C.

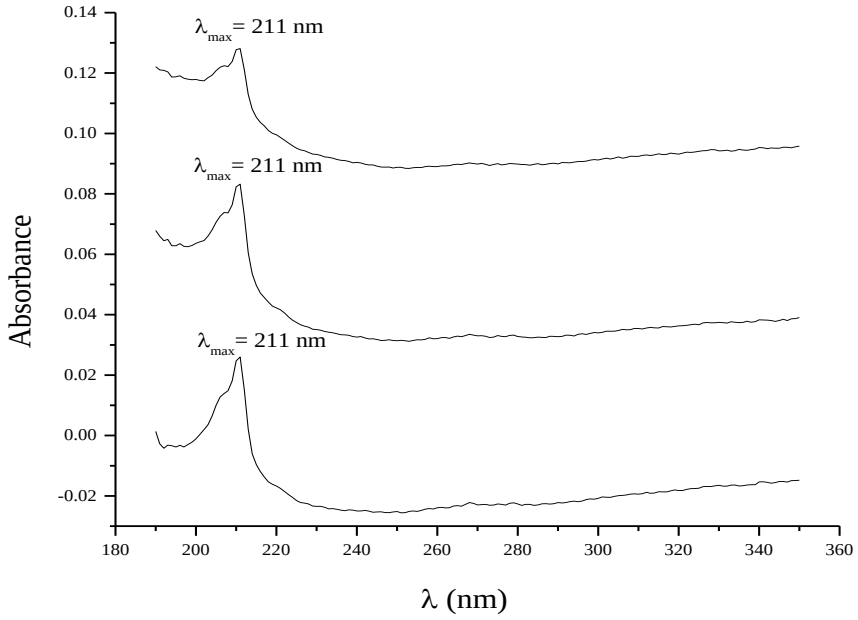

Figure B22. UV-absorbance spectra of the vapor phase of OSU-6 loaded with naphthalene at 20 °C.

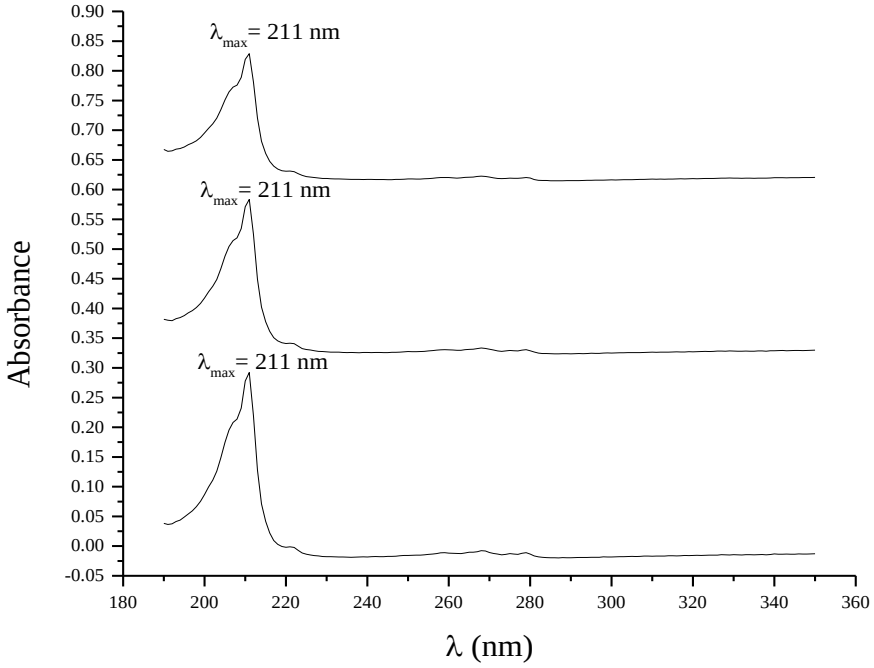

Figure B23. UV-absorbance spectra of the vapor phase of OSU-6 loaded with naphthalene at 50 °C.

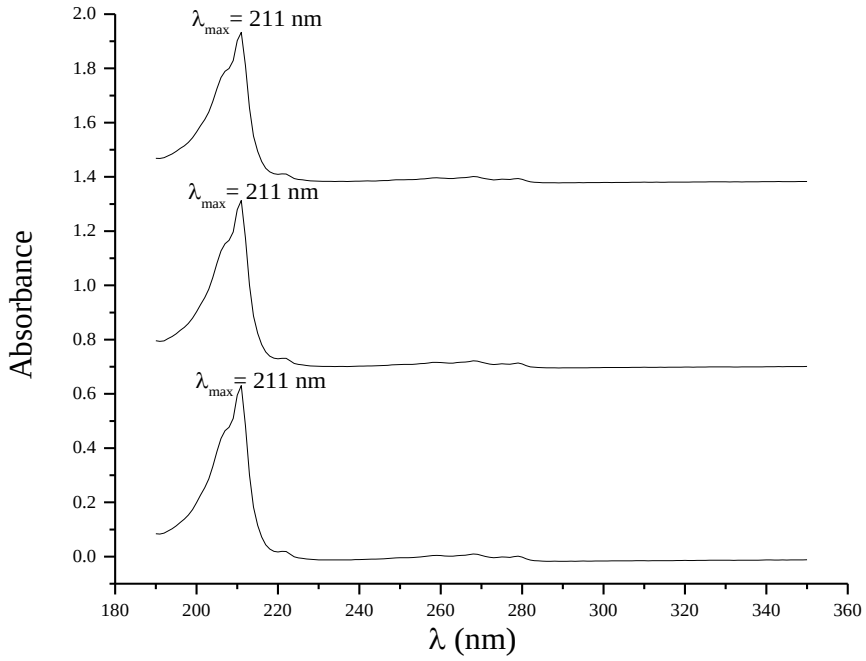

Figure B24. UV-absorbance spectra of the vapor phase of OSU-6 loaded with naphthalene at 70 °C.

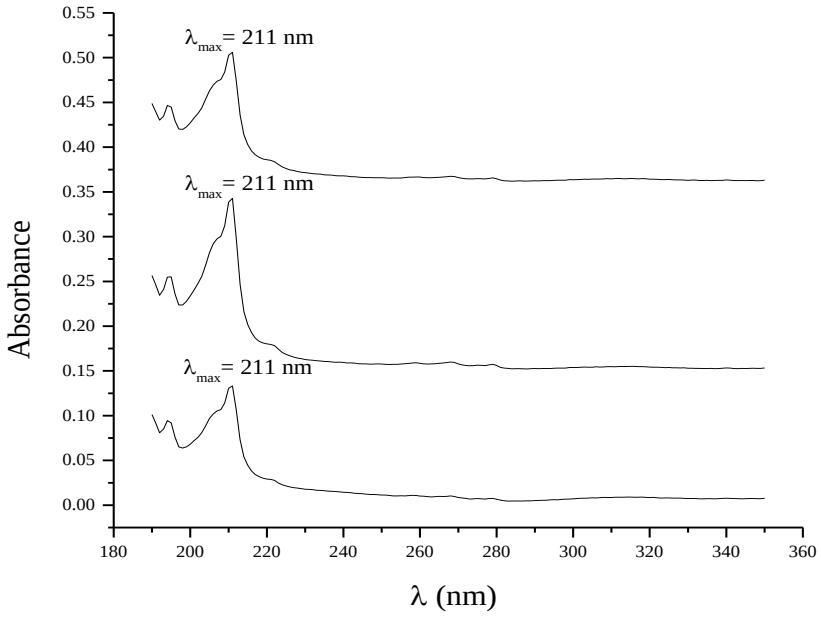

Figure B25. UV-absorbance spectra of the vapor phase of OSU-6 functionalized with hexyltrimethoxysilane loaded with naphthalene at 20 °C.

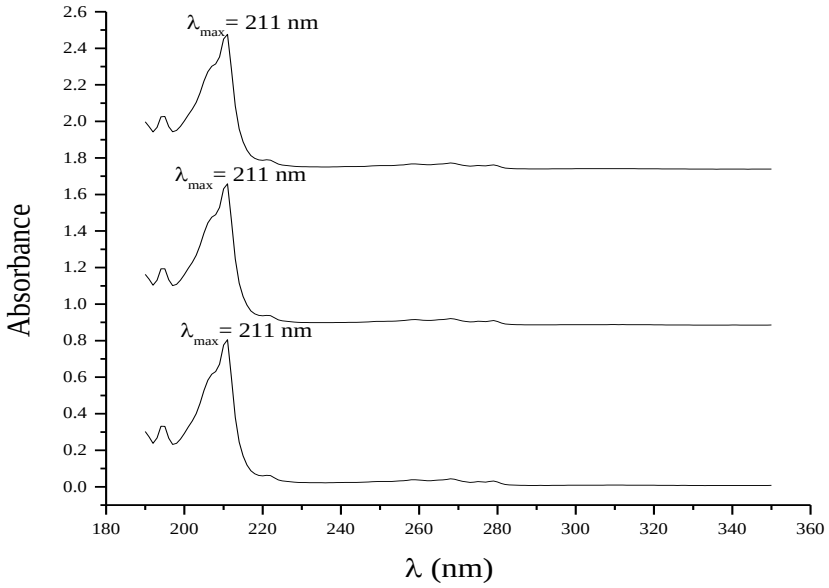

Figure B26. UV-absorbance spectra of the vapor phase of OSU-6 functionalized with hexyltrimethoxysilane loaded with naphthalene at 50 °C.

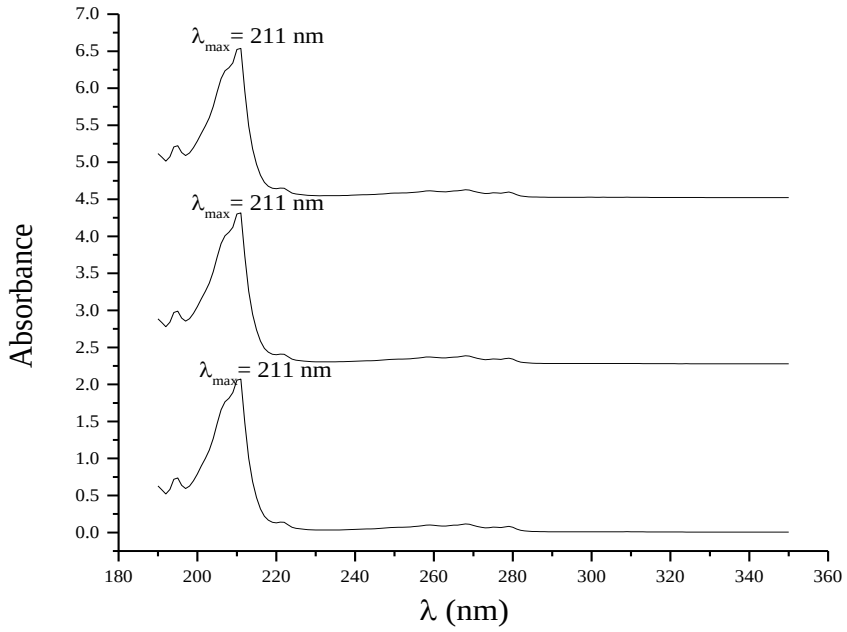

Figure B27. UV-absorbance spectra of the vapor phase of OSU-6 functionalized with hexyltrimethoxysilane loaded with naphthalene at 70 °C.

APPENDIX C – *Enthalpy of evaporation and sublimation tables*, **Chapter IV**

ΔH_{vap} (kJmol^{-1})	**First Scan**	**Second Scan**
1st experiment	28±2	26±2
2nd experiment	31±1	31±1
3rd experiment	27±2	28±2
Average	29±1	29±1

Table C1. Enthalpy of evaporation of toluene.

ΔH_{vap} (kJmol^{-1})	First Scan	Second Scan
1st experiment	28±1	28±1
2nd experiment	29±1	29±1
3rd experiment	35±1	35±1
Average	31±1	31±1

Table C2. Enthalpy of evaporation of OSU-6 loaded with toluene.

ΔH_{vap} (kJmol^{-1})	First Scan	Second Scan
1st experiment	32±1	32±1
2nd experiment	30±2	30±2
3rd experiment	34±1	34±1
Average	32±1	32±1

Table C3. Enthalpy of evaporation of OSU-6 functionalized with hexyltrimethoxysilane loaded with toluene.

ΔH_{vap} (kJmol^{-1})	First Scan	Second Scan
1st experiment	48±2	48±2
2nd experiment	48±2	48±2
3rd experiment	48±2	48±2
Average	48 ±1	48±1

Table C4. Enthalpy of evaporation of nitrobenzene.

ΔH_{vap} (kJmol^{-1})	First Scan	Second Scan
1st experiment	52±6	57±5
2nd experiment	54±5	56±5
3rd experiment	55±5	55±5
Average	54±3	56±3

Table C5. Enthalpy of evaporation of OSU-6 loaded with nitrobenzene.

ΔH_{vap} (kJmol^{-1})	First Scan	Second Scan
1st experiment	48±2	48±3
2nd experiment	40±2	40±2
3rd experiment	50±3	49±3
Average	46±1	46±2

Table C6. Enthalpy of evaporation of OSU-6 functionalized with hexyltrimethoxysilane loaded with nitrobenzene.

ΔH_{sub} (kJmol^{-1})	First Scan	Second Scan
1st experiment	56±6	56±6
2nd experiment	57±6	57±6
3rd experiment	56±7	56±7
Average	56±4	56±4

Table C7. Enthalpy of sublimation of naphthalene.

ΔH_{sub} (kJmol^{-1})	First Scan	Second Scan
1st experiment	31±13	29±12
2nd experiment	34±13	34±13
3rd experiment	38±17	41±20
Average	34±8	34±9

Table C8. Enthalpy of sublimation of OSU-6 loaded with naphthalene.

ΔH_{sub} (kJmol^{-1})	First Scan	Second Scan
1st experiment	48±10	48±10
2nd experiment	44±9	47±9
3rd experiment	48±10	49±10
Average	47±6	48±6

Table C9. Enthalpy of sublimation of OSU-6 functionalized with hexyltrimethoxysilane loaded with naphthalene.

VITA

Shadi Alizadeh Bazazi

Candidate for the Degree of

Doctor of Philosophy

Thesis: FUNCTIONALIZED MESOPOROUS SILICA AND ADSORPTION OF VOLATILE ORGANIC COMPOUNDS

Major Field: Chemistry

Biographical:

Education:

Completed the requirements for the Doctor of Philosophy in Chemistry at Oklahoma State University, Stillwater, Oklahoma in March 12, 2015.

Completed the requirements for the Master of Science in Inorganic Chemistry at University of Tehran, Tehran, Iran in 2006.

Completed the requirements for the Bachelor of Science in Chemistry at Azad University, Tehran, Iran in 2002.

Experience:

Graduate Research and Teaching Assistant, Oklahoma State University, Jan 2010 – Present

Quality Assurance Expert, Osvah (ex-*IRAN MERCK)* Pharmaceutical Company, Iran, Sep 2006-Feb 2009

Research Assistant, University of Tehran, Iran, Aug 2003-Feb 2006

Professional Memberships:

American Chemical Society, Phi Lambda Upsilon Chemical Honorary Society, North American Thermal Analysis Society